

**NOVEL (Cu-Sn) AND (Ni-Sn) CATALYSTS PREPARED BY MECHANICAL  
ALLOYING**

Sakollapath Pithakratanayothin

A Dissertation Submitted in Partial Fulfilment of the Requirements  
for the Degree of Doctor of Philosophy  
The Petroleum and Petrochemical College, Chulalongkorn University  
in Academic Partnership with  
The University of Michigan, The University of Oklahoma,  
and Case Western Reserve University

2018

บทคัดย่อและแฟ้มข้อมูลฉบับเต็มของวิทยานิพนธ์ตั้งแต่ปีการศึกษา 2554 ที่ให้บริการในคลังปัญญาจุฬาฯ (CUIR)  
เป็นแฟ้มข้อมูลของนิสิตเจ้าของวิทยานิพนธ์ที่ส่งผ่านทางบัณฑิตวิทยาลัย

The abstract and full text of theses from the academic year 2011 in Chulalongkorn University Intellectual Repository (CUIR)  
are the thesis authors' files submitted through the Graduate School.

**Thesis Title:** Novel (Cu-Sn) and (Ni-Sn) catalysts prepared by mechanical alloying  
**By:** Sakollapath Pithakratanayothin  
**Program:** Polymer Science  
**Thesis Advisors:** Prof. Sujitra Wongkasemjit  
Dr. Ruangdej Thongsri  
Assoc. Prof. Thanyalak Chaisuwan

---

Accepted by The Petroleum and Petrochemical College, Chulalongkorn University, in partial fulfilment of the requirements for the Degree of Doctor of Philosophy.

..... College Dean  
(Prof. Suwabun Chirachanchai)

**Thesis Committee:**

..... (Assoc.Prof. Dr. Apirat Laobuthee)	..... (Prof. Sujitra Wongkasemjit)
..... (Dr. Ruangdej Thongsri)	..... (Assoc. Prof. Dr. Thanyalak Chaisuwan)
..... (Asst. Prof. Dr. Manit Nithithanakul)	..... (Asst. Prof. Dr. Bussarin Ksapabutr)

**ABSTRACT**

5792008063: Polymer Science Program

Student's Name: Sakollphat Pithakratanayothin

Novel CuSn and NiSn catalysts prepared by mechanical alloying.

Thesis Advisors: Prof. Sujitra Wongkasemjit, Dr. Ruandej Thongsri,

Assoc. Prof. Dr. Thanyalak Chaisuwan 112 pp.

Keywords: Phenol/ Hydroxylation/ Crystal structure/ Catechol/ Hydroquinone

This research was aimed to synthesize intermetallic catalysts using mechanical alloying (Ma) technique. Copper (Cu) and nickel (Ni) were chosen to study since not only their properties are closed to the noble metal properties, e.g. platinum and palladium, but also they are not expensive. However, as also found in noble metals, both Cu and Ni metals are oxidized easily in air. To overcome this problem, either Cu or Ni was mixed with tin (Sn) to obtain bimetallics, viz. CuSn or NiSn, respectively. Therefore, this research was focused on finding the optimal conditions to synthesize both CuSn and NiSn bimetallics using the Ma technique and studied their catalytic activity on phenol hydroxylation and hydrogenation of cinnamaldehyde, as well. Structural characterization was carried out using various instrumental techniques.

## บทคัดย่อ

ชื่อ นายสกลพัฒน์ พิทักษ์รัตนโยธิน: ตัวเร่งปฏิกิริยาโลหะทองแดงผสมดีบุก และ นิกเกิลผสมดีบุกแบบใหม่จากกระบวนการผสมเชิงกล (ภาษาอังกฤษ) Novel CuSn and NiSn catalysts prepared by mechanical alloying. อ. ที่ปรึกษา: ศ. สุจิตรา วงศ์เกษมจิตต์ ดร. เรืองเดช ชงศรี และ รศ.ดร. ธัญญลักษณ์ ฉายสุวรรณ 112 หน้า

งานวิจัยนี้ ได้เน้นถึงการสังเคราะห์ตัวเร่งปฏิกิริยาชนิด intermetallic โดยใช้เทคนิคที่เรียกว่า อัลลอยเชิงกล (Mechanical alloying) โลหะที่เลือกมาศึกษาคือ ทองแดงและนิกเกิล เพราะ โลหะทั้งสองชนิดนี้ ไม่เพียงแต่มีสมบัติคล้ายโลหะประเภทเงินและพลาตินั่ม ยังมีราคาถูก อย่างไรก็ตาม ทั้งโลหะทองแดงและโลหะนิกเกิลมีความว่องไวต่อออกซิเจนในอากาศ ทำให้เสียความสามารถในการทำปฏิกิริยา เช่นเดียวกับเงินและพลาตินั่ม เพื่อแก้ปัญหานี้ จึงต้องผสมโลหะดีบุกลงไปในโลหะทองแดงและโลหะนิกเกิลเพื่อเพิ่มสมบัติในการต่อต้านการเกิดออกไซด์บนผิวโลหะ ทำให้ได้ตัวเร่งปฏิกิริยาชนิด CuSn และ NiSn ดังนั้น งานวิจัยนี้ จึงมุ่งศึกษาสภาวะที่เหมาะสม ของส่วนผสมโลหะทองแดงต่อดีบุก และ โลหะนิกเกิลต่อดีบุก รวมทั้งศึกษาความว่องไวของตัวเร่งปฏิกิริยาในการทำปฏิกิริยาไฮดรอกซีเลชันของฟีนอลและปฏิกิริยาไฮโดรจีเนชันของสารซินนามอลดีไฮด์ สมบัติทางโครงสร้างของตัวเร่งปฏิกิริยาถูกศึกษาด้วยเครื่องมือชนิดต่างๆ



## ACKNOWLEDGEMENTS

This work could not be accomplished without the facilities and supports from the following people. First of all, I am deeply grateful to my advisor and co advisors, Prof. Sujitra Wongkasemjit, Dr.Ruangdej Thongsri, and Assoc. Prof. Thanyalak Chaisuwan , who gave me a great experience and always encouraged me. It was so kind of them to give a chance for doing this research and provide me an international experience, beneficial recommendation, and intensive attention in my dissertation, especially their patience for proofreading my dissertation.

My gratitude is extended to the thesis committees, Assoc. Prof. Apirat laobutee, Asst. Prof. Manit Nithithanakul and Asst. Prof. Bussarin Ksapabutr for their important comments.

I would like to thank for the scholarship and funding supported by the Petroleum and Petrochemical College, Chulalongkorn University, Thailand Research Fund (Senior Research Scholar), the grant for international Research Integration: Chula Research Scholar, the Ratchadaphiseksompote Endowment fund, the powder metallurgy Research and Development Unit (PM\_RDU) of the National Metal and Material Technology Center (MTEC), and Thailand Graduate Institute of Science and Technology (TGIST-TG-33-09-58-058D).

Finally, I would like to take this opportunity to thank Mr. John M. Jackson for proofreading and give appreciation to all entire PPC friends and staffs for their support and help.

Last but not least, I would like to express my very profound gratitude to my parents and my sister for their supports, love, and standing me all time.

## TABLE OF CONTENTS

	<b>PAGE</b>
Title Page	i
Abstract (in English)	iii
Abstract (in Thai)	iv
Graphical abstract	v
Acknowledgements	vi
Table of Contents	vii
List of Tables	x
List of Figures	x
 <b>CHAPTER</b>	
<b>I INTRODUCTION</b>	<b>1</b>
 <b>II BACKGROUND AND LITERATURE REVIEW</b>	 <b>4</b>
 <b>III EXPERIMENTAL</b>	 <b>9</b>
3.1 Equipment	9
3.2 Chemicals	9
3.3 Experiment	9
3.3.1 Catalyst Preparation	10
3.3.2 Catalytic activity testing	10
3.3.3 Catalyst characterization	11
 <b>IV A SIMPLE ROUTE TO <math>\text{Cu}_x\text{Sn}_{100-x}</math> INTERMETALLIC NANOPARTICLE CATALYSTS FOR ULTRA-PHENOL HYDROXYLATION</b>	 <b>12</b>
4.1 Abstract	12

<b>CHAPTER</b>	<b>PAGE</b>
<b>IV</b> 4.2 Introduction	12
4.3 Experimental	14
4.4 Results and Discussion	16
4.5 Conclusions	28
4.6 Acknowledgements	28
4.7 References	29
<b>V</b> <b>INFLUENCES OF M-Sn INTERMETALLICS (M=Ni,Cu)</b> <b>PREARED BY MECHANICAL ALLOYING ON PHENOL</b> <b>HYDROXYLATION</b>	35
5.1 Abstract	35
5.2 Introduction	35
5.3 Experimental	36
5.4 Results and Discussion	38
5.5 Conclusions	53
5.6 Acknowledgements	55
5.7 References	55
<b>VI</b> <b>STRUCTURE EFFECT OF Cu<sub>x</sub>Sn<sub>1-x</sub> INTERMETALLIC</b> <b>CATALYST PREPARED BY MECHANICAL ALLOYING</b> <b>TECHNIQUE IN PHENOL HYDROXYLATION</b>	56
6.1 Abstract	56
6.2 Introduction	56
6.3 Experimental	58
6.4 Results and Discussion	60
6.5 Conclusions	77
6.6 Acknowledgements	77



<b>CHAPTER</b>		<b>PAGE</b>
VI	6.7 References	79
VII	<b>CONCLUSIONS AND RECCOMEMDATIONS</b>	87
	<b>REFERENCES</b>	89
	<b>CURRICULUM VITAE</b>	92

## LIST OF TABLES

<b>TABLE</b>		<b>PAGE</b>
<b>CHAPTER IV</b>		
<b>4.1</b>	Effect of the composition of $\text{Cu}_x\text{Sn}_{1-x}$ on the phenol hydroxylation.	19
<b>CHAPTER V</b>		
<b>5.1</b>	Composition, particle size, and crystallite size of $\text{Ni}_x\text{Sn}_y$ intermetallics on phenol hydroxylation	37
<b>5.2</b>	Optimized conditions for phenol hydroxylation	47
<b>5.3</b>	Phenol hydroxylation catalyzed by different catalytic systems	52
<b>CHAPTER VI</b>		
<b>6.1</b>	Composition, crystallite size, and influence of $\text{Cu}_x\text{Sn}_{1-x}$ intermetallics on phenol	62
<b>6.2</b>	Surface analysis of $\text{Cu}_x\text{Sn}_{1-x}$ intermetallics and $\text{H}_2\text{O}_2$ efficiency	78

## LIST OF FIGURES

<b>CHAPTER IV</b>		
<b>4.1</b>	XRD patterns of $\text{Cu}_{70}\text{Sn}_{30}$ at different milling times of (a) 5, (b) 20, and (c) 30 h	17
<b>4.2</b>	XRD patterns of $\text{Cu}_x\text{Sn}_{1-x}$ nanoparticles milled for 30 h; (a) $\text{Cu}_{100}$ , (b) $\text{Cu}_{70}\text{Sn}_{30}$ , (c) $\text{Cu}_{50}\text{Sn}_{50}$ , (d) $\text{Cu}_{30}\text{Sn}_{70}$ , and (e) $\text{Sn}_{100}$	18
<b>4.3</b>	HRTEM images of catalysts at 30 h milling; (a) $\text{Cu}_{100}$ , (b) $\text{Cu}_{70}\text{Sn}_{30}$ , (c) $\text{Cu}_{50}\text{Sn}_{50}$ , (d) magnification 2 nm scale in red rectangular of $\text{Cu}_{50}\text{Sn}_{50}$ (e) $\text{Cu}_{30}\text{Sn}_{70}$ , and (f) $\text{Sn}_{100}$	21

## LIST OF FIGURES

FIGURE		PAGE
<b>CHAPTER IV</b>		
4.4	The phenol conversion and the product selectivity of Cu <sub>30</sub> Sn <sub>70</sub> (30 mg) using 1:3 Phenol:H <sub>2</sub> O <sub>2</sub> at (a) 303, (b) 323, (c) 343, and (d) 363 K for 300 min reaction time	23
4.5	The phenol conversion and the product selectivity of different Cu <sub>30</sub> Sn <sub>70</sub> contents using 1:3 phenol:H <sub>2</sub> O <sub>2</sub> at 343 K for 1 h reaction time	24
4.6	The phenol conversion and the product selectivity of Cu <sub>30</sub> Sn <sub>70</sub> (monoclinic η-Cu <sub>6</sub> Sn <sub>5</sub> phase, 50 mg) using various phenol:H <sub>2</sub> O <sub>2</sub> molar ratios at 343 K for 1 h reaction time	26
4.7	(a) XRD patterns, (b) Raman spectra of Cu <sub>50</sub> Sn <sub>50</sub> before and after reaction	27
4.8	(a) XRD patterns, (b) Raman spectra of Cu <sub>50</sub> Sn <sub>50</sub> after 1 <sup>st</sup> and 2 <sup>nd</sup> cycles	28
<b>CHAPTER V</b>		
5.1	XRD patterns of Maed intermetallic catalysts a) Sn b) Ni <sub>57</sub> Sn <sub>43</sub> c) Ni <sub>42</sub> Sn <sub>58</sub> d) Ni <sub>27</sub> Sn <sub>73</sub> e) Ni	38
5.2	XRD patterns of Maed intermetallic catalysts: a) Sn, b) Cu <sub>30</sub> Sn <sub>70</sub> c) Cu <sub>30</sub> Sn <sub>70</sub> (HT), d) Cu	39
5.3	Selected area electron diffraction (SAED) of a) Ni <sub>57</sub> Sn <sub>43</sub> (Ni <sub>3</sub> Sn) b) Ni <sub>42</sub> Sn <sub>58</sub> (Ni <sub>3</sub> Sn <sub>2</sub> ) c) Ni <sub>27</sub> Sn <sub>73</sub> (Ni <sub>3</sub> Sn <sub>4</sub> ) d) Cu <sub>30</sub> Sn <sub>70</sub> (Cu <sub>6</sub> Sn <sub>5</sub> ) e) Cu <sub>30</sub> Sn <sub>70</sub> (HT) (Cu <sub>6</sub> Sn <sub>5</sub> (HT))	40
5.4	FE-SEM-EDS elemental mapping and black scattering images (BSE) of a-c) Ni <sub>3</sub> Sn, d-f) Ni <sub>3</sub> Sn <sub>2</sub> , g-i) Ni <sub>3</sub> Sn <sub>4</sub> , j-l) Cu <sub>6</sub> Sn <sub>5</sub> , and m-o) Cu <sub>6</sub> Sn(HT)	41
5.5	Sn 3d <sub>5/2</sub> spectra of a) Ni <sub>3</sub> Sn, b) Ni <sub>3</sub> Sn <sub>2</sub> , and c) Ni <sub>3</sub> Sn <sub>4</sub>	42
5.6	Sn 3d <sub>5/2</sub> spectra of a) Cu <sub>6</sub> Sn <sub>5</sub> and b) Cu <sub>6</sub> Sn <sub>5</sub> (HT)	43
5.7	Relationship between number of facets and TON value of Ni <sub>x</sub> Sn <sub>y</sub> intermetallic catalysts ; TON = mole of converted substrate/ mole of catalyst	44

## LIST OF FIGURES

FIGURE		PAGE
<b>CHAPTER V</b>		
5.8	Phenol conversion and the product distributions of Ni <sub>3</sub> Sn <sub>4</sub> (50 mg) using 1:3 phenol:H <sub>2</sub> O <sub>2</sub> at a) 343 and b) 363 K	46
5.9	Catalytic activity profiles versus time of Ni <sub>3</sub> Sn, Ni <sub>3</sub> Sn <sub>4</sub> , Cu <sub>6</sub> Sn <sub>5</sub> , Cu <sub>6</sub> Sn <sub>5</sub> (HT); a) Conversion, b) Concentration of CAT, and c) Concentration of HQ	48
5.10	XRD patterns of spent catalysts a) Cu-Sn series b) Ni-Sn series using 50 mg catalyst, 1:4 phenol:H <sub>2</sub> O <sub>2</sub> , 363 K for 3 h reaction time	50
<b>CHAPTER VI</b>		
6.1	XRD patterns of a) Cu <sub>30</sub> Sn <sub>70</sub> (HT), b) Cu <sub>50</sub> Sn <sub>50</sub> (HT), c) Cu <sub>70</sub> Sn <sub>30</sub> (HT)	61
6.2	Rietveld-XRD plots of a) Cu <sub>50</sub> Sn <sub>50</sub> (HT)	63
6.3	Selected area electron diffraction (SAED) of a) Cu <sub>30</sub> Sn <sub>70</sub> , b) Cu <sub>30</sub> Sn <sub>70</sub> (HT), c) Cu <sub>50</sub> Sn <sub>50</sub> , d) Cu <sub>50</sub> Sn <sub>50</sub> (HT), e) Cu <sub>70</sub> Sn <sub>30</sub> , f) Cu <sub>70</sub> Sn <sub>30</sub> (HT)	65
6.4	Cu 3p <sub>3/2</sub> spectra of a) Cu <sub>30</sub> Sn <sub>70</sub> , b) Cu <sub>50</sub> Sn <sub>50</sub> , and c) Cu <sub>70</sub> Sn <sub>30</sub>	66
6.5	Cu 3p <sub>3/2</sub> spectra of a) Cu <sub>30</sub> Sn <sub>70</sub> (HT), b) Cu <sub>50</sub> Sn <sub>50</sub> (HT), and c) Cu <sub>70</sub> Sn <sub>30</sub> (HT)	67
6.6	Sn 3d <sub>5/2</sub> spectra of a) Cu <sub>30</sub> Sn <sub>70</sub> , b) Cu <sub>50</sub> Sn <sub>50</sub> , and c) Cu <sub>70</sub> Sn <sub>30</sub>	68
6.7	Sn 3d <sub>3/2</sub> spectra of a) Cu <sub>30</sub> Sn <sub>70</sub> (HT), b) Cu <sub>50</sub> Sn <sub>50</sub> (HT), and c) Cu <sub>70</sub> Sn <sub>30</sub> (HT)	69
6.8	FE-SEM-EDS elemental mapping and back scattering images (BSE) of a-c, Cu <sub>30</sub> Sn <sub>70</sub> , d-f, Cu <sub>30</sub> Sn <sub>70</sub> (HT), g-i, Cu <sub>50</sub> Sn <sub>50</sub> , j-l, Cu <sub>50</sub> Sn <sub>50</sub> (HT), 8 m-o, Cu <sub>70</sub> Sn <sub>30</sub> , and p-r, Cu <sub>70</sub> Sn <sub>30</sub> (HT)	71
6.9	Phenol conversion by time of Cu <sub>x</sub> Sn <sub>y</sub> intermetallic catalysts before and after the heat treatment	72
6.10	Crystallite size and product selectivity of single phase catalysts	75

## CHAPTER I

### INTRODUCTION

The challenging step in catalysis hydrogenation is the selective hydrogenation in  $\alpha$ ,  $\beta$ -unsaturated aldehyde. Due to the unsaturated position (C=C) prefer to hydrogenate than carbonyl position (C=O), the specific catalyst should be designed. Many researches reported that there were two types of metal that could have used to selective hydrogenation of  $\alpha$ ,  $\beta$ -unsaturated aldehyde; that were mono-metallics and bi-metallics. Mono-metallics. Noble metals played an important role to hydrogenate  $\alpha$ , $\beta$ -unsaturated aldehyde. The developed catalysts in selective hydrogenation of  $\alpha$ , $\beta$ -unsaturated aldehyde have been done for decades. They found that the most active noble metals that could have given high yield that were Palladium (Pd), Platinum (Pt), Iridium (Ir), Gold (Au), Silver (Ag), and Ruthenium (Ru). Although the noble metals gave yield pretty high; however, some of them such as Pd, Pt, and Ru gave low selectivity of unsaturated alcohol due to high hydrogenation ability; moreover, they were declined in either activity or selectivity in higher temperature and inhibit their applications. Therefore, transition metals such as copper (Cu), iron (Fe), and nickel (Ni) would be the candidates to be an alternative metal to provide selective hydrogenation because they are cheap and practical. (Mertens *et al.*, 2007; Milone *et al.*, 2007; Álvarez-Rodríguez *et al.*, 2012; Du *et al.*, 2012; Ide *et al.*, 2012; Rojas *et al.*, 2012). Copper, Iron, and Nickel have been tested extensively for the selective hydrogenation, found that the Fe seemed to be the most reactive catalyst that provided the selective hydrogenation in  $\alpha$ ,  $\beta$ -unsaturated aldehyde. They found that the Fe<sup>4+</sup> of Fe(BF)<sub>4</sub> showed the highest selectivity to unsaturated alcohol (Wienhöfer *et al.*, 2013). Copper was a moderate reactivity for selective hydrogenation of  $\alpha$ , $\beta$ -unsaturated aldehyde. Recently research showed that copper nanoparticles without supported had a good reactivity for selective hydrogenation in  $\alpha$ , $\beta$ -unsaturated aldehyde (Gutiérrez *et al.*, 2013). Nickel was a poor selective hydrogenation in  $\alpha$ , $\beta$ -unsaturated aldehyde but excellent in hydrogenation on both conjugated and carbonyl positions.

Owing to the low selectivity of unsaturated alcohol in noble metals catalysts, besides, the noble metals were expensive and limited resource. Bi-metallic is a challenging catalyst which promising to perform two functions, which activate

carbonyl group and provide the selective hydrogenation at carbonyl position to unsaturated alcohol. Recently researches on bimetallic catalyst, Tin (Sn) were added to elevate the selectivity of unsaturated alcohol which succeeded to dramatically increase the selectivity closely to 100%. Generally, bi-metallic catalysts have been prepared by the incipient wetness co-impregnation technique, deposit-precipitation, reductive deposition precipitation, and etc. on the support but these techniques need either precision or accuracy of experimental details and take a long time period to prepare including reduction, evaporation, and many others processes, in addition, those processes can produce catalyst in a small scale and the noble metal precursors either highly sensitive to air and moisture or are expensive.

To cope with these problems that are high catalyst cost and small quantity in production. Powder techniques such as mechanical alloying (MA) and blending technique are the solution because those processes can produce catalyst in high scale, blending technique is simple technique which size of metal is not reduced. The two metals are mixed like shaking, where the surface of them reacts each other in solid-solid reaction. The surface of the metal is merge by the one another after sintering in furnace at high temperature. This technique will produce the catalyst in metallic pattern of random homogeneous alloy or sub-cluster segregated alloys. MA has been extensively investigated to prepare metal alloys, nano-crystallines, and various intermetallic compounds which is the powerful technique that can produce nanosize powders and nanocomposite materials; moreover, MA can accomplish the reaction in solid state and overcome the presence of oxygen and moisture during the process.

At present, there has been no research to use intermetallic compounds or alloy materials as a catalyst in the selective hydrogenation reaction. Therefore, the bi-metallic catalysts are going to prepare by the Copper (Cu) or Nickel (Ni) that will be used instead of noble metals to provide the hydrogenation with Tin (Sn) that activates the carbonyl group. The objectives of this study are

1. To characterize Cu-Sn and Ni-Sn intermetallic compounds as catalysts and elucidate the activity of Cu:Sn and Ni:Sn without support as a catalyst in the selective hydrogenation.
2. To elucidate the ratio of Cu:Sn and Ni:Sn to find the optimal ratio that could produce the highest conversion and selectivity of unsaturated alcohol.

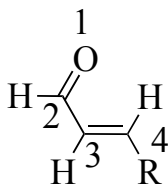
3. To determine the reaction time and chemical kinetic either Cu:Sn or Ni:Sn.
4. To compare the conversion and selectivity of unsaturated alcohol by using differences sources of hydrogen such as hydrogen gas or formic acid in different solvents (e.g. isopropanol, amyl alcohol, and THF).

## CHAPTER II

### BACKGROUND AND LITERATURE REVIEW

#### 2.1 $\alpha$ , $\beta$ -unsaturated aldehyde

The unsaturated aldehyde is the carbonyl compound that consists of two electrophilic sites: the carbonyl carbon (1,2-position) and the double bond at  $\beta$ -carbon (3,4-position) as shown in Figure 1. Due to the delocalization of electron among double bond and carbonyl group, nucleophile can add either carbonyl carbon position or  $\beta$ -carbon to give derivative compounds via conjugate reaction or 1,4-addition reaction. This chemical molecular is also called  $\alpha$ ,  $\beta$ -unsaturated aldehyde. This molecule is interesting and challenging in catalysis because it can convert to several functional groups that depends on the catalysis.



R= -Ph, -CH<sub>3</sub>, -H, and alkyl

Figure 2.1. Illustrate the carbonyl carbon (1,2-position) and C=C double bond (3,4-position) in  $\alpha$ ,  $\beta$ -unsaturated aldehyde.

Interestingly, the unsaturated alcohols (e.g. allylic alcohols and Furfural) are play an important role in the pharmaceuticals, perfumes, cosmetics, and advanced material. All of them are attribute to hydrogenate preferably at carbonyl group of  $\alpha$ ,  $\beta$ -unsaturated aldehyde at 1,2-position ( $\alpha$ -carbon) ([Chapuis and Jacoby, 2001](#); [Serra \*et al.\*, 2005](#)). On the other hand, the conventional hydrogenation catalysts prefer to hydrogenate on 3,4-position ( $\beta$ -carbon) of  $\alpha$ ,  $\beta$ -unsaturated aldehyde because it is more reactive than the carbonyl carbon ([Chapuis and Jacoby, 2001](#); [Serra \*et al.\*, 2005](#); [Mertens \*et al.\*, 2009](#)). The selective hydrogenation of  $\alpha, \beta$ -unsaturated aldehyde has become a challenging issue since 1990. Many researches reported that there were two types of metal that could have used to selective hydrogenation of  $\alpha$ ,  $\beta$ -unsaturated aldehyde; that were mono-metallics and bi-metallics.



## 2.2 Mono-metallic catalysts

### 2.2.1 Noble Metals

Mono-metallics such noble metals played an important role to hydrogenate  $\alpha,\beta$ -unsaturated aldehyde. The developed catalysts in selective hydrogenation of  $\alpha,\beta$ -unsaturated aldehyde has been done for decades. They found that the most active noble metals that could have given high yield that were Palladium (Pd), Platinum (Pt), Iridium (Ir), Gold (Au), Silver (Ag), and Ruthenium (Ru) ([Mertens et al., 2007](#); [Milone et al., 2007](#); [Álvarez-Rodríguez et al., 2012](#); [Du et al., 2012](#); [Ide et al., 2012](#); [Rojas et al., 2012](#)). Milone et al. studied the Au activity for the selective hydrogenation on  $\alpha,\beta$ -unsaturated aldehyde and ketone. The results showed that the gold on goethite gave the 50% conversion which selected to unsaturated alcohol at 91%; moreover, the  $\alpha,\beta$ -unsaturated aldehyde were selective to hydrogenation than  $\alpha,\beta$ -unsaturated ketone ([Milone et al., 2007](#)). Mertens studied the Ag, Pt, Co, and Ru metal for selective hydrogenation in various solvents (e.g. DMF, ethanol, butanol, and pentanol), found that Pt in DMF showed the highest conversion (87%) while was giving low selectivity (23%) unsaturated alcohol. Whereas Ag gave conversion in rang 55-65 % with high selectivity ([Mertens et al., 2007](#)). Rojas and colleges demonstrated Au and Ir on SiO<sub>2</sub> in the selective hydrogenation  $\alpha,\beta$ -unsaturated aldehyde, found that the Ir gave high conversion but low selectivity while Au gave low conversion but high selectivity ([Rojas et al., 2012](#)).

## 2.3 Transition Metals

### 2.3.1 Iron (Fe)

Wienhöfer studied the Fe(BF)<sub>4</sub> homogeneous catalyst for selective hydrogenation on  $\alpha,\beta$ -unsaturated aldehyde by using formic acid as a hydrogen source. The results showed that the higher of iron loading gave the higher conversion and selectivity of unsaturated alcohol. Moreover, they reported that the solvents (e.g. THF and tert-amyl alcohol) induced the reaction gave the selectivity more than 99 % on unsaturated alcohol (Wienhöfer et al., 2013).

### 2.3.2 Nickel (Ni)

Lin and coworkers studied the activity of Ni when added in the Ir by deposition-precipitation. The modified of Ni with Ir showed that cinnamaldehyde was hydrogenated to hydrocinnamaldehyde, which conversion was 97.8 % but did not selective to unsaturated alcohol. As consequence, they concluded that Ni was a powerful metal that could have provided the hydrogenation reaction (Lin *et al.*, 2013).

### 2.3.3 Copper (Cu)

Recently, many researches studied on Cu to be an alternative metal to provide hydrogenation in selective hydrogenation in  $\alpha,\beta$ -unsaturated aldehyde because it was cheap and abundance in natural resource. The factors that effected on the reactivity of copper in the selective hydrogenation of  $\alpha,\beta$ -unsaturated aldehyde were particle sizes of metals, and support. Generally, support is used to increase the catalyst activity by increasing the surface area; until Victorial research group elucidated the activity of Cu on many supports. In 2012, Victorial used MCM-48 for testing selective hydrogenation of cinnamaldehyde, the conversion was 10 % and selectivity was 50 % when compared with SiO<sub>2</sub> support, MCM-48 gave higher conversion and selectivity than SiO<sub>2</sub> (Gutierrez *et al.*, 2012). Year later, Victorial studied the surface area that effected on the conversion and selectivity of cinnamaldehyde hydrogenation by using MCM-41, CeO<sub>2</sub>, and without supported which surface area were 810, 240, and N/A (m<sup>2</sup>/g) respectively. At 30 % conversion, they gave the selectivity of unsaturated alcohol were 65% on MCM-41, 85% on CeO<sub>2</sub>, and 87 % without supported (Gutiérrez *et al.*, 2013).

## 2.4 Post Transition Metals

### 2.4.1 Tin (Sn)

Furthermore, the other metal that has an ability to activate the carbonyl group is tin (Sn). Sn is categorized in a post transition metal group because they are soft and poor mechanical strength (Huheey and Keiter, 1993). To cope the low selectivity of unsaturated alcohol in  $\alpha,\beta$ -unsaturated aldehyde, Sn was played an activated metal for carbonyl group. In 2001, Margitfalvi and colleagues reported the

activity of Pt/SiO<sub>2</sub> in the selective hydrogenation of crotonaldehyde at 5% conversion that Pt gave high selectivity in saturated alcohol.

## 2.5 Bi-metallic Catalysts

### 2.5.1 Platinum-Tin (Pt-Sn)

When Tin was added on the Pt/SiO<sub>2</sub>, the selectivity of unsaturated alcohol was increased direct proportional to weight; until, the ratio of Sn/Pt to 2.5 the selectivity of unsaturated alcohol closely to be 90 %. Moreover, they found that Sn<sup>4+</sup> could enhance the electrophilicity of carbonyl group owing to high selectivity in unsaturated alcohol (Margitfalvi *et al.*, 2002). While Pt-Sn/SiO<sub>2</sub> gave low conversion, some researches were played on this application due to unique properties. In 2009, Merlo studied the Sn<sub>x</sub>Pt/SiO<sub>2</sub> (where x = 0.3-1) in furfural selective hydrogenation, found that the Sn<sub>0.3</sub>Pt/SiO<sub>2</sub> provided the high selectivity of furfuryl alcohol. Moreover, this catalyst could recycle for three times which retained the efficiency (Merlo *et al.*, 2009). The modification of this catalyst was further studied, Plomp used Pt-Sn/carbon nanofibers (CNF) to study selective hydrogenation which prepared by reductive deposition precipitation method, found that at 50 % conversion, the selectivity of cinnamylalcohol (unsaturated alcohol) was 77 % when compared with the Pt/CNF which gave 59% selectivity (Plomp *et al.*, 2009). Taniya prepared Sn-modified Si-coated Pt (Sn/SP) for selective hydrogenation in crotonaldehyde. They illustrated that Sn/SP was a core shell catalyst which Pt was a core. Hence, Sn activated at carbonyl and Pt directly transferred hydrogen to hydrogenate at the carbonyl group. As a result, at 5 % conversion, the Sn/SP gave 100 % selectivity of crotylalcohol (unsaturated alcohol) at 20 hours (Taniya *et al.*, 2012). Therefore, many researchers looked forward to enhance conversion and selectivity of unsaturated alcohol by combining noble metals with tin by means of co-impregnation and many others techniques on the support. The bi-metallics were promising to perform two functions, which are activated carbonyl group and provide the selective hydrogenation at carbonyl group to unsaturated alcohol. According to literature reviews, Sn dramatically enhanced the selectivity of the unsaturated alcohol dramatically increase from 1.4 % to 100 % (Taniya *et al.*, 2012) when tin was co-impregnated with the noble-metal, the reaction mechanism revealed that Sn activated the oxygen atom at carbonyl group and was thus

to increase the electrophilicity at  $\alpha$ -carbon atom; therefore, the competitive hydrogenation would have favored at  $\alpha$ -carbon (C=O carbonyl group) than  $\beta$ -carbon (C=C double bond) due to the thermodynamic properties (Margitfalvi *et al.*, 2002; Merlo *et al.*, 2009; Plomp *et al.*, 2009; Taniya *et al.*, 2012).

## **CHAPTER III**

### **EXPERIMENTAL**

#### **3.1 Equipment**

1. Three neck round bottom flask
2. Condenser
3. Hydrogen regulator
4. Agilent Technology Gas Chromatography 7890 (GC)
5. Capillary column
6. Furnace Linn High Temp
7. Sieves, 140 and 200 mesh
8. Alumina tube
9. Cucible
10. Mechanical alloying
11. Ball mill

#### **3.2 Chemicals**

1. Cinnamaldehyde
2. Naphthalene
3. Copper powder
4. Tin powder
5. Formic acid
6. Hydrogen gas
7. Isopropanol
8. Standard cinamyl alcohol
9. Standard hydrocinamaldehyde
10. Standard 3-phenyl-1-propanol

#### **3.3 Experiment**

##### **3.3.1 Catalyst Preparation**

Mechanical alloying is carried out under argon atmosphere at room temperature. Pure Cu (99.99 %), Ni (99.99%), and Sn (99.99%) are used as starting materials. To obtain the desired stoichiometric catalyst composition, these materials are mixed into ratio of Cu:Sn as (100:0, 70:30, 50:50, 30:70, 0:100) %wt and Ni:Sn also repeat the same ratio. The mechanical alloying rotates at the speed of 500 rpm with ball to powder ratio 5:1. The vial and ball material are made from stainless steel, which diameter of balls are 4.7 mm. The powders are sieved to get the same particle size with sieve 140 and 200 mesh. The powders are mix with the naphthalene and packed in alumina tube for sintering at 700°C for 30 minutes to create foam catalyst.

### 3.3.2 Catalyst activity test

#### 3.3.2.1 Liquid phase hydrogenation

Catalytic hydrogenation of cinnamaldehyde is carried out in a modified three-necked round bottom flask in an oil bath at 100 °C with hydrogen flow rate 150 ml/min. 0.2 g of catalysts are added in 25 ml of isopropanol as a solvent. Prior testing, the hydrogen gas is purged for 1 h into the mixture to avoid the trace of oxygen. The cinnamaldehyde with concentration of 1 mM with volume 25 ml is added. The stirring rate is 700 rpm. To follow the progress of the reaction, sampling a sufficient amount in order to observe the conversion and selectivity. The liquid sample was analyzed by means of Gas Chromatography (Agilent Technology-7890, rtx-50 capillary column) using a flame ionization detector. Hydrocinnamaldehyde, cinamyl alcohol, and 3-phenyl-1-propanol are detected as reaction products, which are quantified by using o-xylene as the internal standard substance.

### 3.3.3 Catalyst characterization

#### 3.3.3.1 Transmission electron microscopy (TEM)

The Cu-Sn and Ni-Sn nanoparticle are observed by transmission electron microscopy. For TEM study, the samples (after air calcination and H<sub>2</sub> reduction) are ultrasonically dispersed in ethanol by adding drops of 2-dimethylaminoethanol as a dispersant, and the ethanol solution is dropped on a carbon film supported on a Cu grid.

### 3.3.3.2 Adsorption capacity

Temperature-programmed reduction (TPR) tests are carried out in a conventional reactor equipped with a thermal conductivity detector with a feeding flow of 25 cm<sup>3</sup> min<sup>-1</sup> (5% H<sub>2</sub> in N<sub>2</sub>) at a heating rate of 10 °C min<sup>-1</sup>. H<sub>2</sub> and CO chemisorption measurements are performed in a static volumetric apparatus at ambient temperature.

### 3.3.3.3 X-ray fluorescence (XRF)

The ratios of Cu-Sn and Ni-Sn catalysts are estimated by XRF spectroscopy. The sample was excited with the Pd X-ray tube operated at 40 kV and 1.25 mA.

### 3.3.3.4 X-ray diffraction (XRD)

X-ray diffraction powder patterns of Cu-Sn and Ni-Sn intermetallic compounds are measured at room temperature Cu K $\alpha$  radiation. X-ray tube was operated at 40 kV and 40 mA.

### 3.3.3.5 X-ray photoelectron spectra (XPS)

XPS spectra are acquired with a multi-technique system (SPECS) equipped with a Al-K $\alpha$  100 W X-ray source and a hemispherical electron analyzer, operated in fixed analyzer transmission (FAT) mode. The spectra are collected at an energy pass of 30 eV. The powder samples are pressed to form a disc and mounted onto a manipulator that allowed the transfer from the pretreatment chamber to the analysis chamber. In the pretreatment chamber, the samples are reduced for 1 h at 400 °C in flowing H<sub>2</sub>. The spectra are recorded once the pressure in the analysis chamber reached a residual pressure of less than  $5 \times 10^{-9}$  mbar. The binding energies are referenced to the C 1s line at 284.6 eV. The intensities are estimated by calculating the integral of each peak after subtracting the S-shaped background and fitting the experimental peak to a Lorentzian/Gaussian mix of variable proportion, using the XPS program.

## CHAPTER IV

### A SIMPLE ROUTE TO $\text{Cu}_x\text{Sn}_{100-x}$ INTERMETALLIC NANOPARTICLE CATALYSTS FOR ULTRA-PHENOL HYDROXYLATION

#### 4.1 Abstract

A practical methodology and novel, economical materials were proposed to successfully prepare nanoparticle catalysts for phenol hydroxylation. The preparation was carried out via mechanical alloying (MA) of  $\text{Cu}_x\text{Sn}_{100-x}$  powder mixtures (where  $x = 30, 50, 70,$  and  $100$  %wt). The mechanical alloyed nanoparticles were characterized using various techniques. X-ray diffraction patterns indicated that  $\eta\text{-Cu}_6\text{Sn}_5$ ,  $\epsilon\text{-Cu}_3\text{Sn}$ , and  $\text{CuSn}$  phases could be formed in the mechanical alloyed  $\text{Cu}_x\text{Sn}_{100-x}$  materials. Transmission electron micrographs and selected area electron diffraction patterns confirmed the presence of  $\eta\text{-Cu}_6\text{Sn}_5$ ,  $\epsilon\text{-Cu}_3\text{Sn}$ , and  $\text{CuSn}$  phases. Activity of the catalysts, using the optimal conditions of  $70$  °C reaction temperature for  $1$  h,  $50$  mg of  $\text{Cu}_{0.5}\text{Sn}_{0.5}$ , and  $1:3$  phenol: $\text{H}_2\text{O}_2$  ratio, provided more than  $98\%$  conversion with  $70\%$  catechol (CAT) and  $29\%$  hydroquinone (HQ). Experimental results suggested that the presence of the  $\epsilon\text{-Cu}_3\text{Sn}$  phase gave higher activity while Sn reduced benzoquinone (BQ) to HQ. The catalyst maintained its stability with no structural collapse for more than  $24$  h.

**Keywords:** Mechanical alloying,  $\eta\text{-Cu}_6\text{Sn}_5$ ;  $\epsilon\text{-Cu}_3\text{Sn}$ ;  $\text{CuSn}$ ; Phenol hydroxylation

#### 4.2 Introduction

Due to the growth of industry, an increase in wastewater containing organic compounds and affecting to the environment has become a major concern. Phenol is one component that has received much attention since it is toxic, carcinogenic, and mutagenic (Busac *et al.* (2008); Zapico *et al.* (2015)). Many researchers have attempted to solve this problem by converting phenol to more value-added components, such as catechol (CAT) and hydroquinone (HQ) because these two compounds are useful, especially in the pharmaceutical area. For instance, CAT can



be used as an antioxidant, astringent, antiseptic, etc., while HQ and its derivatives are also used in allergic disease treatment (Abbo *et al.* (2004)).

One way to convert phenol to CAT and HQ is to carry out a process through phenol hydroxylation reaction. Many types of heterogeneous catalysts were studied to optimize the oxidation of phenol. Xia *et al.* incorporated Cu and Fe on MCM-41 and found that Cu played a major role in promoting the catalytic performance on phenol hydroxylation using H<sub>2</sub>O<sub>2</sub> under mild conditions at low pH (Xia *et al.* (2011)). In addition, Kumar and Srinivas studied the hydroxylation of Ti on both SBA-12 and SBA-16, and showed both catalysts gave low conversions of 24.1 and 13.3%, respectively. Ti-SBA-12 exhibited a higher activity with a higher selectivity of HQ than Ti-SBA-16 (Kumar *et al.* (2013)). Silva *et al.* prepared Au/ZnO for the phenol hydroxylation and found that double impregnation procedure was needed to obtain excellent conversion of 98%. Moreover, the preparation was suitable for only the lab-scale (Silva *et al.* (2014)). Ahmed *et al.* studied microwave-enhanced degradation of phenol using Ni/ZnO and found that Zn, NiO, and Ni(OH)<sub>2</sub> were leached and the structure significantly collapsed (Ahmed *et al.* (2014)). Moreover, Maneesuwan *et al.* studied synthesized Fe-Ti-TUD-1 for phenol hydroxylation and found that not only was the structure collapsed by strong oxidant, but also the metals were leached from the framework (Maneesuwan *et al.* (2016)). Unfortunately, the studied catalysts either were unstable or resulted from the leaching problem. In terms of economical issue, many scientists have turned to Cu (II) complex solution and copper metal as a catalyst for phenol hydroxylation (Casto *et al.* (2009); Inchaurredo *et al.* (2012)). Moreover, it was reported that the presence of Sn<sup>4+</sup> enhanced the H<sub>2</sub>O<sub>2</sub> efficiency and conversion in phenol hydroxylation (Mal *et al.* (1996); Niphadkar *et al.* (2009)).

Although bi-metallic nanoparticle catalysts can be achieved by many techniques (e.g. chemical reduction), thermal decomposition of appropriate precursors, electrochemical synthesis, etc., the procedures are complicated and can be conducted only on a laboratory scale (Sankar *et al.* (2012)). Mechanical alloying (MA) is a powerful technique in producing nanosize powders (Saboor *et al.* (2015)) and nanocomposite materials on a larger scale (Zamani *et al.* (2012)). Most

importantly, the obtained product is stable to oxygen and moisture during the process and is thus easier to handle (Mostann *et al.* (2012)).

Up to now, there has been no research reported on the catalyst produced from the MA technique. In this study, nanoparticles of Cu and Sn metals and  $\text{Cu}_x\text{Sn}_{100-x}$  intermetallics were synthesized via the MA technique and used as catalysts for phenol hydroxylation to increase the selectivity of CAT and HQ. The influence parameters, such as contents of Sn, reaction temperature and time, amount of catalyst, and amount of oxidant were investigated to observe the optimal conversion and selectivity. The catalysts were characterized using various techniques. The catalysts' reusability and stability were also investigated.

### 4.3 Experimental

#### 4.3.1 Materials

Copper (Cu, 99.99 %wt) and tin (Sn, 99.99 % wt) powders were produced using gas atomization, as detailed in elsewhere (Morakotjinda *et al.* (2010)). Methanol ( $\text{CH}_3\text{OH}$ , 99.99%) was purchased from Labscan, Thailand; catechol (CAT, 99%), hydroquinone (HQ, 99%), 1,4-benzoquinone (BQ, 98%) from Sigma-Aldrich, USA; phenol detached crystals and hydrogen peroxide ( $\text{H}_2\text{O}_2$ , 30 %w/v) from Fisher Scientific, UK. All chemicals were used without purification.

#### 4.3.2 Characterization

X-ray diffraction (XRD) patterns were recorded on a Rigaku X-ray diffractometer with  $\text{CuK}\alpha$  radiation and the crystallite sizes were determined using MDI JADE 9 software, relating to the Scherrer formula, with a residual error of less than 10% (Kurian *et al.* (2012); Maurya *et al.* (2003); Fathima *et al.* (2008)). X-ray fluorescence (XRF) spectrometer (PANalytical AXIOS PW 4400) was used to analyze elements in the samples. Materials characterization by Transmission electron micrographs (TEM) and high resolution transmission electron micrographs (HRTEM) were conducted using JEOL JEM-2010. Gas chromatography with a flame ionization detector (GC-FID, Agilent 6890) equipped with a 30 m ZB-WAX capillary column was used to analyze the products from phenol hydroxylation.

Raman spectra were obtained using Senterra Dispersive Raman Microscope (Bruker Optics) equipped with Laser excitation wavelength 532 nm and the power laser was kept at 5 mw to analyze the coke formation on the catalyst.

#### 4.3.3 Synthesis of Cu, Sn, and Cu<sub>x</sub>Sn<sub>y</sub> nanoparticles

Cu (32 > μm) and Sn (32 > μm) were used to prepare Cu, Sn, and Cu<sub>x</sub>Sn<sub>100-x</sub> nanoparticles. The Cu<sub>x</sub>Sn<sub>100-x</sub> alloys was prepared by varying Sn contents (30, 50, 70, and 100 %wt) balanced with Cu powder. Elemental Cu and Sn powders and Cu<sub>x</sub>Sn<sub>100-x</sub> powder mixtures were mechanically alloyed (MAed) in an attritor. The MA conditions were as follows: 5:1 ball-to-powder ratio, 300 rpm MA speed, and 30h milling time. The MAed powders were further characterized using various techniques.

#### 4.3.4 Catalytic activity study

Phenol hydroxylation was carried out to study the activity of the synthesized catalysts by adding phenol (1.88g, 20mmol), H<sub>2</sub>O<sub>2</sub> (6.84g, 60 mol), and water (10 ml) into a 250 ml two-necked round bottom flask fitted with a condenser. The studied reaction temperature was varied from 303 to 363K for various reaction times (30 min to 5h). The tar content was filtered and washed with a mixture of 1:1 water:ethanol by volume. The products in the reaction liquid were analyzed using GC. The reactions were repeated three times and the results averaged for both accuracy and precision.

#### 4.3.5 Reusability and thermal stability study

The first-run catalysts were filtered, washed with acetone to remove tar, followed by a rinse with distilled water, and dried at 373 K for 1 h before conducting the second run. The coke formation was determined using Raman spectroscopy technique. To test its stability, the catalysts were run at 343 K for 6, 12, 18, and 24 h. The catalysts were filtered, washed with acetone and distilled water, and dried at 373 K for 1 h before analysis with XRD.

## 4.4 Results and Discussion

### 4.4.1 Preparation and characterization of catalyst

$\text{Cu}_x\text{Sn}_{1-x}$  catalysts prepared by MA at 30 h with various amounts of Sn (30, 50, 70, and 100 %wt) are shown in Figure 4.1. Figure 4.1(a)-(e) show XRD patterns of  $\text{Cu}_{100}$  (JCPDS Card No. 04-0836),  $\text{Cu}_{70}\text{Sn}_{30}$  (JCPDS Card No. 65-3434 of sorosite),  $\text{Cu}_{50}\text{Sn}_{50}$  (JCPDS card No. 47-1575 of monoclinic  $\eta$ - $\text{Cu}_{6.25}\text{Sn}_5$ , JCPDS Card No. 45-1488 of monoclinic  $\eta$ - $\text{Cu}_6\text{Sn}_5$ , and JCPDS Card No. 01-1240 of orthorhombic  $\epsilon$ - $\text{Cu}_3\text{Sn}$ ),  $\text{Cu}_{30}\text{Sn}_{70}$  (JCPDS Card No. 45-1488 of monoclinic  $\eta$ - $\text{Cu}_6\text{Sn}_5$ ), and  $\beta$ -Sn phase (JCPDS Card No. 04-0673), respectively. All the XRD patterns show broad peaks which can be attributed to the small crystallite sizes, as listed in Table 4.1. The crystallite size was determined using the Scherrer formula, see eq.1 (Buarod *et al.* (2015));

$$d = \frac{0.9\lambda}{B\cos\theta} \quad (1)$$

where  $d$  is the average crystallite size,  $\lambda$  is the wavelength of the X-ray,  $B$  is the full width at half maximum intensity of Bragg diffraction peak at diffraction angle  $\theta$  (in radians). The MDI JADE software was used to calculate the crystallite size, as related to the Scherrer formula (Howard *et al.* (1989); Callister *et al.* (2003); Cullity *et al.* (2001)), to obtain more accuracy and precision. From the results, it was found that the crystallite size of Sn was the biggest since Sn, having its melting point at 231 °C, was possibly melted and agglomerated into large particle size during the mechanical alloying process, generating heat at around 200° – 220 °C (Takacs and McHenry (2006)). As the Sn content was higher, viz.,  $\text{Cu}_{30}\text{Sn}_{70}$ , the agglomerate of Sn became a concern. To achieve nanocrystallite size of  $\text{Cu}_{30}\text{Sn}_{70}$ , the mechanical alloying process took 30 h.

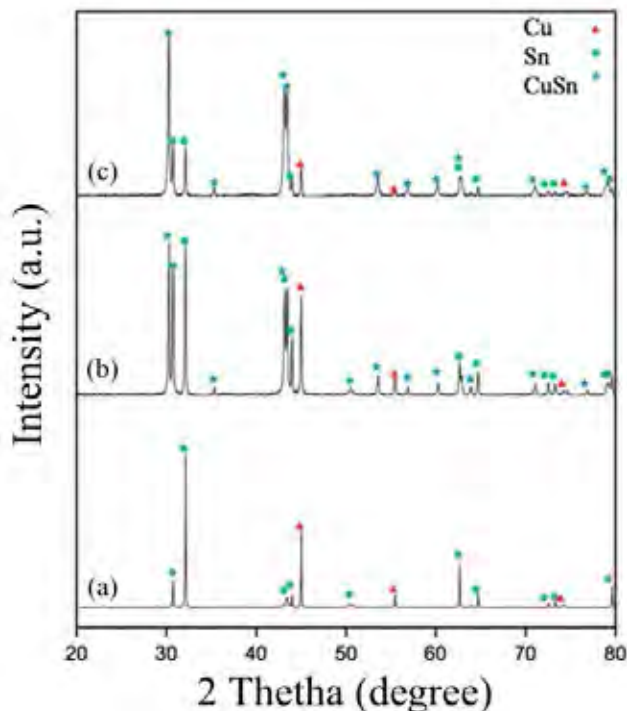


**Figure 4.1** XRD patterns of  $\text{Cu}_{70}\text{Sn}_{30}$  at different milling times of (a) 5, (b) 20, and (c) 30 h.

#### 4.4.1.1 Determination of suitable MA time

The mixed  $\text{Cu}_{30}\text{Sn}_{70}$  powder was chosen to determine the MA time. As can be seen in Figure 4.2, at 5 and 20 h, the Cu peak (JCPDS Card No. 04-0836) and  $\beta$ -Sn peak (JCPDS Card No. 04-0673) were predominant and sharp due to the big crystallite size. At 30 h, the monoclinic  $\eta$ - $\text{Cu}_6\text{Sn}_5$  peak (JCPDS Card No. 47-1488) was overwhelmingly formed and showed broad XRD peaks, attributing to small particles with the average crystallite size of 55.3 nm, analyzed by MDI JADE 9 (Howard *et al.* (1989); Callister *et al.* (2003); Cullity *et al.* (2001)). Therefore, the optimal MA time to prepare  $\text{Cu}_a\text{Sn}_b$  intermetallics in  $\text{Cu}_{30}\text{Sn}_{70}$  and other  $\text{Cu}_x\text{Sn}_{(100-x)}$  materials in the attritor was at 30 h.

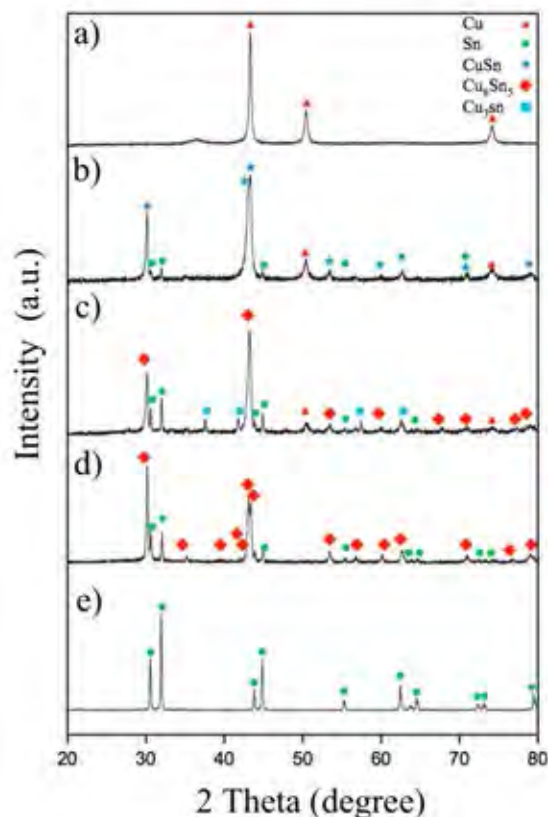


**Figure 4.2** XRD patterns of  $\text{Cu}_x\text{Sn}_{1-x}$  nanoparticles milled for 30 h; (a)  $\text{Cu}_{100}$ , (b)  $\text{Cu}_{70}\text{Sn}_{30}$ , (c)  $\text{Cu}_{50}\text{Sn}_{50}$ , (d)  $\text{Cu}_{30}\text{Sn}_{70}$ , and (e)  $\text{Sn}_{100}$ .

#### 4.4.1.2 Characterization of $\text{Cu}_x\text{Sn}_{1-x}$

Bright field TEM images shown in Figure 4.3 indicated that the MAed  $\text{Cu}_x\text{Sn}_{(100-x)}$  powder particles were agglomerated and overlapped to each other, as can be seen in thick and dark area. The powder particle agglomeration is due to the larger surface energy of metal nanoparticles that needs to be reduced by surface area reduction (Kao *et al.* (2004); Benjamin *et al.* (1974)). The selected area electron diffraction (SAED) patterns of the MAed metal powders (the insets of Figure 4.3(a) for  $\text{Cu}_{100}$  and Figure 4.3(f) for  $\text{Sn}_{100}$ ) show diffraction spots. Whereas the SAED patterns of  $\text{Cu}_a\text{Sn}_b$  intermetallics (the insets of Figure 4.3(b) for  $\text{Cu}_{70}\text{Sn}_{30}$ , Figure 4.3(c) for  $\text{Cu}_{50}\text{Sn}_{50}$ , and Figure 4.3(e) for  $\text{Cu}_{30}\text{Sn}_{70}$ ) showed diffraction rings. The ring diffraction patterns are due to the presence of polynanocrystalline in the microstructure of a material (Du *et al.* (2004)). Evidently, the  $\text{Cu}_a\text{Sn}_b$  intermetallics with nanosize were formed during the MA technique. This result also confirms the

XRD results in Table 4.1.

**Table 4.1** Effect of the composition of  $\text{Cu}_x\text{Sn}_{1-x}$  on the phenol hydroxylation

Catalyst	Composition <sup>a</sup>		Particle Size <sup>b</sup>		Conversion (%)	Selectivity (%)			Tar content <sup>c</sup> (%)
	Cu	Sn	Size	Residual		CA	HQ	BQ	
	(%wt)	(%wt)	(nm)	error (%)	T				
No catalyst	-	-	-	-	2.3	43.4	-	56.6	0
$\text{Cu}_{100}$	99.6	-	30	6.5	94.3	99.6	-	0.4	6.2
$\text{Cu}_{70}\text{Sn}_{30}$	68.4	31.4	29	5.9	85.3	82	17.3	0.8	4.4
$\text{Cu}_{50}\text{Sn}_{50}$	49.5	50.0	46.3	8.2	98.4	74.2	25.2	0.6	2.5
$\text{Cu}_{30}\text{Sn}_{70}$	30.94	68.3	55.3	9.8	87.4	68.6	29.7	1.8	0.9
$\text{Sn}_{100}$	-	99.5	70.1	9.1	17.2	100	-	-	0

Reaction conditions : phenol: $\text{H}_2\text{O}_2$  = 1:3, catalyst = 50 mg, T= 323 K, reaction time = 1 h.

<sup>a</sup>Data were obtained from XRF.

<sup>b</sup>Data were obtained from XRD by using MDI JADE 9 software with residual error is less than 10 %.

<sup>c</sup> Tar content (%) = (tar (g) / phenol (g)) $\times$ 100

To verify the  $\text{Cu}_x\text{Sn}_{100-x}$  intermetallics, the d-spacing values were calculated from the SADE patterns and matched with the d-spacing values given in the JCPDS references in order to index the Miller indices of the corresponding intermetallics (Yu *et al.* (2013)). The calculated d-spacing values from the SAED pattern of the MAed  $\text{Cu}_{70}\text{Sn}_{30}$  powder were 1.761 and 1.532 Å, which were corresponding to the d-spacing values of the (201) and (103) planes of the hexagonal Sorosite, respectively. The calculated d-spacing value of 2.06 Å, from the

SAED pattern of the MAed Cu<sub>50</sub>Sn<sub>50</sub> powder, was corresponding to the d-spacing value of the (422) planes of the monoclinic  $\eta$ -Cu<sub>6</sub>Sn<sub>5</sub> intermetallic. Also in the MAed Cu<sub>50</sub>Sn<sub>50</sub> powder, the d-spacing value of 2.08 Å, measured from the HRTEM image (Figure 4.3(d)), was in agreement with that of the (2120) planes of the orthorhombic  $\epsilon$ -Cu<sub>3</sub>Sn intermetallic. In both the MAed Cu<sub>50</sub>Sn<sub>50</sub> and Cu<sub>30</sub>Sn<sub>70</sub> powder, the calculated d-spacing value of 1.71 Å was found to match well with the d-spacing value of the (241) planes of the monoclinic  $\eta$ -Cu<sub>6</sub>Sn<sub>5</sub> intermetallic. In addition, the calculated d-spacing values from the SAED pattern of the MAed Cu<sub>30</sub>Sn<sub>70</sub> powder were 2.46 and 1.75 Å corresponding to that of the (222) and (315) planes of the monoclinic  $\eta$ -Cu<sub>6</sub>Sn<sub>5</sub> (JCPDS card No. 072-8761), respectively. As a result, it could be stated that the CuSn intermetallic with crystal structure corresponding to hexagonal Sorosite existed the MAed Cu<sub>30</sub>Sn<sub>70</sub> powder. The mixed  $\eta$ -Cu<sub>6</sub>Sn<sub>5</sub> and  $\epsilon$ -Cu<sub>3</sub>Sn intermetallics were formed in the MAed Cu<sub>50</sub>Sn<sub>50</sub> powder. In the MAed Cu<sub>70</sub>Sn<sub>30</sub> powder, the main intermetallic was  $\eta$ -Cu<sub>6</sub>Sn<sub>5</sub>.



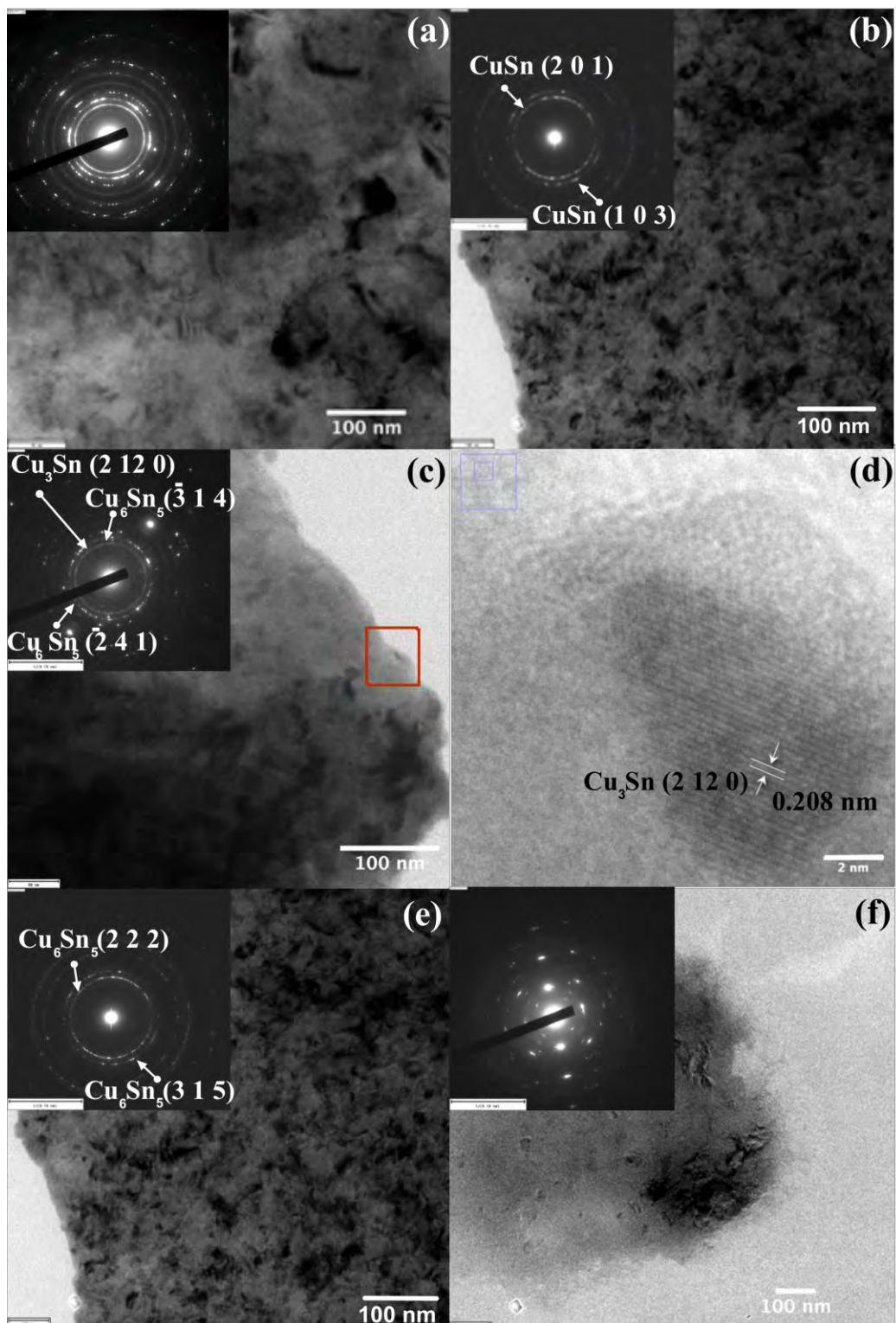


**Figure 4.3** HRTEM images of catalysts at 30 h milling; (a)  $\text{Cu}_{100}$ , (b)  $\text{Cu}_{70}\text{Sn}_{30}$ , (c)  $\text{Cu}_{50}\text{Sn}_{50}$ , (d) magnification 2 nm scale in red rectangular of  $\text{Cu}_{50}\text{Sn}_{50}$  (e)  $\text{Cu}_{30}\text{Sn}_{70}$ , and (f)  $\text{Sn}_{100}$ .

#### 4.4.2 Activity study of MAed Cu, Sn, and Cu<sub>x</sub>Sn<sub>100-x</sub> catalysts

##### 4.4.2.1 *Effects of reaction temperature and reaction time*

Generally, phenol hydroxylation takes place using an H<sub>2</sub>O<sub>2</sub> oxidizing agent to convert phenol to CAT, HQ, and BQ. To achieve a higher conversion of phenol, a higher amount of hydroxyl radical generated from the H<sub>2</sub>O<sub>2</sub> dissociation is required. However, temperature and time are also important parameters that need to be considered. As discussed previously in the MA time study, the mixed Cu<sub>30</sub>Sn<sub>70</sub> powder could form metal and intermetallic mixture. Thus, the activity study commenced by using the MAed Cu<sub>30</sub>Sn<sub>70</sub> catalyst with 1:3 phenol:H<sub>2</sub>O<sub>2</sub> ratio to optimize the reaction time and temperature for the phenol hydroxylation, as shown in the results in Figure 4.4. The study was conducted at the temperature range of 303 K (ambient temperature) to 363 K. At ambient temperature in the absence of the catalyst, the conversion was only 4.6 % after 300 min reaction time (not shown) and the product obtained was mainly BQ due to the conversion of intermediate HQ to BQ after such a long reaction time, as studied by Saito *et al.* [31]. After adding Cu<sub>30</sub>Sn<sub>70</sub>, the conversion was improved to 37 % at the same reaction time and temperature. The products were a mixture of CAT, HQ, and BQ with 87, 8, and 5 % selectivity, respectively. This result indicates that the MAed Cu<sub>30</sub>Sn<sub>70</sub> catalyst helps dissociate H<sub>2</sub>O<sub>2</sub> from hydroxyl radical. When raising the temperature from ambient to 323 K, the conversion increased from 37 to 48% and became steady after 60 min, giving a 51% CAT selectivity. With an increase in the reaction temperature to 343 K, the conversion also increased to 71% at 60 min reaction time with 73% CAT selectivity before starting to decline to about 60 %. This change can probably be attributed to the tar formation, occurring from the over-oxidation of BQ, over the active surface of the catalyst [18]. At such high temperatures as 363 K, the conversion decreased to 59 % and remained nearly constant after 60 min reaction time with 59% CAT selectivity. This result could be again attributable to the over-oxidation of BQ to tar on the catalyst surface. In conclusion, the optimal condition was at 343 K for 60 min, resulting in the highest conversion and selectivity.

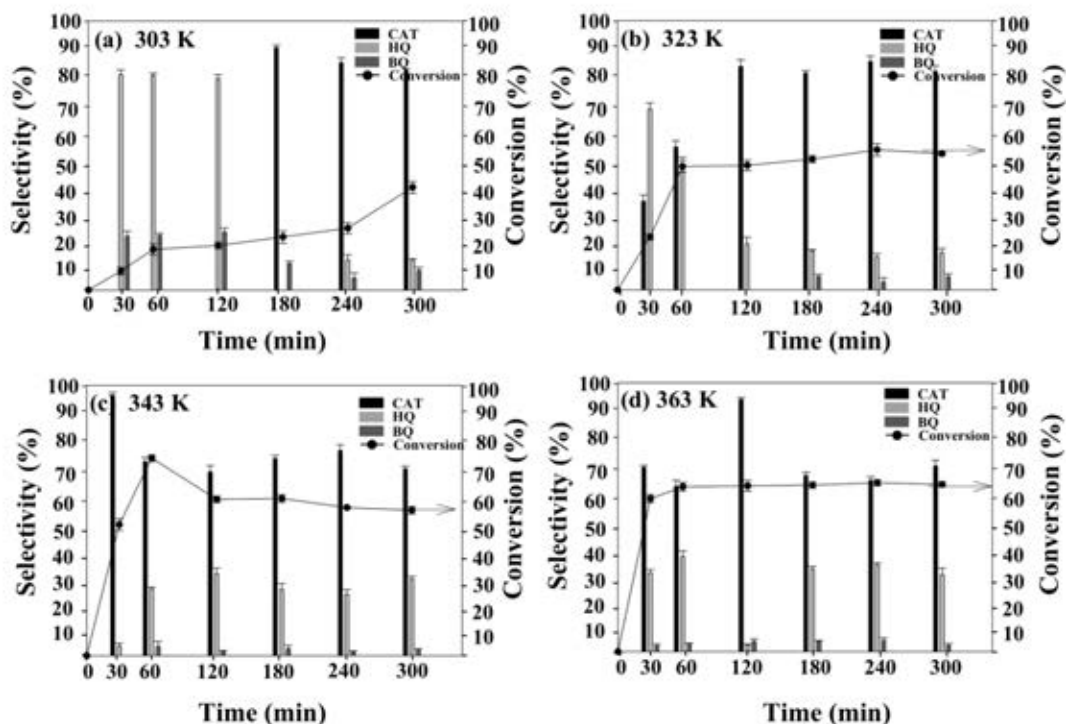


**Figure 4.4** The phenol conversion and the product selectivity of  $\text{Cu}_{30}\text{Sn}_{70}$  (30 mg) using 1:3 Phenol: $\text{H}_2\text{O}_2$  at (a) 303, (b) 323, (c) 343, and (d) 363 K for 300 min reaction time.

#### 4.4.2.2 Effect of catalyst content

The investigation of catalyst content was observed by varying the content from 10 to 60 mg, and the results are shown in Figure 4.5. The highest conversion found was 80 %, with 83% CAT selectivity when using 50 mg of catalyst. It is worth noting that at 10 mg of the catalyst, BQ was the only product obtained while at 20 or 60 mg of the catalyst, no BQ was observed. The % conversion kept increasing with the catalyst content due to the higher amount of hydroxyl radicals generated (Maurya *et al.* (2003); Mal *et al.* (1996); Niphadkar *et al.* (2009)). However, when too much hydroxyl radicals were generated, as seen in the case of 60 mg of the catalyst content, the % conversion dropped to 59 %. The reason was that BQ was over-oxidized to tar over the active surface of catalyst (Kurian *et al.* (2012)). As a result, the optimal catalyst content, which gave the highest conversion of 80% with 83, 14, and 3% CAT, HQ, and BQ selectivities, respectively, was 50 mg.

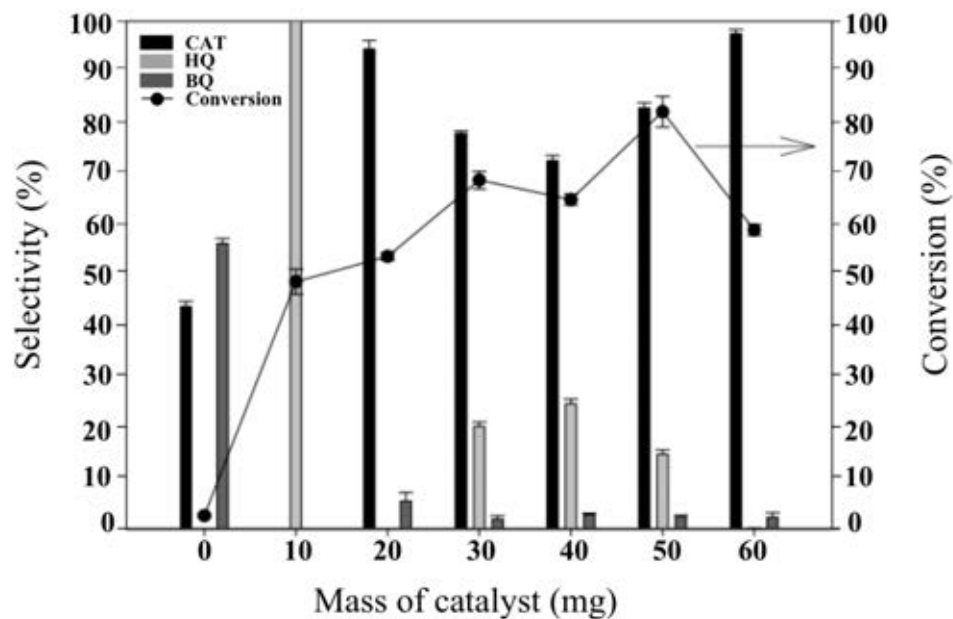


**Figure 4.5** The phenol conversion and the product selectivity of different  $\text{Cu}_{30}\text{Sn}_{70}$  contents using 1:3 phenol: $\text{H}_2\text{O}_2$  at 343 K for 1 h reaction time.

#### 4.4.2.3 Effect of phenol: $\text{H}_2\text{O}_2$ molar ratio

The important reactive species to convert phenol to their derivatives was hydroxy radical generated from  $\text{H}_2\text{O}_2$ . Thus, it is interesting to study the amount of  $\text{H}_2\text{O}_2$  by varying the phenol: $\text{H}_2\text{O}_2$  molar ratio, and the results are shown in Figure 4.6. A twofold increase in the phenol amount (by increasing the phenol: $\text{H}_2\text{O}_2$  molar ratio from 1:1 to 2:1), did not impressively increase the conversion (from 39 to 47%). This result is due to not only the limited amount of the hydroxy radicals generated from  $\text{H}_2\text{O}_2$ , but also the occurrence of two competed reactions, via oxidation of phenol and hydroxy radical scavenging (Fathima *et al.*(2008); Inchaurredo *et al.* (2012)). This result was in fact in agreement with those reported elsewhere (Huang *et al.* (2015); Yusuf *et al.* (2007)). In addition, the selectivity of HQ also increased from 28 to 37% while that of CAT dropped from 71 to 62%. This drop results from the limited amount of the hydroxy radicals that would prefer to react with phenol at the more favorable position, which is the para position, rather than the more steric hindrance position, which is the ortho position (Perego *et al.* (2007); Esposito *et al.* (1985)). On the other hand, an increase in the  $\text{H}_2\text{O}_2$  amount (phenol: $\text{H}_2\text{O}_2$  molar ratio from 1:1 to 1:2) caused the conversion to drastically

increase from 39 to 64% with a higher selectivity of CAT (71%) over HQ (28%). Obviously, the phenol conversion likely depended on the concentration of the hydroxy radicals generated from H<sub>2</sub>O<sub>2</sub> in the system (Hamshary *et al.* (2011)), giving more satisfactory results in both conversion and selectivity. When the phenol:H<sub>2</sub>O<sub>2</sub> molar ratio was further increased to 1:3, the conversion continued to increase from 64 to 73%, with an increase in the CAT selectivity from 70 to 78%, meaning that the higher concentration of the hydroxy radicals resulted in the higher conversion of the phenol. CAT is the most thermodynamically stable due to the intramolecular hydrogen bonding at the ortho position (Winstanley *et al.* (2007)). Meanwhile, the selectivity of HQ dropped from 29 to 18% and BQ started to form (3%), indicating further oxidation of HQ to BQ and BQ to tar since BQ is less thermodynamically stable (Fu *et al.* (2000)). Thus, to avoid tar formation, the phenol:H<sub>2</sub>O<sub>2</sub> molar ratio of 1:3 was chosen as the optimal condition for further study.

#### 4.4.2.4 Effect of MAed Cu, Sn, and Cu<sub>x</sub>Sn<sub>100-x</sub> catalysts

As can be seen from Table 4.1, the contents of MAed Cu and Sn in Cu<sub>x</sub>Sn<sub>100-x</sub> catalysts were studied. It was found that, without H<sub>2</sub>O<sub>2</sub>, the reaction containing only catalysts hardly took place due to the absence of the hydroxyl radicals to react with phenol. Similarly, without a catalyst, the reaction containing only H<sub>2</sub>O<sub>2</sub> resulted in a very small conversion (2.6 %) due to no active sites to cleavage H<sub>2</sub>O<sub>2</sub> to the hydroxyl radicals. The reaction containing both Cu<sub>100</sub> nanoparticles and H<sub>2</sub>O<sub>2</sub> gave an impressive conversion (up to 94.3%), implying that H<sub>2</sub>O<sub>2</sub> was well absorbed on the surface of the MAed Cu<sub>100</sub> metal in acid condition to form hydroxyl radicals (Stewart *et al.* (2007)), which rapidly reacted with phenol to form CAT (99.6%) and BQ (0.4%). The conversion obtained from the MAed Sn<sub>100</sub> was much less than the MAed Cu<sub>100</sub> (17.3 %), but only CAT was obtained and no tar was observed.

For the MAed Cu<sub>x</sub>Sn<sub>100-x</sub> catalysts, the tar content increased with the Cu content due to over oxidation of BQ to tar, as shown in Table 4.1. The results show that the MAed Cu<sub>70</sub>Sn<sub>30</sub> and the MAed Cu<sub>30</sub>Sn<sub>70</sub> catalysts gave slightly different conversion (85 and 87%, respectively) while the MAed Cu<sub>50</sub>Sn<sub>50</sub> catalyst gave a higher conversion (98%). As a consequence, with the increase of the Sn

content in the MAed  $\text{Cu}_x\text{Sn}_{(100-x)}$  catalysts from 30, 50, to 70 wt%, the tar content gradually decreased from 6.2 to 1 with a noticeable increase in HQ. These results suggest that the higher Sn content provided a greater reduction of BQ to HQ.

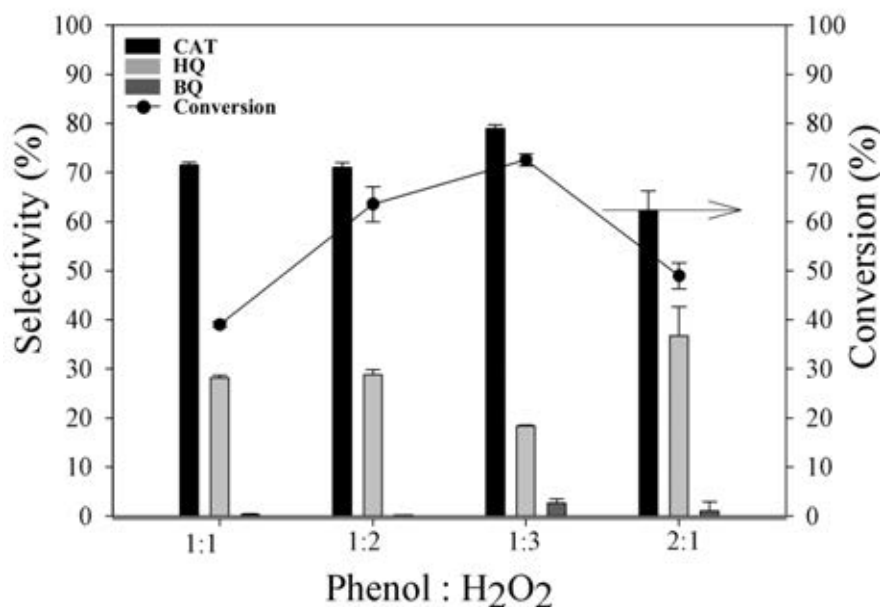


**Figure 4.6** The phenol conversion and the product selectivity of  $\text{Cu}_{30}\text{Sn}_{70}$  (monoclinic  $\eta$ - $\text{Cu}_6\text{Sn}_5$  phase, 50 mg) using various phenol: $\text{H}_2\text{O}_2$  molar ratios at 343 K for 1 h reaction time.

#### 4.4.2.5 Thermal stability of catalysts

The catalysts were tested for stability by conducting the experiment for 6, 12, 18, and 24 h, as shown in Figure 4.7. The XRD patterns in Figure 4.7 (a) reveal that a longer contacting time resulted in the slightly sharper XRD peaks, suggesting that the crystallite size of the catalyst grows slowly. In general, the components and their crystal structures in the catalyst did not change for the times of up to 24 h. This indicates that under these experimental conditions, the thermal stability of the catalyst is excellent. Since the catalyst performance does not only rely on its thermal stability but also on its surface condition, the coke formation on the catalysts surface is of interest. Figure 4.7 (b) shows the Raman spectrum fingerprints of graphite at G-band of  $\sim 1580\text{ cm}^{-1}$  and D-band of  $\sim 2685\text{ cm}^{-1}$  for the samples conducted for 6 to 24 h. Due to the experimental data (Figure 4.7 (b)) and the information given in (Hodkiewicz *et al.* (2008)), it can be concluded that the coke is indeed formed after 6 h.

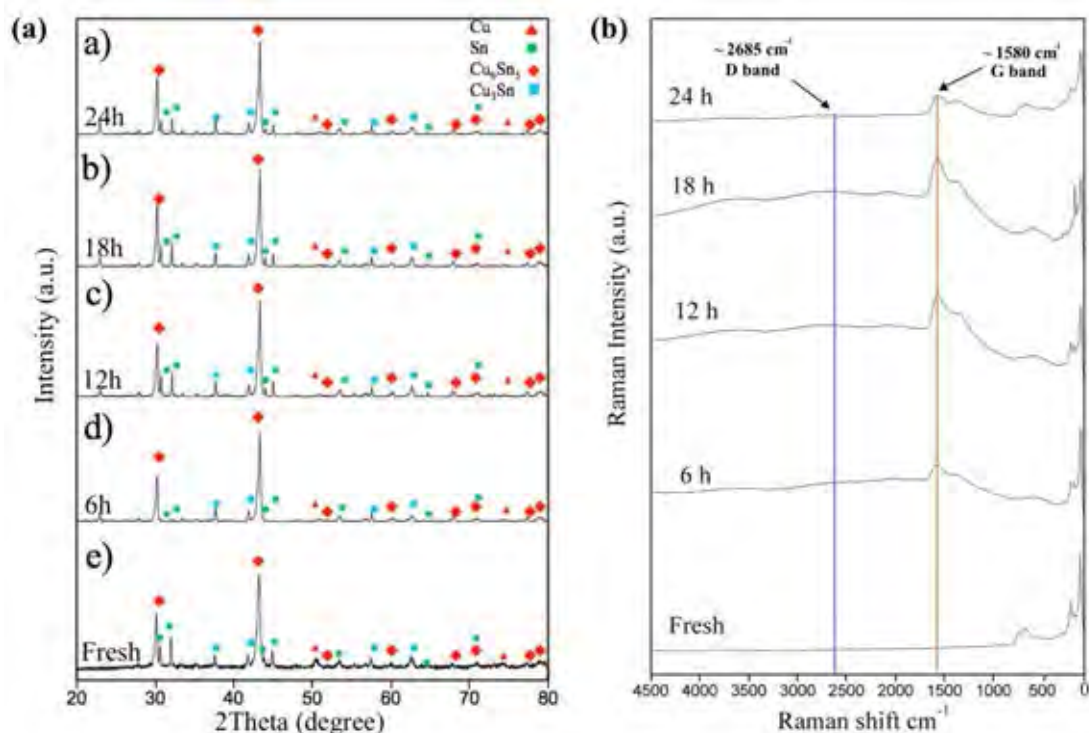


**Figure 4.7** (a) XRD patterns, (b) Raman spectra of Cu<sub>50</sub>Sn<sub>50</sub> before and after reaction.

#### 4.4.2.6 Reusability of catalysts

The study was carried out to identify the catalyst efficiency after each run. Figure 4.8 (a), showing XRD patterns of the MAed Cu<sub>50</sub>Sn<sub>50</sub> catalyst before and after the test, indicates that the catalyst after use gave sharper peaks due to the bigger crystallite size caused by the coke formation on the catalyst surface, meaning that the coke formation on the catalyst surface was already found from the 1<sup>st</sup> cycle. As confirmed by Raman spectroscopy in Figure 4.8 (b), the fingerprints of graphite were observed at G-band of ~1580 cm<sup>-1</sup> and D-band of ~2685 cm<sup>-1</sup> (Hodkiewicz *et al.* (2008)). After the second cycle, the conversion dropped to 75 % with selectivity of CAT, HQ, and BQ of 72.5, 26.6, and 0.9 %, respectively. It is evidently that the coke formation on the catalyst surface is detrimental to its performance.

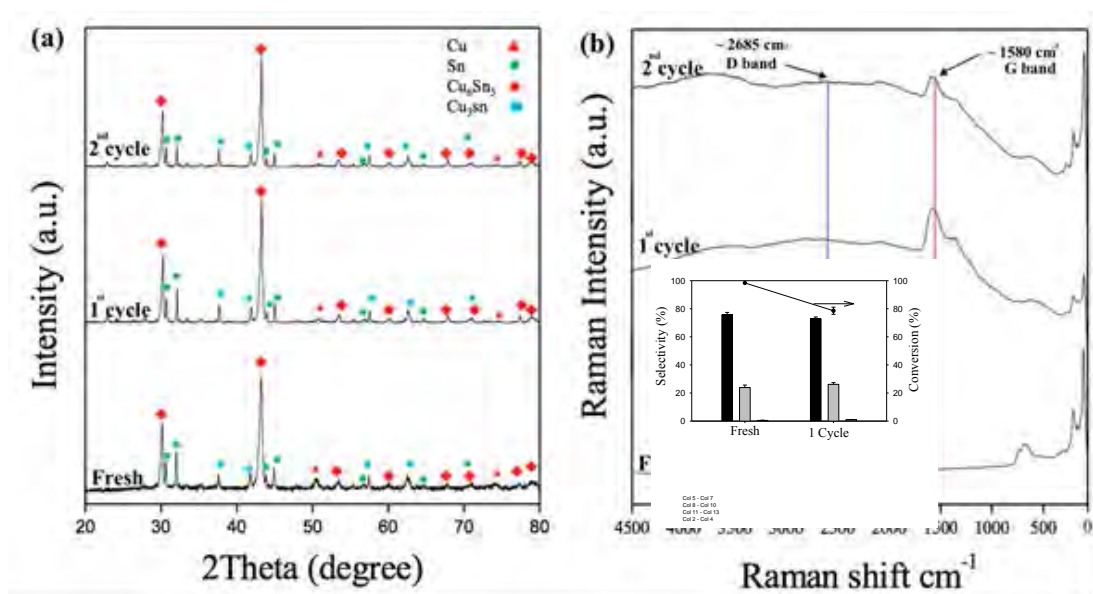


**Figure 4.8** (a) XRD patterns, (b) Raman spectra of Cu<sub>50</sub>Sn<sub>50</sub> after 1<sup>st</sup> and 2<sup>nd</sup> cycles.

#### 4.5 Conclusion

The MAed Cu<sub>x</sub>Sn<sub>(100-x)</sub> catalysts ( $x = 30, 50, 70$  wt.%) were successfully prepared via mechanical alloying technique for phenol hydroxylation. The synthesized catalysts were MAed Cu<sub>70</sub>Sn<sub>30</sub>, MAed Cu<sub>50</sub>Sn<sub>50</sub> and MAed Cu<sub>30</sub>Sn<sub>70</sub> powders. The activity study revealed that the MAed Cu<sub>50</sub>Sn<sub>50</sub> catalyst consisting of both  $\eta$ -Cu<sub>6</sub>Sn<sub>5</sub> (monoclinic) and  $\epsilon$ -Cu<sub>3</sub>Sn (orthorhombic) phases gave the highest conversion (98%) with 71% CAT selectivity. The increase in the Sn content decreased the amount of BQ, increased the amount of HQ, and decreased the tar content. The components and their crystal structures in the MAed Cu<sub>50</sub>Sn<sub>50</sub> catalyst structure still maintained after 24 h reaction time.

#### 4.6 Acknowledgements

The authors gratefully acknowledge the mutual supports or the partial scholarship from Thailand Graduate Institute of Science and Technology (TIGIST-TG-33-09-58-058D), The Petroleum and Petrochemical College, Chulalongkorn University, and Powder Metallurgy Research and Development Unit (PM\_RDU) of the National Metal and Materials Technology Center (MTEC). The authors also would like to thank Mr. John M. Jackson for proof-reading the paper.



#### 4.7 References

- G. Busca, S. Berardinelli, C. Resini, L. Arrighi, J. Technologies for the removal of phenol from fluid streams: a short review of recent developments, Hazard Material, 160 (2008) 265-288.
- R.R. Zapico, P. Marín, F.V. Díez, S. Ordóñez, Influence of operation conditions on the copper-catalysed homogeneous wet oxidation of phenol: development of a kinetic model, Chemical Engineering Journal, 270 (2015) 122-132.
- H.S. Abbo, S.J.J. Titinchi, C. Shri, R. Prasad, Investigation of [Ni {Me4Bzo2 [14] aneN4}] Cl2 catalyzed selective hydroxylation of phenol to catechol by H2O2 in the homogeneous medium, Journal Molecular Catalysis A: Chemical, 218 (2004) 125-132.
- M. Xia, M. Long, Y. Yang, C. Chen, W. Cai, B. Zhou A highly active bimetallic oxides catalyst supported on Al-containing MCM-41 for Fenton oxidation of phenol solution, Applied Catalysis, B: Environment, 110 (2011) 118-125.
- A. Kumar, D. Srinivas, Hydroxylation of phenol with hydrogen peroxide catalyzed by Ti-SBA-12 and Ti-SBA-16, Journal Molecular Catalyst A: Chemical, 368-369 (2013) 112-118.
- C.G. Silva, M.J. Sampaio, S.A.C. Carabineiro, J.W.L. Oliveira, D.L. Baptista, R. Bacsá, B.F. Machado, P. Serp, J.L. Figueiredo, A.M.T. Silva, J.L. Faria, Developing highly active photocatalysts: gold-loaded ZnO for solar phenol oxidation, Journal Catalysis, 316 (2014) 182-190.

- A.B. Ahmed, B. Jibril, S. Danwittayahul, J. Dutta, Microwave-enhanced degradation of phenol over Ni-loaded ZnO nanorods catalyst, Applied Catalysis B. Environment., 156-157 (2014) 456-465.
- H. Maneesuwan, S. Tantisriyanurak, T. Chaisuwan, S. Wongkasemjit, On the synergistic catalytic properties of bimetallic mesoporous materials containing aluminum and zirconium: the prins cyclisation of citronellal, Applied Catalysis., A: General., 2016.
- I.U. Castro, F. Stüber, A. Fabregat, J. Font, A. Fortuny, C. Bengoa, Supported Cu (II) polymer catalysts for aqueous phenol oxidation, Journal of Hazardous. Materials, 163 (2009) 809-815.
- N.S. Inchaurreondo, P. Massa, R. Fenoglio, J. Font, P. Haure, Efficient catalytic wet peroxide oxidation of phenol at moderate temperature using a high-load supported copper catalyst, Chemical Engineering Journal, 198–199 (2012) 426-434.
- N.K. Mal, A.V. Ramaswamy, Hydroxylation of phenol over Sn-silicalite-1 molecular sieve: solvent effects, Journal Molecular Cataysis A: Chemical., 105 (1996) 149-158.
- P.S. Niphadkar, M.S. Kotwal, S.S. Deshpande, V.V. Bokade, P.N. Joshi, Tin-silicalite-1: Synthesis by dry gel conversion, characterization and catalytic performance in phenol hydroxylation reaction, Material Chemistry Physics., 114 (2009) 344-349.
- M. Sankar, N. Dimitratos, P.J. Miedziak, P.P. Wells, C.J. Kiely, G.J. Hutchings, Designing bimetallic catalysts for a green and sustainable future, Chemical Society Review, 41 (2012) 8099-8139.

- E. Saboor Bagherzadeh, M. Dopita, T. Mütze, U.A. Peuker, Morphological and structural studies on Al reinforced by Al<sub>2</sub>O<sub>3</sub> via mechanical alloying, Advance Powder Technology., 26 (2015) 487-493.
- S. Zamani, H.R. Bakhsheshi-Rad, A. Shokuhfar, M.R. Vaezi, M.R.A. Kadir, M.R.M. Shafiee, Synthesis and characterization of MoSi<sub>2</sub>-Mo<sub>5</sub>Si<sub>3</sub> nanocomposite by mechanical alloying and heat treatment, International Journal Refract Met Hard Material, 31 (2012) 236-241.
- H. Mostaan, F. Karimzadeh, M.H. Abbasi, Thermochim. Synthesis and formation mechanism of nanostructured NbAl<sub>3</sub> intermetallic during mechanical alloying and a kinetic study on its formation, Acta, 529 (2012) 36-44.
- M. Morakotjinda, K. Fakpan, T. Yotkaew, N. Tosangthum, R. Krataitong, A. Daraphan, P. Siriphol, P.Wila, B. Vetayanugul, R. Tongstri, Gas atomization of low melting-point metal powders, Chiang Mai Journal Science 37 (2010) 55-63
- Kurian M., Eldhose A., Thasleenabi R.M., Mild temperature oxidation of phenol over rare earth exchanged aluminum pillared montmorillonites, International Environment Reserve., 6 (2012) 669-375.
- M.R. Maurya, S.J.J. Titinchi, S. Chand, Oxidation of phenol with H<sub>2</sub>O<sub>2</sub> catalysed by Cu (II), Ni (II) and Zn (II) complexes of N, N' -bis-(salicylidene) diethylenetriamine (H<sub>2</sub>saldien) encapsulated in Y-zeolite, Journal Molecular Catalysis A: Chemical, 201 (2003) 119-130.
- N.N. Fathima, R. Aravindhan, J.R. Rao, B.U. Nair, Dye house wastewater treatment through advanced oxidation process using Cu-exchanged Y zeolite: A heterogeneous catalytic approach, Chemosphere, 70 (2008) 1146-1151.

- E. Buarod, S. Pithakratanayothin, S. Naknaka, P. Chaiyasith, T. Yotkaew, N. Tosangthum, R. Tongstri, Facile synthesis and characterization of tenorite nanoparticles from gas-atomized Cu powder, Powder Technology, 269 (2015) 118-126.
- SA Howard, K. Preston, Profile Fitting of Powder Diffraction Patterns, Mineralogical Society of America, Washington DC, 1989.
- W.D. Callister, "Materials Science and Engineering: An Introduction", Wiley & Sons 2003.
- B.D. Cullity, "Elements of X-ray Diffraction:", 2<sup>nd</sup> ed., Addison-Wesley Publishing Company Inc. 2001.
- L. Takacs, J.S. McHenry, Temperature of the milling balls in shaker and planetary mills, Journal Material Science 41 (2006) 5246-5249.
- S.-T. Kao, J.-G. Duh, Effect of Cu concentration on morphology of Sn-Ag-Cu solders by mechanical alloying, Journal Electron Material, 33 (2004) 1445-1451.
- J.S. Benjamin, T.E. Volin, MT, Artificial neural network modeling of mechanical alloying process for synthesizing of metal matrix nanocomposite powders, Materials Science and Technology, 5 (1974) 1929-1934.
- G.H. Du, G. Van Tendeloo, Cu (OH) 2 nanowires, CuO nanowires and CuO nanobelts, Chemical Physics Letter, 393 (2004) 64-69.
- F. Yu, W. Zhou, Progress in Natural Science: Alloying and dealloying of CuPt bimetallic nanocrystals, Material International, 23 (2013) 331-337.
- R. Tongstri, T. Yotkaew, R. Krataitong, P. Wila, A. Sir-on, P. Muthitamongkol, N. Tosangthum, Characterization of Cu<sub>6</sub>Sn<sub>5</sub> intermetallic powders produced

- by water atomization and powder heat treatment, Material Characterization 86 (2013) 167-176.
- K.I. Toranosuke Saito, Hiroki Tsunomachi, Katsuya Sakaguchi, PROCESS FOR THE PREPARATION OF P-BENZOQUINONE, United States Patent, Sanko Kaihatsu, Kagaku Kenkyusho, USA, 1990.
- N. Inchaurreondo, J. Cechini, J. Font, P. Haure, Strategies for enhanced CWPO of phenol solutions, Applied Catalysis, B, 111–112 (2012) 641-648.
- K. Huang, Y. Xu, L. Wang, D. Wu, Heterogeneous catalytic wet peroxide oxidation of simulated phenol wastewater by copper metal–organic frameworks, RSC Advances, 5 (2015) 32795-32803.
- Y. Yusuf, K. A. Savas, O. Ulker Bakir, Chemical Engineering Technology, 30 (2007) 548-552.
- C. Perego, A. Carati, P. Ingallina, M.A. Mantegazza, G. Bellussi, Production of titanium containing molecular sieves and their application in catalysis, Applied Catalysis, A, 221 (2001) 63-72.
- (a) Esposito, A.; Neri, C; Taramasso, M. Hydroxylation of Phenol. 1985; (b) Esposito, A.; Neri, C.; Buonomo, F. Hydroxylation of Aromatic Hydrocarbon. 1983-3309669, 19830317, 1983.
- H. El-Hamshary, M.H. El-Newehy, S.S. Oxidation of phenol by hydrogen peroxide catalyzed by metal-containing poly (amidoxime) grafted starch Al-Deyab, Molecules, 16 (2011) 9900-9911.
- K.J. Winstanley, D.K. Smith, Ortho-substituted catechol derivatives: the effect of intramolecular hydrogen-bonding pathways on chloride anion recognition, Journal Organic Chemistry, 72 (2007) 2803-2815.

Z. Fu, J. Chen, D. Yin, D. Yin, L. Zhang, Y. Zhang, Highly effective Cu-HMS catalyst for hydroxylation of phenol, Catalysis Letter, 66 (2000) 105-108.

K.L. Stewart, A.A. Gewirth, Highly effective Cu-HMS catalyst for hydroxylation of phenol, Langmuir, 23 (2007) 9911-9918.

J. Hodkiewicz, Characterizing Graphene with Raman Spectroscopy, Thermo Fisher Scientific, Madison, WI, USA.

**CHAPTER V**  
**INFLUENCES OF M-Sn INTERMETALLICS (M=Ni, Cu) PREPARED BY**  
**MECHANICAL ALLOYING ON PHENOL HYDROXYLATION**

### **5.1 Abstract**

This work discusses the effect of the crystal structure of Ni-Sn and Cu-Sn intermetallic catalysts on phenol hydroxylation. All catalysts were prepared via mechanical alloying (MA) technique which is a green process for catalyst preparation. The results showed that the prepared catalysts consisted of monoclinic (Ni<sub>3</sub>Sn<sub>4</sub> and Cu<sub>6</sub>Sn<sub>5</sub>) and hexagonal (Ni<sub>3</sub>Sn and Cu<sub>6</sub>Sn<sub>5</sub>(HT)) crystal structures. Catalytic activity of all synthesized catalysts on phenol hydroxylation demonstrated that both Ni<sub>3</sub>Sn<sub>4</sub> and Ni<sub>3</sub>Sn performed better catalytic activity than Cu<sub>6</sub>Sn<sub>5</sub> and Cu<sub>6</sub>Sn<sub>5</sub>(HT), and Ni<sub>3</sub>Sn, having a hexagonal crystal structure, showed the best catalytic activity (> 97% conversion) at 363 K, 3 h, 1:4 phenol:H<sub>2</sub>O<sub>2</sub>, 50 mg of the catalyst content, giving CAT (60.28% yield) and HQ (36.82% yield) with no over-oxidation of CAT and HQ as time elapsed.

**Keywords:** Mechanical alloying, η-Cu<sub>6</sub>Sn<sub>5</sub>; ε-Cu<sub>3</sub>Sn; CuSn; Phenol hydroxylation

### **5.2 Introduction**

For a decade phenol hydroxylation has been proposed as a means of producing more valuable dihydroxybenzene, e.g., catechol (CAT) and hydroquinone (HQ), which are used in the pharmaceutical industry (Briganti *et al.*, 2003). Many kinds of catalysts were studied to enhance higher catalytic activity and selectivity. Previous research revealed that the addition of tin (Sn) to mechanical alloyed (MAed) Cu<sub>50</sub>Sn<sub>50</sub> intermetallic catalyst, prepared and used for the phenol hydroxylation, retarded tar formation (Pithakratanayothin *et al.*, 2016). Unfortunately, in this case, the HQ was over-oxidized to benzoquinone (BQ). In addition, other researchers found that Ti, Fe, Mn, and Cu could not give any selectivity in either CAT or HQ, and sometimes observed the over-oxidation of HQ (He *et al.*, 2015; Liang *et al.*, 2013; Mohapatra *et*

*al.*,2003; Shi *et al.*, 2012). To cope with this problem, a change in the catalyst's crystal structure is a new strategy, since the crystal structure alteration can modify an active site by creating a new reaction space on the catalyst (i.e., edge and corner). By different reaction spaces, the incoming molecules showed different reactions and products when they reacted and adsorbed (Recchia *et al.*, 1999; Efremenko *et al.*, 2008; Donazzi *et al.*,2008; Shimizu *et al.*,2012; Bandarenka *et al.*, 2013). Changes in crystal structure can be accomplished by mechanical alloying (MA) technique since it is easy to handle and provides high productivity in either a lab or commercial scale. Moreover, MA technique also results in new phases of intermetallics and produces small grains of materials that exhibit different thermodynamic properties (Borchers *et al.*, 2015).

Nickel (Ni) was reported to be an interesting candidate since it showed a good catalytic decomposition of hydrogen peroxide (H<sub>2</sub>O<sub>2</sub>) for selective hydroxylation of benzene (Morimoto *et al.*, 2015), and Sn was revealed to enhance the H<sub>2</sub>O<sub>2</sub> efficiency and coke retardant in the phenol hydroxylation (Klaewkla *et al.*, 2007). In this study, both Ni and Sn were prepared to form a single phase of Ni<sub>x</sub>Sn<sub>y</sub> intermetallic catalyst via MA technique. This paper reports on the catalyst preparation and the catalytic activity of Ni<sub>x</sub>Sn<sub>y</sub> intermetallics for the phenol hydroxylation employing H<sub>2</sub>O<sub>2</sub> as the oxidant under mild conditions

## 5.3 Experimental

### 5.3.1 Materials

Nickel (Ni, 99.99%wt) and Copper (Cu, 99.99%wt) powders were purchased from Sigma-Aldrich, USA and tin (Sn, 99.99% wt) powders were produced by atomization technique as mentioned elsewhere (Morakotjinda *et al.*, 2010). Methanol (CH<sub>3</sub>OH, 99.99%) was purchased from Labscan, Thailand; catechol (CAT, 99%), hydroquinone (HQ, 99%), and 1,4-benzoquinone (BQ, 98%) from Sigma-Aldrich, USA; phenol detached crystals and hydrogen peroxide (H<sub>2</sub>O<sub>2</sub>, 30% w/v) from Fisher Scientific, UK. All chemicals were used without purification.

### 5.3.2 Characterization

X-ray diffraction (XRD) patterns using CuK $\alpha$  radiation and the



crystallite sizes were determined using MDI JADE 9 software, relating to the Scherrer formula, with a residual error of less than 10% (Maurya *et al.*,2003). X-ray fluorescence (XRF) spectrometer (PANalytical AXIOS PW 4400) was used to analyze elements in the samples. Materials characterization by transmission electron micrographs (TEM) and high resolution transmission electron micrographs (HRTEM) were conducted using JEOL JEM-2010. X-ray photoelectron spectra (XPS) was analyzed using an AXIS ULTRA<sup>DLD</sup> spectrometer to determine the oxidation state of metal. The system was equipped with a monochromatic Al X-ray source and a hemispherical analyzer. All peaks were calibrated from C 1s spectra located at 284.6 eV. Temperature programmed desorption (NH<sub>3</sub>-TPD) was also used to determine the acidity of the catalysts. Acid properties, such as acid strength and acidity were determined on Thermo Finnigan 1100. The samples were analyzed by a UFLC Shimadzu high-performance liquid chromatography (HPLC) equipped with a C-18 reverse-phase column (Inersil ODS-3) and a UV detector (SPD-M20A Shimadzu). All data were analyzed three times and the results averaged for both accuracy and precision.

### 5.3.3 Synthesis of Ni, Sn, and Ni<sub>x</sub>Sn<sub>y</sub> nanoparticles

Ni (32<um) and Sn(32<um) were used to prepare Ni, Sn, and Ni<sub>x</sub>Sn<sub>y</sub>nanoparticles. The Ni<sub>x</sub>Sn<sub>y</sub> alloys were prepared by varying Sn contents (43, 58, 73, and 100%wt) balanced with Ni powder. Elemental Ni and Sn powders and Ni<sub>x</sub>Sn<sub>(100-x)</sub> powder mixtures were milled in an attritor. The MA conditions were as follows: 5:1 ball-to-powder ratio, 300 rpm MA speed, and 30 h milling time. The mechanically alloyed (MAed) powders were heated to complete the reactions between of Ni and Sn and homogenize the phase formations. The synthesized catalysts were further characterized using various techniques.

### 5.3.4 Synthesis of monoclinic-Cu<sub>6</sub>Sn<sub>5</sub> and hexagonal-Cu<sub>6</sub>Sn<sub>5</sub> nanoparticles

Cu (32<um) and Sn (32<um) were used to prepare monoclinic and hexagonal-Cu<sub>6</sub>Sn<sub>5</sub> nanoparticles. The monoclinic-Cu<sub>6</sub>Sn<sub>5</sub> intermetallic was prepared by mixing 70 %wt Sn contents balanced with Cu powder before mechanically alloying in an attritor. The conditions used were as follows: 5:1 ball-to-powder ratio, 300 rpm

Ma speed, and 30 h milling time. The hexagonal-Cu<sub>6</sub>Sn<sub>5</sub>(HT) intermetallic prepared by heating monoclinic-Cu<sub>6</sub>Sn<sub>5</sub> intermetallics in a vacuum chamber for metal diffusion. The Maed powders were further characterized using various techniques.

### 5.3.5 Catalytic activity study

Phenol hydroxylation was carried out to study the activity of the synthesized catalysts by adding phenol (1.88 g, 20 mmol), H<sub>2</sub>O<sub>2</sub> (6.84 g, 60 mmol), and water (10 ml) into a 250 ml two-necked round-bottom flask fitted with a condenser. The catalytic activity results of the Ni<sub>x</sub>Sn<sub>y</sub> intermetallics were compared at 343 K using 50 mg of catalyst, 1:3 phenol:H<sub>2</sub>O<sub>2</sub> molar ratio, and 24 min reaction time. The condition was fixed for the phenol hydroxylation of Cu<sub>50</sub>Sn<sub>50</sub> intermetallic in order to observe the effect of the second metal on tin <sup>2</sup>

## 5.4 Results and Discussion

### 5.4.1 Characterization of catalyst

The phases in the prepared catalysts were identified by using XRD and TEM selected area electron diffraction (SAED). The crystallite sizes of the synthesized catalysts were examined from XRD peak half width. XRD patterns of Ni, Sn, and Ni<sub>x</sub>Sn<sub>y</sub> intermetallic catalysts containing various Sn amounts (43, 58, and 73 wt%) are shown in Figure. 5.1a-e belonging to Sn<sub>100</sub> (JCPDS Card No. 04-006-2820 of tetragonal β-Sn), Ni<sub>57</sub>Sn<sub>43</sub> (JCPDS Card No. 035-1362 of hexagonal Ni<sub>3</sub>Sn), Ni<sub>42</sub>Sn<sub>58</sub> (JCPDS Card No. 065-1315 of orthorhombic Ni<sub>3</sub>Sn<sub>2</sub>), Ni<sub>27</sub>Sn<sub>73</sub> (JCPDS Card No. 004-0845 of monoclinic Ni<sub>3</sub>Sn<sub>4</sub>), and Ni (JCPDS card No. 001-1258 of cubic Ni), respectively. Figure. 5.2a-b shows XRD patterns of Cu<sub>30</sub>Sn<sub>70</sub> (JCPDS Card No. 01-072-8761 of monoclinic η-Cu<sub>6</sub>Sn<sub>5</sub>) and Cu<sub>30</sub>Sn<sub>70</sub>(HT) (JCPDS Card No. 04-045-1488 of hexagonal η-Cu<sub>6</sub>Sn<sub>5</sub>). The Scherrer formula was used to calculate the crystallite size of the prepared catalysts, as listed in Table 5.1 (Perego *et al.*,2001).

$$d = \frac{0.9\lambda}{B\cos\theta} \quad (1)$$

**Table 5.1** Composition, particle size, and crystallite size of Ni<sub>x</sub>Sn<sub>y</sub>intermetallicson phenol hydroxylation.

Catalysts	Composition (%wt)						Crystallite size <sup>a</sup>	Particle size <sup>b</sup>	Conversion (%)	Selectivity (%)		
	Nominal		XRF		SEM-EDS		Size	Size	CAT	HQ	BQ	
	Ni or Cu	Sn	Ni or Cu	Sn	Ni or Cu	Sn	(nm)	(nm)				
Ni	100	-	99	-	99	-	-	-	38	8	91	0
Ni <sub>3</sub> Sn	60	40	57	43	60	39	7.78 ± 1.85	18.5	29	0	10	0
Ni <sub>3</sub> Sn <sub>2</sub>	40	60	42	58	42	57	10.62 ± 2.66	20.5	22	10	89	0
Ni <sub>3</sub> Sn <sub>4</sub>	30	70	27	73	29	70	13.48 ± 2.38	22.5	42	0	10	0
Cu <sub>6</sub> Sn <sub>5</sub>	30	70	32	70	32	67	18.78± 3.38	25	-	-	-	-
Cu <sub>6</sub> Sn <sub>5</sub> (HT)	30	70	30	70	31	69	33.57± 3.24	55	-	-	-	-

Reaction conditions: phenol:H<sub>2</sub>O<sub>2</sub> = 1:3, catalyst = 50 mg, T= 343 K, reaction time = 24 min.

<sup>a</sup>Data were obtained from XRD by using MDI JADE 9 software with residual error is less than 10 %.

<sup>b</sup>Data were obtained from bright filed TEM

All data were repeated 3 replicat

Where  $d$  is the average crystallite size,  $\lambda$  is the wavelength of the X-ray,  $\beta$  is the full width at half maximum intensity of Bragg diffraction peak at diffraction angle  $\theta$  (in

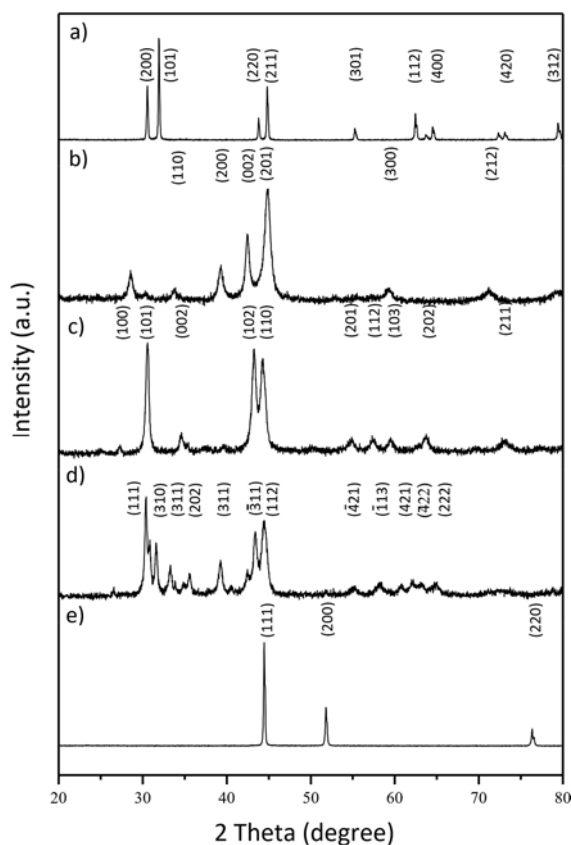


**Figure 5.1** XRD patterns of Maed intermetallic catalysts a) Sn b)  $\text{Ni}_{57}\text{Sn}_{43}$  c)  $\text{Ni}_{42}\text{Sn}_{58}$  d)  $\text{Ni}_{27}\text{Sn}_{73}$  e) Ni.

-radians). The MDI JADE software was used to calculate the crystallite size, as related to the Scherrer formula. With an increase in the Sn content, the crystallite size also increased. As can be seen from Table 5.1, Sn was found to have the biggest crystallite size. Because Sn has a melting point of 504 K, it may have melted and agglomerated into a larger particle size during the MA process which generates heat around 473 – 493 K (James *et al.*, 2012). The single phases of  $\text{Ni}_x\text{Sn}_y$  intermetallic catalysts were verified using TEM SAED patterns matching with the  $d$ -spacing values given in the JCPDS reference in order to index the miller indices of the corresponding intermetallic (Pino *et al.*, 2001). It was found that the calculated  $d$ -spacing values from the SAED pattern of the synthesized  $\text{Ni}_3\text{Sn}$  powder were 1.75 and 2.02 Å, corresponding to the  $d$ -spacing values of the {210} and {201} planes of the hexagonal phase (see Figure.

5.2a). The calculated  $d$ -spacing values of the synthesized  $\text{Ni}_3\text{Sn}_2$  powder were 2.07 and 2.90 Å, which corresponded to {102} and {101} planes of the orthorhombic phase, while those values of the synthesized  $\text{Ni}_3\text{Sn}_4$  powder were 2.06 and 2.95 Å, corresponding to {-511} and {111} planes of the monoclinic phase, as shown in Figure. 5.3 b-c. The calculated  $d$ -spacing values of the synthesized  $\eta\text{-Cu}_6\text{Sn}_5$  powder were 2.15 and 2.96 Å, which corresponded to {132} and {-113} planes of the monoclinic phase, while those values of the synthesized  $\eta\text{-Cu}_6\text{Sn}_5(\text{HT})$  powder were 2.10 and 2.94 Å, corresponding to {132} and {22-1} planes of the hexagonal phase, as shown in Figure. 5.3 d-e. Since there were no XRD peaks corresponding to Cu, Ni and Sn metals and TEM characterization indicated only  $d$ -spacings corresponding to those of  $\text{Ni}_x\text{Sn}_y$  and  $\text{Cu}_a\text{Sn}_b$  intermetallics, it may therefore be concluded that the synthesized  $\text{Ni}_x\text{Sn}_y$  and  $\text{Cu}_a\text{Sn}_b$  intermetallic catalysts are single phase. Interestingly, the crystallite and the particle sizes given in Table 5.1 exhibit the same increasing trends as the Sn content.

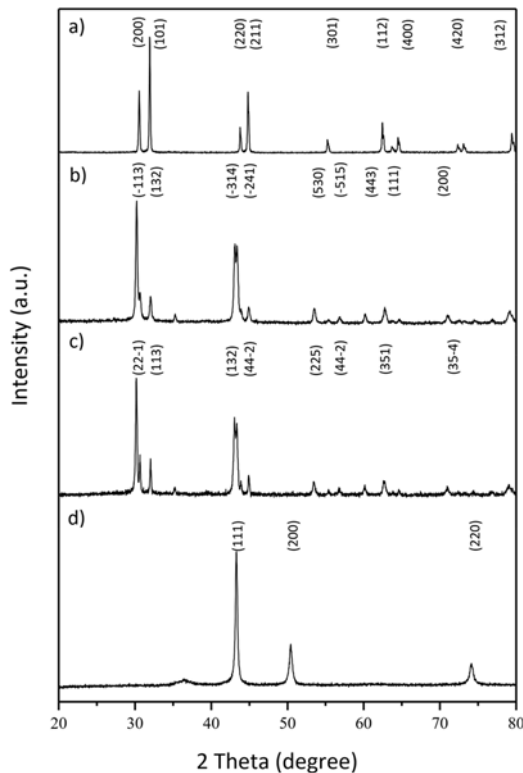


**Figure 5.2.** XRD patterns of Maed intermetallic catalysts: a) Sn, b)  $\text{Cu}_{30}\text{Sn}_{70}$  c)  $\text{Cu}_{30}\text{Sn}_{70}(\text{HT})$ , d) Cu.

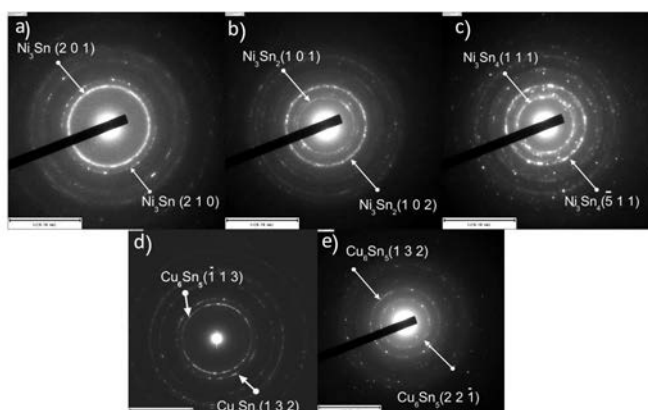


**Figure 5.3.** Selected area electron diffraction (SAED) of a)  $\text{Ni}_{57}\text{Sn}_{43}$  ( $\text{Ni}_3\text{Sn}$ ) b)  $\text{Ni}_{42}\text{Sn}_{58}$  ( $\text{Ni}_3\text{Sn}_2$ ) c)  $\text{Ni}_{27}\text{Sn}_{73}$  ( $\text{Ni}_3\text{Sn}_4$ ) d)  $\text{Cu}_{30}\text{Sn}_{70}$  ( $\text{Cu}_6\text{Sn}_5$ ) e)  $\text{Cu}_{30}\text{Sn}_{70}$ (HT) ( $\text{Cu}_6\text{Sn}_5$  (HT)).

#### 5.4.2. Surface studies of $\text{Ni}_x\text{Sn}_y$ and $\text{Cu}_x\text{Sn}_y$ intermetallic catalysts

Figure 5.4, showing Fe-SEM-EDS elemental maps and black scattering images (BSE) of Cu-Sn and Ni-Sn intermetallic catalysts (Figure. 5.4 a-c,  $\text{Ni}_3\text{Sn}$ , Figure 5.4 d-f,  $\text{Ni}_3\text{Sn}_2$ , Figure 5.4 g-i,  $\text{Ni}_3\text{Sn}_4$ , Figure 5.4 j-l,  $\text{Cu}_6\text{Sn}_5$ , and Figure 5.4 m-o,  $\text{Cu}_6\text{Sn}_5$ (HT)) confirmed the composition uniformity in the samples. Table 5.1, showing the compositions of Cu/Sn and Ni/Sn on the  $\text{Cu}_x\text{Sn}_y$  and the Ni-Sn intermetallic catalysts, respectively, indicated that the values was close to the nominal weighing. In addition, the morphology of all prepared catalysts had random sphere shapes. Evidently, these results confirmed that the MA technique was a good method to successfully prepare the  $\text{Cu}_x\text{Sn}_y$  and  $\text{Ni}_x\text{Sn}_y$  intermetallic catalysts.

The oxidation state number of Sn (i.e.  $\text{Sn}^{2+}$  and  $\text{Sn}^{4+}$ ) was identified by XPS. Figures 5.5 (a-c) and 5.6 (a-b), showing the deconvoluted peak profile of Sn in both Cu-Sn and Ni-Sn intermetallic catalysts, and changes in the Sn peak shapes, suggested the presence of the two oxidation states of Sn in the intermetallic. The Sn  $3d_{5/2}$  peak was therefore deconvoluted by Gaussian-Lorentzian curves to fit two oxidation states of  $\text{Sn}^{2+}$  and  $\text{Sn}^{4+}$ . From Figure 5.5a, the Sn  $3d_{5/2}$  peak of  $\text{Ni}_3\text{Sn}$  was 486 eV, corresponding to (IV) (Elzovic *et al.*,2015) whereas Figure 5.5b shows the Sn  $3d_{5/2}$  peaks of

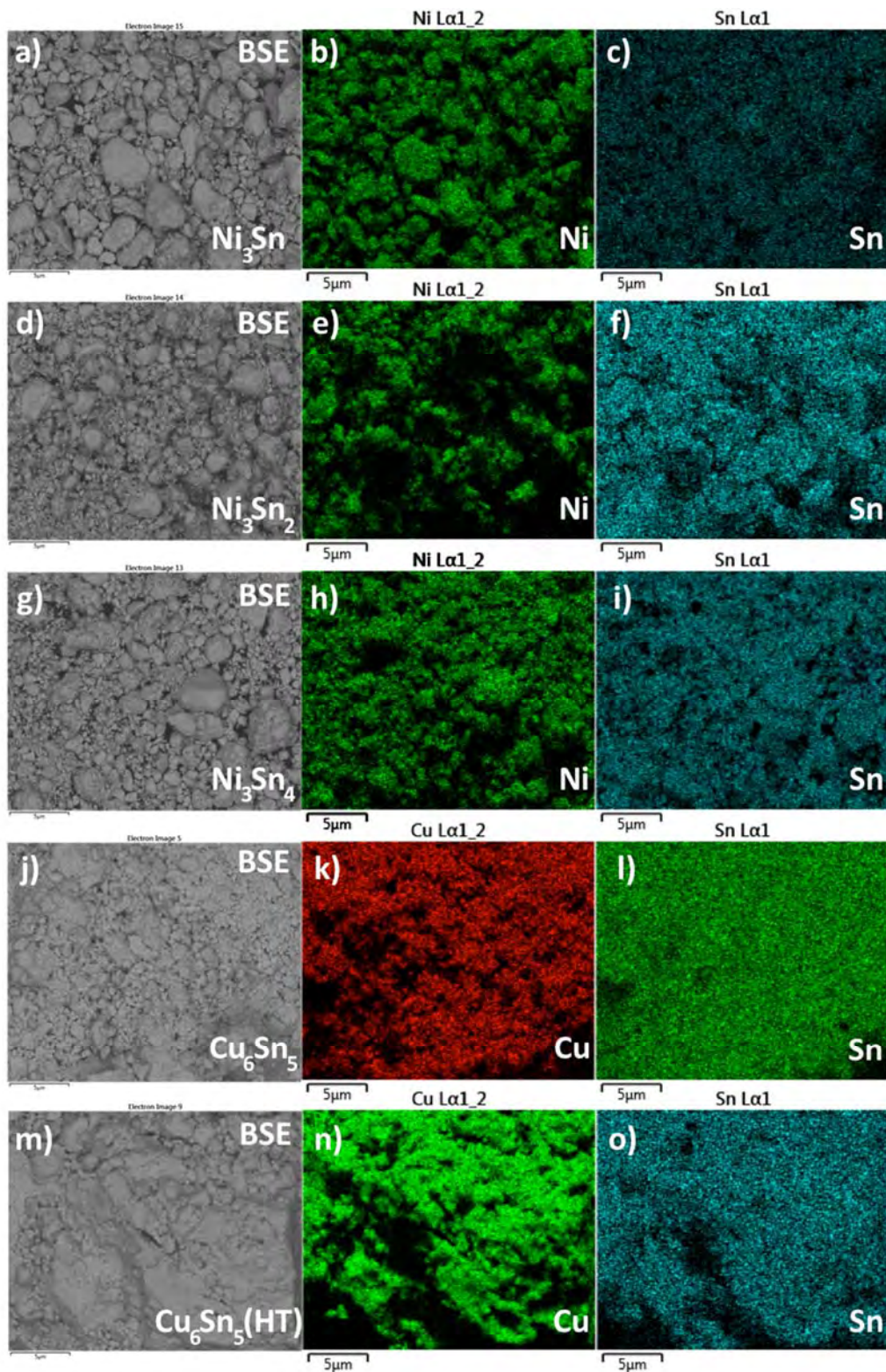


**Figure.5.4** FE-SEM-EDS elemental mapping and black scattering images (BSE) of a-c)  $\text{Ni}_3\text{Sn}$ , d-f)  $\text{Ni}_3\text{Sn}_2$ , g-i)  $\text{Ni}_3\text{Sn}_4$ , j-l)  $\text{Cu}_6\text{Sn}_5$ , and m-o)  $\text{Cu}_6\text{Sn}_5(\text{HT})$ .

$\text{Ni}_3\text{Sn}_2$  at 485.7 (13.3%) and 487.2 eV (86.7%), corresponding to Sn (II) (Virnovskaia *et al.*, 2007), and Sn(IV). Figure 5.5c shows the Sn  $3d_{5/2}$  peaks of  $\text{Ni}_3\text{Sn}_4$  at 485.5 (20%) and 487.4 eV (80%), corresponding to Sn(II) (Virnovskaia *et al.*, 2007) and Sn (IV) (Elzovic *et al.*, 2015). The Sn  $3d_{5/2}$  peak of  $\text{Cu}_6\text{Sn}_5$ , see Figure 5.6a, was 487.3 eV (92%), corresponding to Sn (II). The Sn  $3d_{5/2}$  peaks of  $\text{Cu}_6\text{Sn}_5(\text{HT})$  in Figure 5.6b was found at 487.7 eV (94.1%), corresponding to Sn(II). The XPS results indicated that the binding energy (Bes) of Sn metallics (485.0 – 485.5 eV) shifted to higher BEs since Ni or Cu diffused into interstitial site of Sn and formed the metal-metal bonds, as found the two oxidation states of Sn, as discussed earlier.

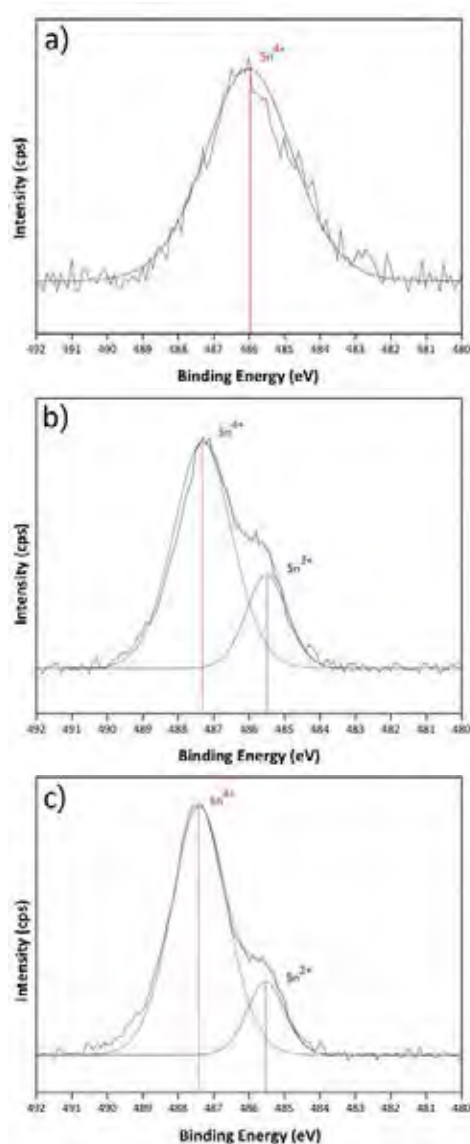


**Figure 5.5.** Sn  $3d_{5/2}$  spectra of a)  $\text{Ni}_3\text{Sn}$ , b)  $\text{Ni}_3\text{Sn}_2$ , and c)  $\text{Ni}_3\text{Sn}_4$ .



The number of the acid sites was investigated and calculated using  $\text{NH}_3$ -TPD, and found that the numbers of strong acid sites of  $\text{Ni}_3\text{Sn}$ ,  $\text{Ni}_3\text{Sn}_2$ , and  $\text{Ni}_3\text{Sn}_4$  were 0.031, 0.084, and 0.478 mmol/g, respectively. These values are indicated that the more Sn content provided the higher number of the acid strength and the acid sites. The strong acid site numbers of  $\text{Cu}_6\text{Sn}_5$  and  $\text{Cu}_6\text{Sn}_5(\text{HT})$  were 0.092 and 0.056 mmol/g, respectively.

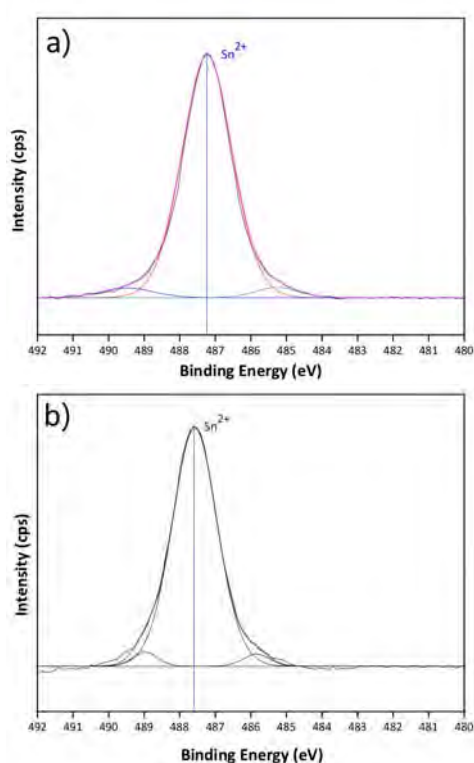


**Figure 5.6.** Sn  $3d_{5/2}$  spectra of a)  $\text{Cu}_6\text{Sn}_5$  and b)  $\text{Cu}_6\text{Sn}_5(\text{HT})$ .

#### 5.4.3 Catalytic activity of $\text{Ni}_x\text{Sn}_y$ intermetallic catalysts

The effects of differences in crystal structure of  $\text{Ni}_x\text{Sn}_y$  intermetallic catalysts were tested and the results were compared (see Figure. 5.7). The three catalysts have close crystallite sizes. The crystallite size and the surface area have an effect on activity and selectivity; therefore, in order to compare the effects of  $\text{Ni}_x\text{Sn}_y$  intermetallics, it is critical that catalysts with different compositions should have close particle sizes and surface area. The  $\text{N}_2$  adsorption-desorption isotherm revealed that the prepared catalysts had surface area in a range of 4.2-4.9 ( $\text{m}^2/\text{g}$ ). The

intermetallic catalysts,  $\text{Ni}_3\text{Sn}$ ,  $\text{Ni}_3\text{Sn}_2$ , and  $\text{Ni}_3\text{Sn}_4$ , were tested for phenol hydroxylation. Figure 5.7 shows that the increases of Sn contents in the  $\text{Ni}_x\text{Sn}_y$  intermetallics result in a decreasing number of facets on the crystal structure in conjunction with increases in the turnover number (TON). Experimental results revealed that the increase of Sn content enhanced both  $\text{H}_2\text{O}_2$  efficiency and active sites on the catalysts, as shown in Table 5.1. Moreover, changes in crystal structure that affected the kinetic and product selectivity could be best explained by the geometric effect, the number of acid sites, and the quantity of  $\text{Sn}^{2+}$  ion. This observation is because a decrease in the coordination of the edge and the corner (i.e. facets) atoms of the nanoparticle caused changes in the kinetics. (Henry *et al.*, 1985; Dahl *et al.*, 1999) As the experimental results are in agreement with theoretical prediction and related articles cited elsewhere (Vines *et al.*, 2009; Ludwig *et al.*, 2010; Schauer mann *et al.*, 2015), it can be concluded that as the facets of  $\text{Ni}_x\text{Sn}_y$  intermetallic nanoparticles decreased, the diffusion rate of the hydroxyl radical over the surface and subsurface increased. Hence the hydroxyl radicals were strongly facilitated to react with phenol. Furthermore, the cubic and orthorhombic crystal structure produced a mixture of CAT and HQ, whereas the hexagonal and monoclinic crystal structure produced only HQ, as listed in Table 5.1.

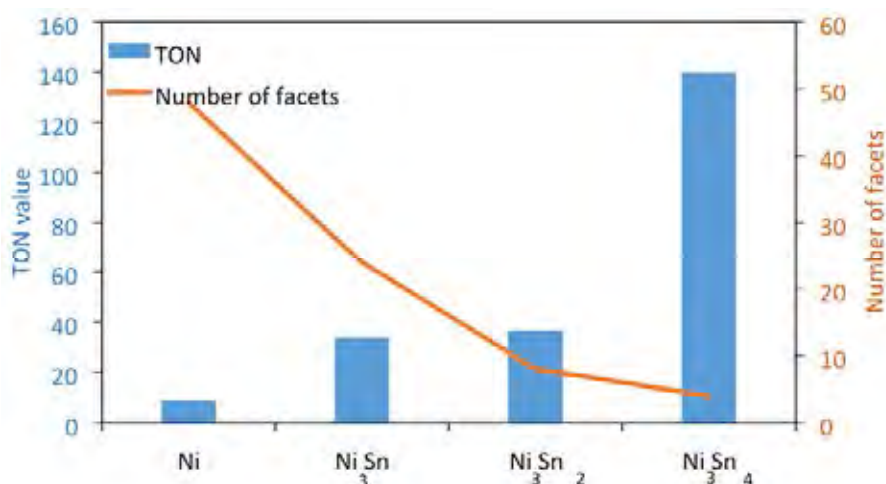


**Figure 5.7.** Relationship between number of facets and TON value of  $\text{Ni}_x\text{Sn}_y$  intermetallic catalysts ; TON = mole of converted substrate/ mole of catalyst.

These results indicate that the product selectivity depends on the crystal structure of either hexagonal or monoclinic crystal facets, the replicas of internal structures, on the  $\text{Ni}_x\text{Sn}_y$  intermetallics are preferential sites for phenol to react and form HQ. Additionally, these phenomena could be best supported and confirmed by the number of the strong acid sites and the  $\text{Sn}^{2+}$  ion generated since they were reported that a large number of strong acid site prevented the scavenging of  $\text{H}_2\text{O}_2$  and improved the absorption of phenol on the surface (Huang *et al.*, 2003). Moreover, a large number of  $\text{Sn}^{2+}$  on the catalyst were active for the phenol hydroxylation, meaning that a large number of the strong acid sites and the  $\text{Sn}^{2+}$  ion comprehended to be active in the phenol hydroxylation (Klaewkla *et al.*, 2003). The experimental result showed that the monoclinic  $\text{Ni}_3\text{Sn}_4$  intermetallic provided the highest yield, compared to other investigated catalysts because it contained the highest numbers of the strong acid sites and the  $\text{Sn}^{2+}$  ions. Therefore, it can be concluded that the crystal structure, a number of the strong acid sites, and a number of  $\text{Sn}^{2+}$  of  $\text{Ni}_x\text{Sn}_y$  intermetallics have influences on the phenol hydroxylation

#### 5.4.4 Optimizing conditions of phenol hydroxylation

To distinguish the catalytic activity of  $\text{Ni}_3\text{Sn}_4$  and  $\text{Ni}_3\text{Sn}$ , the optimum conditions, viz., time and temperature, amount of catalyst, and phenol: $\text{H}_2\text{O}_2$ , were required and thus investigated. In this study,  $\text{Ni}_3\text{Sn}_4$  was first studied at two different temperatures, 343 and 363 K. Figure 5.8a-b shows the time effect at both temperatures, respectively. At 343 K, the conversion kept increasing with time and stayed steady after 240 min, giving 88% conversion whereas at 363 K, the conversion of 90% became steady after 180 min. The reason could be that there were no more hydroxyl radicals generated from  $\text{H}_2\text{O}_2$  in the system after 240 and 180 min at 343 and 363 K, respectively. As for the product distributions, BQ was predominant at the first 60 min, especially at 343 K, and decreased as the time increased. After 240 min reaction time, BQ was hardly observed. On the other hand, CAT content increased with an increase in the reaction time, although it was observed at the lower temperature and slightly decreased after 240 min. Interestingly, HQ started to occur after 240 and 180 min at 343 and 363 K, respectively. As a result, CAT had higher selectivity than HQ due to

its strong thermodynamic stability by intra hydrogen bonding.<sup>34</sup> Therefore, 363 K and 180 min reaction temperature and time, respectively, were chosen to study for other effects.

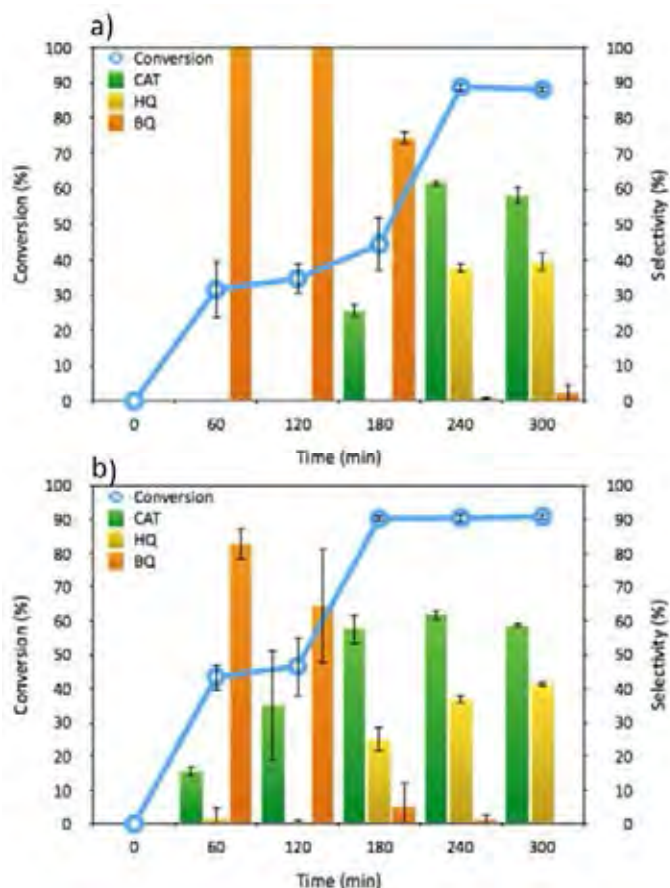


**Figure 5.8.** Phenol conversion and the product distributions of  $\text{Ni}_3\text{Sn}_4$  (50 mg) using 1:3 phenol: $\text{H}_2\text{O}_2$  at a) 343 and b) 363 K.

The results of studying the effect of catalyst amount are listed in Table 5.2. As the amount of the catalyst increased from 50 to 60 and 70 mg, the % conversions and the product selectivity of both CAT and HQ were slightly different. Therefore, the 50 mg amount of catalyst was used for other studies.

For phenol: $\text{H}_2\text{O}_2$  ratios of 1:4 and 1:5, the results are also shown in Table 5.2. As can be seen, both ratios provided nearly the same % conversion and the product selectivity of both CAT and HQ (97% with 60.3% CAT and 36.8% HQ for

1:4 and 98% with 64.1% CAT and 34.7% HQ for 1:5). It can be concluded that there was not much influence from H<sub>2</sub>O<sub>2</sub> on both the % conversion and the product selectivity since phenol was almost converted to the products and hydrogen peroxide scavenging might occur when it was applied in excess (Lou and Liu 2005; Klaewkla *et al.*, 2007). As a result, the yields of CAT and HQ increased around 10% yield when 1:4 phenol:H<sub>2</sub>O<sub>2</sub> was applied, as compared to those when using 1:3 phenol:H<sub>2</sub>O<sub>2</sub>. In summary, H<sub>2</sub>O<sub>2</sub> played an important role in oxidizing phenol to dihydroxybenzene at 363K for 180 min, using 1:4 phenol:H<sub>2</sub>O<sub>2</sub> and 50 mg of the catalyst.

**Table 5.2** Optimized conditions for phenol hydroxylation

Parameter	Conversion (%)	Yield (%)		
		CAT	HQ	BQ
Temperature <sup>a</sup>				
343 K	44.29	11.36	0	32.92
363 K	90.24	51.92	22.69	4.4
Amount of catalyst <sup>b</sup>				
60 mg	89.75	54.04	35.70	0
70 mg	91.50	53.55	37.94	0
Phenol : H <sub>2</sub> O <sub>2</sub> <sup>c</sup>				
1:4	97.10	60.28	36.82	0
1:5	98.79	64.07	34.71	0

<sup>a</sup>Reaction conditions: phenol:H<sub>2</sub>O<sub>2</sub>= 1:3, Catalyst= 50 mg, reaction time = 3 h.

<sup>b</sup>Reaction conditions: phenol:H<sub>2</sub>O<sub>2</sub>= 1:3, Temperature 363 K, reaction time = 3 h.

<sup>c</sup>Reaction conditions: Catalyst = 50 mg, Temperature 363 K, reaction time = 3 h.

#### 5.4.5 Influences of crystal structure and second metal on tin

To identify the effect of the crystal structure between monoclinic and hexagonal crystal structures on phenol hydroxylation, the catalysts were categorized in groups of monoclinic and hexagonal crystal structures for comparison. Monoclinic and hexagonal crystal structures consist of Ni<sub>3</sub>Sn<sub>4</sub>, Cu<sub>6</sub>Sn<sub>5</sub> and Ni<sub>3</sub>Sn, Cu<sub>6</sub>Sn<sub>5</sub>(HT), respectively. It was found that the catalytic activity of all catalysts, except Cu<sub>6</sub>Sn<sub>5</sub>(HT),

was not significantly different, as shown in Figure 5.9(a), giving conversion in a range of 95-97%, similarly, the conversion of  $\text{H}_2\text{O}_2$  was nearly 100% for all catalysts. However, when specifying the product yields of CAT, HQ, and BQ, only Ni-containing Tin intermetallic catalyst having hexagonal crystal structure seems to be the most powerful in phenol hydroxylation, giving high yields of CAT and HQ as

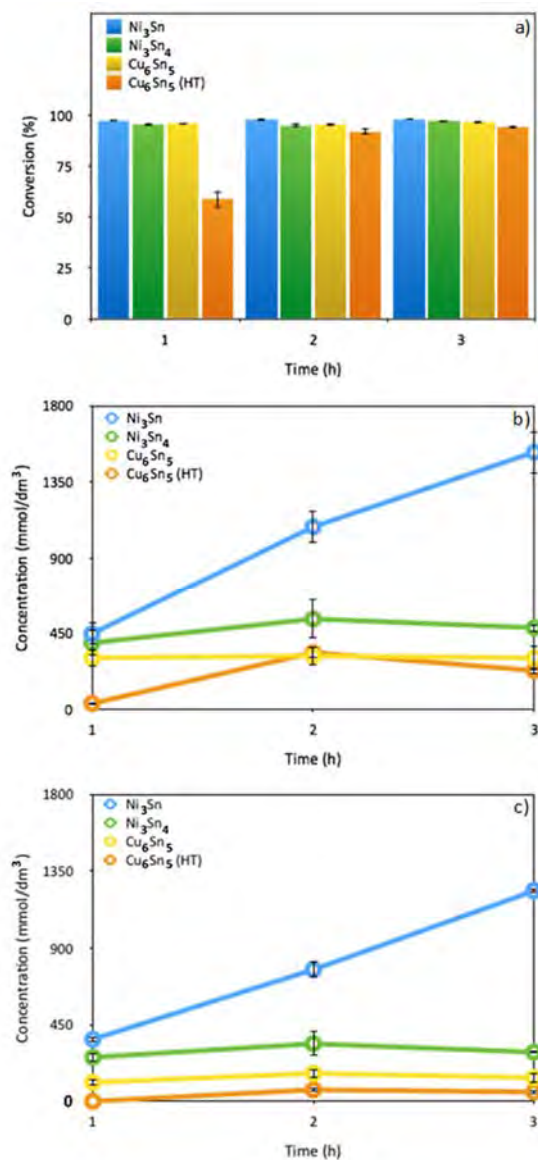


**Figure 5.9.** Catalytic activity profiles versus time of  $\text{Ni}_3\text{Sn}$ ,  $\text{Ni}_3\text{Sn}_4$ ,  $\text{Cu}_6\text{Sn}_5$ ,  $\text{Cu}_6\text{Sn}_5(\text{HT})$ ; a) Conversion, b) Concentration of CAT, and c) Concentration of HQ

reaction time increases, as seen in Figure 5.9b-c. The other catalysts may be too strong for this type of reaction since much tar was observed together with low yields of the products due to the numbers of the strong acid sites and the  $\text{Sn}^{2+}$  ions governing the tremendous reaction, resulting in over oxidation of products. The surface analysis results revealed the number of strong acid sites in a decreasing order, as follows; monoclinic  $\text{Ni}_3\text{Sn}_4$  > monoclinic  $\text{Cu}_6\text{Sn}_5$  > hexagonal  $\text{Ni}_3\text{Sn}$  > hexagonal  $\text{Cu}_6\text{Sn}_5(\text{HT})$ , and the number of the  $\text{Sn}^{2+}$  ion in a decreasing order of; monoclinic  $\text{Cu}_6\text{Sn}_5$  (92%) > hexagonal  $\text{Cu}_6\text{Sn}_5(\text{HT})$  (90%) > monoclinic  $\text{Ni}_3\text{Sn}_4$  (19.4%) > hexagonal  $\text{Ni}_3\text{Sn}$  (12%).  $\text{Ni}_3\text{Sn}$  had high ability to allow oxygen and  $\text{H}_2\text{O}_2$  to rapidly diffuse, thus no over-oxidation was observed (Zhao *et al.*, 2014). It is worth noting that  $\text{Ni}_3\text{Sn}_4$  still gave higher product yields than Cu-containing Tin catalysts after 1 h reaction time, indicating that the doping of Ni on Tin enhanced the phenol hydroxylation. The phenol consumption over  $\text{Ni}_3\text{Sn}_4$  intermetallic catalyst was compared with those using other catalysts reported elsewhere (Winstanley *et al.*, 2007; Shi *et al.*, 2011; Zhang *et al.*, 2011; Inchaurredo *et al.*, 2012; Antonin *et al.*, 2013), as summarized in Table 5.3. Up-to date, no one from literatures had ever studied on any types of Ni-Sn bimetallics on the phenol hydroxylation. Clearly,  $\text{Ni}_3\text{Sn}_4$  intermetallic catalyst showed the best catalytic activity on phenol hydroxylation.

#### 5.4.6 Structure of the spent catalysts

Due to the powerful reaction of those catalysts in terms of % conversion, the structures of the catalysts were thus carefully studied after 3 h

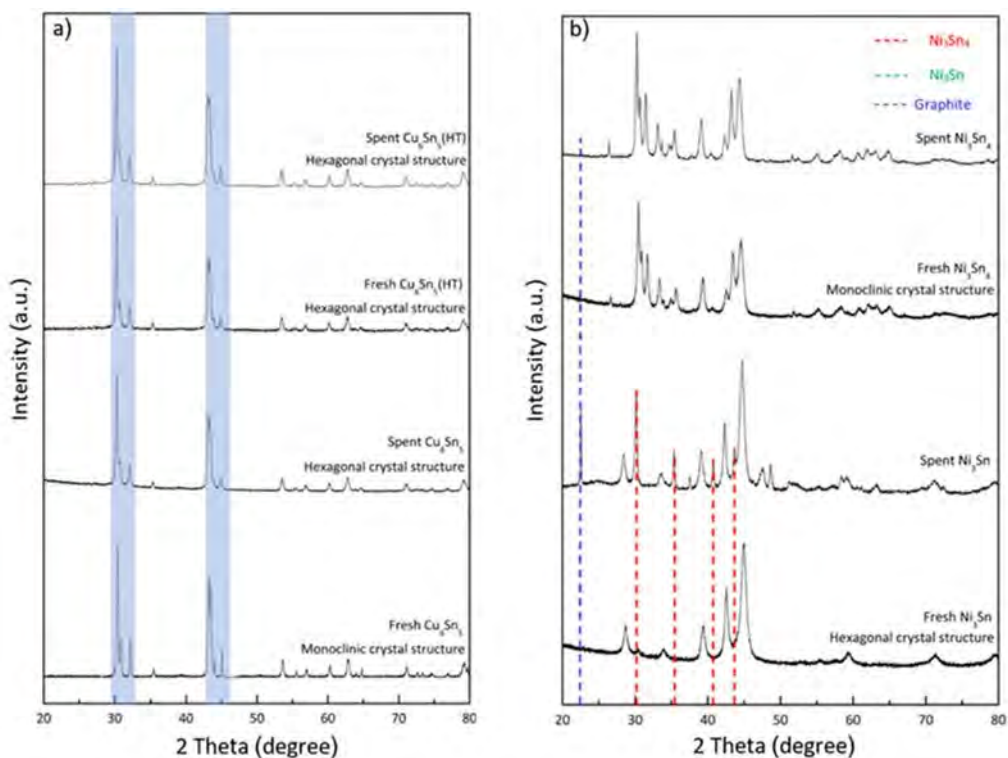


**Figure 5.10.** XRD patterns of spent catalysts a) Cu-Sn series b) Ni-Sn series using 50 mg catalyst, 1:4 phenol:H<sub>2</sub>O<sub>2</sub>, 363 K for 3 h reaction time.

reaction time. Figure 5.10 showing XRD patterns of both the fresh and the spent catalysts revealed that the monoclinic Cu<sub>6</sub>Sn<sub>5</sub>(HT), as expected, did not show any change in the crystal- structure because the hexagonal-Cu<sub>6</sub>Sn<sub>5</sub>(HT) crystal structure was thermodynamically stable; meanwhile, the monoclinic-Cu<sub>6</sub>Sn<sub>5</sub> crystal structure possessed a metastable structure (Larsson *et al.*, 1994). According to the phase diagram of Cu-Sn, allotropic transformation occurs at 406.6 K, where the monoclinic structure of Cu<sub>6</sub>Sn<sub>5</sub> transforms completely into the hexagonal-Cu<sub>6</sub>Sn<sub>5</sub> crystal structure, as depicted in Figure 5.10a. As for the Ni-Sn series, the Ni<sub>3</sub>Sn and Ni<sub>3</sub>Sn<sub>2</sub> phases are thermodynamically stable while the Ni<sub>3</sub>Sn<sub>4</sub> phase can keep growing during the reaction (Shen *et al.*, 2009). Therefore, the spent Ni<sub>3</sub>Sn<sub>4</sub> catalyst showed sharp XRD peaks due to the grain growth caused by the heat generated from the reaction. On the other hand,



the spent  $\text{Ni}_3\text{Sn}$  catalyst showed the mixed phases of  $\text{Ni}_3\text{Sn}$  and  $\text{Ni}_3\text{Sn}_4$  since the reaction was a powerful oxidation, a part of  $\text{Ni}_3\text{Sn}$  was broken and transformed to the less thermodynamically stable phase as  $\text{Ni}_3\text{Sn}_4$ , as shown in Figure 5.10b (Lis *et al.*,2016). Moreover, another evidence of having the coke on some part of the active site of  $\text{Ni}_3\text{Sn}$  was also observed, as can be seen by the sharp peak of graphite at  $23^\circ 2\theta$  (Girgis *et al.*,2007). It can be concluded that the structure of catalysts still maintained without any collapse, only the phase was transformed. The spent catalyst was tested its catalytic activity and found that the conversion dropped to 73%, consisting of 18.5% CAT and 54.5% BQ. It is evident that the coke formation on the catalyst surface is detrimental to its performance, as depicted in Figure 5.10.

## 5.5 Conclusion

The remarkable catalytic ability of the synthesized  $\text{Ni}_x\text{Sn}_y$  intermetallic catalysts was successfully demonstrated for direct phenol hydroxylation for the first time. The MA technique also showed benefits on catalyst preparation not only a large scale production but also a solventless in synthesis processing. Impressive activity enhancement of Cu and Ni can be achieved by adding Sn. The number of the strong acid sites and the  $\text{Sn}^{2+}$  ions increased in conjunction with increasing in Tin content. At 343 K 1:3 phenol: $\text{H}_2\text{O}_2$ , 50 mg of catalyst content, phenol hydroxylation showed that  $\text{Ni}_3\text{Sn}$  and  $\text{Ni}_3\text{Sn}_4$  intermetallic catalysts exhibited a prominent ability to produce only HQ in 30% and 42% yield, respectively. At optimized conditions of

**Table 5.3** Phenol hydroxylation catalyzed by different catalytic systems

Catalyst	Solvent	Phenol : H <sub>2</sub> O <sub>2</sub> molar ratio	Time (min)	Temp (K)	Conversion (%)	Ref.
Ni <sub>3</sub> Sn <sub>4</sub> intermetallic	water	1:4	180	363	98	this study
Al-free Mn-beta	water	1:20	360	353	35.2	3
Ti-HMA	acetic acid	1:2	720	300	20	5
Cu-alginate	water	1:2	120	343	62	6
MgO-Al <sub>2</sub> O <sub>3</sub> -HTS	acetone	1:1	120	353	26	38
CuO-MCM-48	water	1:1	240	333	51	39
TS-1	water	1:2	120	333	37	40
CuFe <sub>2</sub> O <sub>4</sub> -RGO	water	1:1	69	328	35.5	41

363 K, 1:4 phenol:H<sub>2</sub>O<sub>2</sub>, 50 mg of the catalyst content, the Ni<sub>3</sub>Sn and Ni<sub>3</sub>Sn<sub>4</sub> intermetallic catalysts still showed a higher catalytic activity than Cu<sub>6</sub>Sn<sub>5</sub> and Cu<sub>6</sub>Sn<sub>5</sub>(HT) intermetallic catalysts, giving CAT (60.2%) and HQ (36.8%). The merit of this study is to confirm the fact that both the catalyst preparation and the phenol hydroxylation are environmentally friendly.

## 5.6 Acknowledgements

The authors gratefully acknowledge the mutual supports or the partial scholarship from Thailand Graduate Institute of Science and Technology (TIGIST-TG-33-09-58-058D), The Petroleum and Petrochemical College, Chulalongkorn University, and Powder Metallurgy Research and Development Unit (PM\_RDU) of the National Metal and Materials Technology Center (MTEC). The authors also would like to thank Mr. John M. Jackson for proof-reading the paper.

## 5.7 References

- A. Donazzi, B. C. Michael and L. D. Schmidt, Chemical and geometric effects of Ce and washcoat addition on catalytic partial oxidation of CH<sub>4</sub> on Rh probed by spatially resolved measurements, *J. Catal.*, 2008, 260, 270-275.
- A. K. Larsson, L. Stenberg and S. Lidin, The superstructure of domain-twinned η'-Cu<sub>6</sub>Sn<sub>5</sub> *Acta Crystallography. B.*, 1994, 50, 636-643.
- A. S. Bandarenka and M. T. M. Koper, Structural and electronic effects in heterogeneous electrocatalysis: Toward a rational design of electrocatalysts, *J. Catal.*, 2013, 308, 11-24.
- A. Virnovskaia, S. Jørgensen, J. Hafizovic, Ø. Prytz, E. Kleimenov, M. Hävecker, H. Bluhm, A. Knop-Gericke, R. Schlögl and U. Olsbye, In situ XPS investigation of Pt (Sn)/Mg (Al) O catalysts during ethane dehydrogenation experiments, *Surface Science*, 2007, 601, 30-43.
- B.D. Cullity, "Elements of X-ray Diffraction:", 2nd ed., Addison-Wesley Publishing Company Inc. 2001.
- C. Borchers, C. Garve, M. Tiegel, M. Deutges, A. Herz, K. Edalati, R. Pippan, Z. Horita and R. Kirchheim, Nanocrystalline steel obtained by mechanical

- alloying of iron and graphite subsequently compacted by high-pressure torsion , Acta Mater., 2015, 97, 207-215.
- C. Perego, A. Carati, P. Ingallina, M. A. Mantegazza and G. Bellussi, Production of titanium containing molecular sieves and their application in catalysis , Applied Catalysis A: General, 2001, 221, 63-72.
- C. R. Henry and B. Mutaftschiev, Adsorption-desorption kinetics on stepped surfaces by modulated molecular beam techniques, Surface Science, 1985, 163, 409-434.
- C. Xia, L. Long, B. Zhu, M. Lin and X. Shu, Enhancing the selectivity of Pare-dihydroxybenzene in hollow titanium silicalite zeolite catalyzed phenol hydroxylation by introducing acid–base sites, Catalysis Communications, 2016, 80, 49-52.
- F. Shi, Y. Chen, L. Sun, L. Zhang and J. Hu, Hydroxylation of phenol catalyzed by different forms of Cu - alginate with hydrogen peroxide as an oxidant , Catalysis Communications, 2012, 25, 102-105.
- F. Viñes, C. Loschen, F. Illas and K. M. Neyman, Edge sites as a gate for subsurface carbon in palladium nanoparticles , Journal of Catalysis, 2009, 266, 59-63.
- G. Langhendries, D. E. De Vos, G. V. Baron and P. A. Jacobs, Quantitative sorption experiments on Ti-zeolites and relation with  $\alpha$ -olefin oxidation by H<sub>2</sub>O<sub>2</sub> , Journal of Catalysis, 1999, 187, 453-463.
- H. Shi, T. Zhang, B. Li, X. Wang, M. He and M. Qiu, Photocatalytic hydroxylation of phenol with Fe–Al-silicate photocatalyst: A clean and highly selective synthesis of dihydroxybenzenes , Catalysis. Communication., 2011, 12, 1022-1026.
- H.-H. Huang, M.-C. Lu, J.-N. Chen and C.-T. Lee, Influence of surface modification on catalytic activity of activated carbon toward decomposition of hydrogen peroxide and 2-chlorophenol , Journal of Environmental Science and Health, Part A, 2003, 38, 1233-1246.
- I. Efremenko, Implication of palladium geometric and electronic structures to hydrogen activation on bulk surfaces and clusters, J. Mol. Catal. A: Chem., 2001, 173, 19-59.

- K. P. SA Howard, Mineralogical Society of America, Washington DC, 1989.
- K.-i. Shimizu, K. Shimura, K. Kato, N. Tamagawa, M. Tamura and A. Satsuma, Palladium - Catalysed Dehydrogenative Generation of Imines from Amines. A Nature - Inspired Route to Indoles via Cross - Couplings of Amines with Arylhydrazines, J. Mol. Catal. A: Chem., 2012, 353–354, 171-177.
- K.J. Winstanley, D.K. Smith, Ortho-substituted catechol derivatives: the effect of intramolecular hydrogen-bonding pathways on chloride anion recognition, Journal of Organic Chemistry, 2007, 72, 2803-2815
- L.-L. Lou and S. Liu, CuO-containing MCM-48 as catalysts for phenol hydroxylation, Catalysis Communications, 2005, 6, 762-765.
- M. Morakotjinda, K. Fakpan, T. Yotkaew, N. Tosangthum, R. Krataitong, A. Daraphan, P. Siriphol, P. Wila, B. Vetayanugul, R. Tongstri, Gas atomization of low melting-point metal powders, Chiang Mai J. Sci. 37 (2010) 55-63.
- M. R. Maurya, S. J. J. Titinchi and S. Chand, Oxidation of phenol with H<sub>2</sub>O<sub>2</sub> catalysed by Cu (II), Ni (II) and Zn (II) complexes of N, N' -bis-(salicylidene) diethylenetriamine (H<sub>2</sub>saldien) encapsulated in Y-zeolite, Journal of Molecular Catalysis A: Chemical, 2003, 201, 119-130.
- N. Inchaurredo, J. Cechini, J. Font and P. Haure, strategies for enhanced CWPO of phenol solutions, Applied Catalysis B, 2012, 111–112, 641-648.
- N. R. Elezovic, V. R. Radmilovic, J. Kovac, B. M. Babic, L. M. Gajic-Krstajic and N. V. Krstajic, Pt nanoparticles on tin oxide based support as a beneficial catalyst for oxygen reduction in alkaline solutions, RSC Advances, 2015, 5, 15923-15929.
- R. Klaewkla, S. Kulprathipanja, P. Rangsunvigit, T. Rirksomboon and L. Nemeth, Phenol hydroxylation using Ti-and Sn-containing silicalites, Chemical Communications, 2003, DOI: 10.1039/B303455K, 1500-1501.
- R. Klaewkla, S. Kulprathipanja, P. Rangsunvigit, T. Rirksomboon, W. Rathbun and L. Nemeth, Kinetic modelling of phenol hydroxylation using titanium and tin silicalite-1s: Effect of tin incorporation, Chemical Engineering Journal, 2007, 129, 21-30.

- R. Klaewkla, T. Rirkomboon, S. Kulprathipanja, L. Nemeth and P. Rangsunvigit, Light sensitivity of phenol hydroxylation with TS-1, Catalysis Communications, 2006, 7, 260-263.
- S. Dahl, A. Logadottir, R. C. Egeberg, J. H. Larsen, I. Chorkendorff, E. Törnqvist and J. K. Nørskov, Role of Steps in Activation on Ru(0001), Physical Review Letters, 1999, 83, 1814-1817.
- S. Dahl, E. Törnqvist and I. Chorkendorff, Dissociative adsorption of N<sub>2</sub> on Ru (0001): a surface reaction totally dominated by steps , Journal of Catalysis, 2000, 192, 381-390.
- S. K. Mohapatra, F. Hussain and P. Selvam, Titanium substituted hexagonal mesoporous aluminophosphates: Highly efficient and selective heterogeneous catalysts for the oxidation of phenols at room , Catalysis Communications, 2003, 4, 57-62.
- S. L. James, C. J. Adams, C. Bolm, D. Braga, P. Collier, T. Friscic, F. Grepioni, K. D. M. Harris, G. Hyett, W. Jones, A. Krebs, J. Mack, L. Maini, A. G. Orpen, I. P. Parkin, W. C. Shearouse, J. W. Steed and D. C. Waddell, Mechanochemistry: opportunities for new and cleaner synthesis, Chemical Society Reviews, 2012, 41, 413-447.
- S. Pithakratanayothin, R. Tongsrri, T. Chaisuwan and S. Wongkasemjit, A simple route to CuxSn (100– x) intermetallic nanoparticle catalyst for ultra-phenol hydroxylation , Materials Chemistry and Physics, 2016, 181, 452-461.
- S. Recchia, C. Dossi, N. Poli, A. Fusi, L. Sordelli and R. Psaro, Outstanding performances of magnesia-supported platinum–tin catalysts for citral selective hydrogenation, J. Catal., 1999, 184, 1-4.
- S. Schauermaun and H.-J. Freund, Model approach in heterogeneous catalysis: kinetics and thermodynamics of surface reactions, Model approach in heterogeneous catalysis: kinetics and thermodynamics of surface reactions , Account of Chemical Research, 2015, 48, 2775-2782.
- T. Pino, P. Bréchnignac, E. Dartois, K. Demyk and L. d'Hendecourt, Electronic spectroscopy of a cyclopentafused PAH cation, the fluorene<sup>+</sup>: comparison between gas phase and matrix spectra , Chemical Physics Letters, 2001, 339, 64-70.

- V. S. Antonin, M. H. M. T. Assumpção, J. C. M. Silva, L. S. Parreira, M. R. V. Lanza and M. C. Santos, Synthesis and characterization of nanostructured electrocatalysts based on nickel and tin for hydrogen peroxide electrogeneration, Electrochimica Acta, 2013, 109, 245-251.
- W. Ludwig, A. Savara, S. Schauermaun and H.-J. Freund, Role of Low - Coordinated Surface Sites in Olefin Hydrogenation: A Molecular Beam Study on Pd Nanoparticles and Pd (111) , Chem. Phys. Chem., 2010, 11, 2319-2322.
- W.D. Callister, "Materials Science and Engineering: An Introduction", Wiley & Sons 2003.
- X. Liang, R. Yang, G. Li and C. Hu, Phenol hydroxylation over Fe-incorporated mesoporous materials prepared by coprecipitation, Microporous and Mesoporous Materials, 2013, 182, 62-72.
- Y. Morimoto, S. Bunno, N. Fujieda, H. Sugimoto and S. Itoh, Direct hydroxylation of benzene to phenol using hydrogen peroxide catalyzed by nickel complexes supported by pyridylalkylamine ligands , Journal of the American Chemical Society, 2015, 137, 5867-5870.
- Y. Zhao, G. He, W. Dai and H. Chen, High Catalytic Activity in the Phenol Hydroxylation of Magnetically Separable CuFe<sub>2</sub>O<sub>4</sub>-Reduced Graphene Oxide, Industrial & Engineering Chemistry Research, 2014, 53, 12566-12574.
- Z. He, J. Wu, B. Gao and H. He, Hydrothermal synthesis and characterization of aluminum-free Mn- $\beta$  zeolite: a catalyst for phenol hydroxylation, ACS Applied Materials & Interfaces, 2015, 7, 2424-2432.

**CHAPTER VI**  
**STRUCTURAL EFFECT OF  $\text{Cu}_x\text{Sn}_{1-x}$  INTERMETALLIC CATALYST**  
**PREPARED BY MECHANICAL ALLOYING TECHNIQUE IN PHENOL**  
**HYDROXYLATION**

### **6.1 Abstract**

There are three main factors that alter the “catalytic activity”, namely, changing the support material, changing the catalyst size, and adding a second metal (i.e., alloying or intermetallic). The latter two factors result in changing electronic and geometric effects. In this work, both electronic and geometric effects were studied, using Cu and Sn as the active metals and phenol hydroxylation as a molecular probe study for catalytic activity. After the mechanically alloyed processing of Cu and Sn, the results showed that the geometric effect strongly influenced the catalytic activity, and the cubic sorosite crystal structure provided the dominant active site. Moreover, the ensemble crystal structures of monoclinic  $\eta\text{-Cu}_6\text{Sn}_5$  and orthorhombic  $\varepsilon\text{-Cu}_3\text{Sn}$  could govern the conversion upto 84%. On the other hand, the electronic effect strongly depended on the surface structure, and the particle size indicated that the monoclinic  $\eta\text{-Cu}_6\text{Sn}_5$  crystal structure gave higher catechol (CAT) selectivity than the cubic phase crystal structure, while the influence of orthorhombic  $\varepsilon\text{-Cu}_3\text{Sn}$  resulted in greater selectivity of catechol.

**Keywords:** Mechanical alloying; Geometric effect; Electronic effect; Crystal structure; Particle size.

### **6.2 Introduction**

Questions are often raised on the heterogeneous catalysis in which the active site of the catalyst is affected. Nørskov *et al.* studied the molecular level of heterogeneous catalysts and found two major factors, viz., electronic and geometric effects (Nørskov *et al.*, 2008). The electronic effect results from the metal surface which is aligned in different environments and has a slightly different local



electronic structure from the original structure; for example, the change in the metal content and the particle size (degree of charge transfer and hybridization), and surface geometry or ensemble crystal structures (Childers *et al.*,2014). As a consequence, the incoming molecules showed different reactions and results when they reacted and adsorbed. The geometric effect is different in configuring the molecule for bonding, i.e. crystal structure, shape, and size (Recchia *et al.*,1999; Efremenko *et al.*,2001; Donazzi *et al.*,2008; Bandarenka *et al.*,2013).

Changes in the crystal structure can be done by coprecipitation (Fuller *et al.*,1974; Xia *et al.*,2016), annealing (Ahmadi *et al.*, 2012; Wang *et al.*,2015), double impregnation (Childers *et al.*,2014; Kittisakmontree *et al.*, 2013; Rio *et al.*, 2014) and mechanical alloying (Adabavazeh *et al.*,2012; Zamani *et al.*, 2012; Gogebakan *et al.*, 2013; Dudina *et al.*, 2015; Mehrizi *et al.*, 2016; Pothin *et al.*,2016). Among these techniques, mechanical alloying is the most practical technique, because it is easy to handle and provides high productivity in either lab or commercial scale. Moreover, the mechanically alloyed (MAed) technique also results in new phases of intermetallics and produces small grains of materials that exhibit different thermodynamic properties (Corchers *et al.*,2015).

The nature of the mechanical alloying process results in fracturing and welding (Besson *et al.*,2015). The process contributes the surface diffusion mechanism, resulting in the formation of more free surfaces, grain boundaries, surface diffusion driven by the reduction of surface area and radius of the crack tip (Pasebani *et al.*,2013). For a new crystal structure formation from two elements, the smaller atomic diameters are better interstitial sites to form solid solution, resulting in alloys or intermetallics. The diffusion process is very rapid during mechanical alloying (Chithra *et al.*, 2011). Thereby, changes in the crystal structure by the mechanical alloying technique promise to show changes in the electronic and geometric effect.

The results of our previous study on  $\text{Cu}_x\text{Sn}_{(100-x)}$ (Pithakratanayothin *et al.*, 2016), led us to choose Cu and Sn in studying the effects of the crystal structure change by schematic analysis of phenol hydroxylation which was found to provide a high efficiency if Cu was used to oxidize the phenol to their derivatives. Unfortunately, the reaction was over oxidation, resulting in an undesirable product, tar (Karakhanov *et al.*,2010; Shi *et al.*, 2012). Tin, Sn, on the other hand, increases

hydrogen peroxide efficiency (Klaewkla *et al.*,2007) and retards coke formation (Vu *et al.*,2011; Gianotti *et al.*,2014). Owing to the advantages of Cu, Sn, and mechanical alloying technique, it was, thus, attractive to study what were the factors that affected the catalytic activity.

To study the catalytic activity of the Maed  $\text{Cu}_x\text{Sn}_{1-x}$ , different compositions were prepared by following the phase diagrams, as studied elsewhere (Furtauer *et al.*,2013) to obtain various crystal structures of  $\text{Cu}_x\text{Sn}_{1-x}$  intermetallics. The main factors for this study were the number of acid sites,  $\text{Cu}^{2+}$ ,  $\text{Sn}^{2+}$  ions, the phases of  $\text{Cu}_x\text{Sn}_{1-x}$  intermetallics before and after the heat treatment, and different crystallite sizes in the same crystal structure. The criteria was to evaluate the rate constant of phenol, selectivity of CAT, hydroquinone (HQ), and benzoquinone (BQ) in order to compare their catalytic activity tested at 343K using 50 mg of catalyst, and 1:3 phenol:hydrogen peroxide.

### 6.3 Experimental

#### 6.3.1 Materials

Copper (Cu, 99.99 %wt) and tin (Sn, 99.99 % wt) powders were produced using gas atomization (. Methanol ( $\text{CH}_3\text{OH}$ , 99.99%) was purchased from Labscan, Thailand; catechol (CAT, 99%), hydroquinone (HQ, 99%), 1,4-benzoquinone (BQ, 98%) from Sigma-Aldrich, USA; phenol-detached crystals and hydrogen peroxide ( $\text{H}_2\text{O}_2$ , 30 %w/v) from Fisher Scientific, UK. All chemicals were used without purification.

#### 6.3.2 Characterization

X-ray diffraction (XRD) patterns were recorded on a Rigaku X-ray diffractometer with  $\text{CuK}\alpha$  radiation and the crystallite sizes were determined using MDI JADE 9 software, relating to the Scherrer formula, with a residual error of less than 10%. XRD X-ray fluorescence (XRF) spectrometer (PANalytical AXIOS PW 4400) was used to analyze elements in the samples. Transmission electron micrographs and high resolution transmission electron micrographs (HRTEM) were conducted using JEOL JEM-2010. Scanning electron micrograph

(SEM) was obtained on a Hitachi S-4800. X-ray photoelectron spectra (XPS) were analyzed on AXIS ULTRA<sup>DLD</sup> spectrometer to determine the oxidation state of metal. The system was equipped with a monochromatic Al X-ray source and a hemispherical analyzer. All peaks were calibrated from C 1s spectra located at 284.6 eV. Temperature programmed desorption (NH<sub>3</sub>-TPD) was also used to determine the acid properties, such as acid strength and acidity, of the catalysts using Thermo Finnigan 1100. The samples were analyzed by a UFLC Shimadzu high performance liquid chromatography (HPLC) equipped with a C-18 reverse-phase column (Inertsil ODS-3) and a UV detector (SPD-M20A Shimadzu). All reactions were performed in triplicate and average values were used in the data presentation.

### 6.3.3 Synthesis of Cu, Sn, and Cu<sub>x</sub>Sn<sub>1-x</sub> nanoparticles

Cu (32  $\leq$   $\mu$ m) and Sn (32  $\leq$   $\mu$ m) were used to prepare Cu, Sn, and Cu<sub>x</sub>Sn<sub>1-x</sub> nanoparticles. The Cu<sub>x</sub>Sn<sub>1-x</sub> intermetallics were prepared by varying Sn contents (30, 50, 70, and 100 %wt) balanced with Cu powder. Elemental Cu and Sn powders and Cu<sub>x</sub>Sn<sub>1-x</sub> powder mixtures were mechanically alloyed (Maed) in an attritor. The conditions used followed the paper cited elsewhere [27]. After milling, the materials were heated in a vacuum chamber for metal diffusion. The Maed powders were further characterized using various techniques.

### 6.3.4 Catalytic activity study

Phenol hydroxylation was conducted to study the activity of the synthesized catalysts by adding phenol (1.88g, 20mmol), H<sub>2</sub>O<sub>2</sub> (6.84g, 60 mmol), and water (10 ml) into a 250 ml two-necked round bottom flask fitted with a condenser. The catalytic activity results of Cu<sub>x</sub>Sn<sub>1-x</sub> intermetallics before and after heat treatment were compared at 343K using 50 mg of catalyst and 1:3 phenol:H<sub>2</sub>O<sub>2</sub> by considering the rate constants of phenol, CAT, HQ, BQ, and conversion.

## 6.4 Results and Discussion

### 6.4.1 Effect of Sn content

To identify the phases contained in the synthesized catalysts, quantitative analysis using Reference Intensity Ratio (RIR) method was conducted because the whole-pattern fitting approach provides much greater accuracy and precision than any peak-intensity based method. The RIR method was based upon all diffraction data of the reference materials where the RIR values were accompanied with the international center for diffraction data (ICDD) found in the JCPDS card of each phase (Bish and Howard, 1988; Chipera and Bish, 2002). To obtain the amount of each phase, the diffraction data was analyzed using Rietveld refinement with residual error, in which the value was less than 10 % using MDI JADE 9.0 software in order to obtain the greater accuracy and precision data (Snyder *et al.*, 1989). The background was corrected using a Chebyshev polynomial (Rivlin, 1974). A peak profile function was modelled using a convolution of the Thompson–Cox–Hastings pseudo-Voigt (pV-TCH) function (Thompson *et al.*, 1978) with the asymmetry function described by Finger *et al.*, which accounts for the asymmetry of the axial divergence (Finger *et al.*, 1994).

As a result, XRD patterns(not shown) of Sn, Cu, and  $\text{Cu}_x\text{Sn}_{1-x}$  catalysts prepared by Ma technique using various amounts of Sn (30, 50, 70, and 100 %wt) were consistent with the paper cited elsewhere (Pithkaratanayothin *et al.*, 2016), viz.  $\text{Sn}_{100}$  (JCPDS Card No. 04-006-2820 of tetragonal  $\beta$ -Sn);  $\text{Cu}_{30}\text{Sn}_{70}$  (JCPDS Card No. 04-014-9975 of monoclinic  $\eta$ - $\text{Cu}_6\text{Sn}_5$  (89.50 %wt), JCPDS Card No. 04-004-9064 of cubic copper (5.20 %wt), and JCPDS Card No. 04-006-2820 of tetragonal  $\beta$ -Sn (5.30 %wt),  $\text{Cu}_{50}\text{Sn}_{50}$  (JCPDS card No. 04-014-9975 of monoclinic  $\eta$ - $\text{Cu}_6\text{Sn}_5$  (60.5 %wt), and JCPDS Card No. 03-065-5721 of orthorhombic  $\varepsilon$ - $\text{Cu}_3\text{Sn}$  (18.5 %wt), JCPDS Card No. 04-004-9064 of cubic copper (12.40 %wt), and JCPDS Card No. 04-006-2820 of tetragonal  $\beta$ -Sn (8.40 %wt),  $\text{Cu}_{70}\text{Sn}_{30}$  JCPDS Card No. 03-065-3434 of cubic sorosite (89.4 %wt), and JCPDS Card No. 04-006-2820 of tetragonal  $\beta$ -Sn (4.7 %wt), and  $\text{Cu}_{100}$  (JCPDS Card No. 04-004-9064 of cubic copper). All patterns show broad peaks which can be attributed to the small

crystallite sizes, in agreement with the calculation using the Scherrer formula (eq.1), as summarized in Table 6.1.

$$d = \frac{0.9\lambda}{B\cos\theta} \quad (1)$$

Where  $d$  is the average crystallite size,  $\lambda$  is the wavelength of the X-ray, and  $B$  is the full width at half maximum intensity of Bragg diffraction peak at diffraction angle  $\theta$  (in radians). The MDI JADE software was used to calculate the crystallite size, as related to the Scherrer formula, to obtain more accuracy and precision. From the results, it was found that the crystallite size of Sn was the largest; Sn, having its melting point at 504 K, was possibly melted and agglomerated into larger particle sizes during the Ma process, generating heat around 473–493 K (Xi *et al.*, 2008).

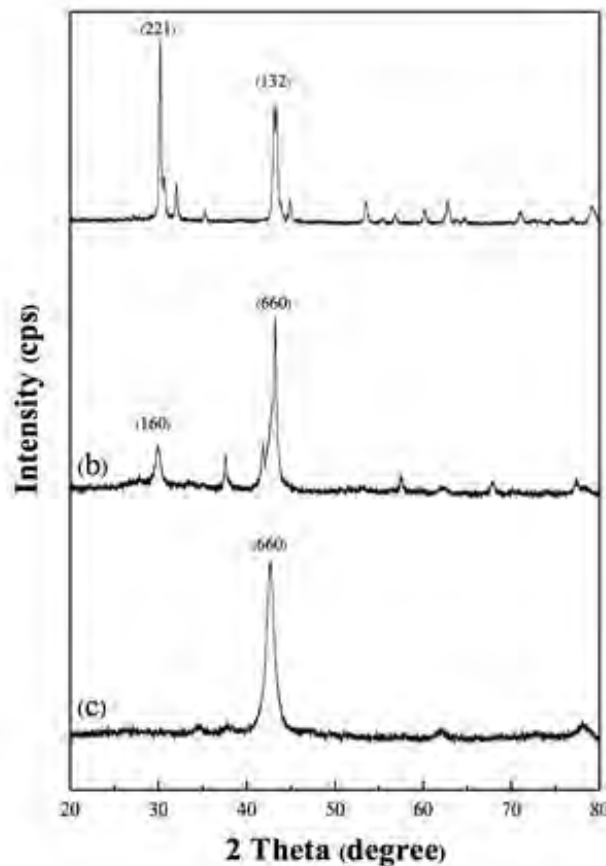


**Figure 6.1** XRD patterns of a)  $\text{Cu}_{30}\text{Sn}_{70}(\text{HT})$ , b)  $\text{Cu}_{50}\text{Sn}_{50}(\text{HT})$ , c)  $\text{Cu}_{70}\text{Sn}_{30}(\text{HT})$

**Table 6.1** Composition, crystallite size, and influence of Cu<sub>x</sub>Sn<sub>1-x</sub> intermetallics on phenol

hydroxylation Catalyst	Composition (%wt)				Particle size <sup>a</sup>	Rate	Conversion (%)	Selectivity (%)		
	Nominal		XPS		Size	Constant <sup>b</sup>		CAT	HQ	BQ
	Cu	Sn	Cu	Sn	(nm)	(dm <sup>3</sup> /mol.s)				
Cu <sub>100</sub>	100	-	99.99	-	30.0	$37.8 \times 10^{-5}$	88.82	54.21	45.78	-
Cu <sub>70</sub> Sn <sub>30</sub>	70.00	30.00	69.20	30.80	29.0	$10.3 \times 10^{-5}$	83.38	43.66	48.33	8.00
Cu <sub>70</sub> Sn <sub>30</sub> (HT)	70.00	30.00	68.15	31.85	50.0	$1.66 \times 10^{-5}$	42.71	50.04	28.43	21.15
Cu <sub>50</sub> Sn <sub>50</sub>	50.00	50.00	49.84	50.16	46.3	$6.87 \times 10^{-5}$	78.47	61.96	30.84	7.19
Cu <sub>50</sub> Sn <sub>50</sub> (HT)	50.00	50.00	48.75	51.25	23.2	$10.5 \times 10^{-5}$	84.56	56.91	43.08	-
Cu <sub>30</sub> Sn <sub>70</sub>	30.00	70.00	29.84	70.16	55.3	$1.25 \times 10^{-5}$	35.20	50.28	22.58	27.12
Cu <sub>30</sub> Sn <sub>70</sub> (HT)	30.00	70.00	29.55	70.45	27.5	$1.41 \times 10^{-5}$	39.97	28.08	41.54	30.36
Sn <sub>100</sub>	-	100	-	99.50	70.1	$0.19 \times 10^{-5}$	7.53	61.15	38.84	-

Reaction conditions : phenol:H<sub>2</sub>O<sub>2</sub> = 1:3, catalyst = 50 mg, T= 323 K, reaction time = 24 min.

(HT) = After heat treatment

<sup>a</sup>Data were obtained from XRD by using MDI JADE 9 software with residual error is less than 10 %.

<sup>b</sup>Data were calculated from the slope of second order kinetic expression.

All data were repeated 3 replicates.

#### 6.4.2. Effect of heat treatment

From the phase diagrams of  $\text{Cu}_x\text{Sn}_{1-x}$  intermetallics, the temperature for the heat treatment was chosen by considering the tin content, thus, 30, 50, and 70% of tin were treated at 573, 673, and 773 K, respectively. Figures 6.1 a-c show XRD patterns of  $\text{Cu}_{30}\text{Sn}_{70}(\text{HT})$  (JCPDS card No. 04-014-9975 of monoclinic  $\eta$ - $\text{Cu}_6\text{Sn}_5$ ),  $\text{Cu}_{50}\text{Sn}_{50}(\text{HT})$  (JCPDS card No. 03-065-7047 of cubic  $\delta$ - $\text{Cu}_{41}\text{Sn}_{11}$  (53.3%), JCPDS card No.04-014-9975 of monoclinic  $\eta$ - $\text{Cu}_6\text{Sn}_5$  (19.8%), and JCPDS card No. 03-065-5721 of orthorhombic  $\epsilon$ - $\text{Cu}_3\text{Sn}$  (35.9%), as can be seen in Figure 6.2a. Surprisingly, after the heat treatment, XRD peaks showed that the phase of all catalysts was changed; in addition, the traces of copper and tin had vanished. This phenomenon could be due to the driving forces from the lower surface tension and stress during the heat treatment, resulting in diffusion of the smaller-radius atoms into the interstitial sites of one another to form intermetallics (Freitas *et al.*,2006; Xi *et al.*,2008). As a result, the electronic and geometric structures were also changed.

To further verify  $\text{Cu}_x\text{Sn}_{1-x}$  intermetallics before and after the heat treatment, the d-spacing values were calculated from the SADE patterns and matched with the d-spacing values given in the JCPDS references in order to index the Miller indices of the corresponding intermetallics (Tongsri *et al.*,2013). Figure 6.3, showing selected area electron diffraction (SAED), indicates that after the heat treatment, the crystal structure of the catalysts had changed. After the heat treatment,  $\text{Cu}_{30}\text{Sn}_{70}$  changed

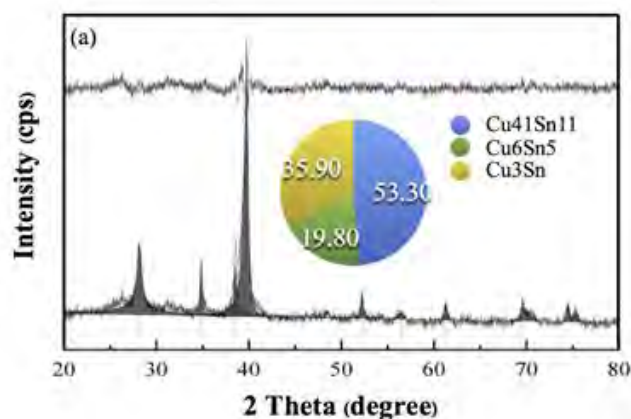


**Figure 6.2** Rietveld-XRD plots of a)  $\text{Cu}_{50}\text{Sn}_{50}(\text{HT})$

from monoclinic  $\eta$ -Cu<sub>6</sub>Sn<sub>5</sub> ( $d = 2.46\text{\AA}\{222\}$  and  $d = 1.70\text{\AA}\{315\}$ , Figure 6.3a) to monoclinic  $\eta$ -Cu<sub>6</sub>Sn<sub>5</sub> ( $d = 2.10\text{\AA}\{132\}$  and  $d = 2.94\text{\AA}\{22-1\}$ , Figure 6.4b), Cu<sub>30</sub>Sn<sub>70</sub>(HT). Cu<sub>50</sub>Sn<sub>50</sub> in Figure 6.3c changed from monoclinic  $\eta$ -Cu<sub>6</sub>Sn<sub>5</sub> ( $d = 1.71\text{\AA}\{-241\}$ ) and orthorhombic  $\varepsilon$ -Cu<sub>3</sub>Sn ( $d = 2.08\text{\AA}\{2120\}$ ) to cubic  $\delta$ -Cu<sub>41</sub>Sn<sub>11</sub> (53.3%,  $d = 2.11\text{\AA}\{660\}$ ) and orthorhombic  $\varepsilon$ -Cu<sub>3</sub>Sn (35.9%,  $d = 3.02\text{\AA}\{160\}$ ), Cu<sub>50</sub>Sn<sub>50</sub>(HT) in Figure 6.3d. Cu<sub>70</sub>Sn<sub>30</sub> changed from cubic sorosite ( $d = 1.761\text{\AA}\{201\}$  and  $d = 1.532\text{\AA}\{103\}$ ) in Figure 6.3e to cubic  $\delta$ -Cu<sub>41</sub>Sn<sub>11</sub> ( $d = 2.11\text{\AA}\{660\}$ ), Cu<sub>70</sub>Sn<sub>30</sub>(HT) in Figure 6.3f. Accordingly, Cu<sub>70</sub>Sn<sub>30</sub> after the heat treatment gave the single phase of cubic  $\delta$ -Cu<sub>41</sub>Sn<sub>11</sub>; Cu<sub>50</sub>Sn<sub>50</sub> gave mixed phases of cubic  $\delta$ -Cu<sub>41</sub>Sn<sub>11</sub> (53.3%), monoclinic  $\eta$ -Cu<sub>6</sub>Sn<sub>5</sub> (10.8%), and orthorhombic  $\varepsilon$ -Cu<sub>3</sub>Sn (35.9%); and Cu<sub>30</sub>Sn<sub>70</sub> gave single phase of monoclinic  $\eta$ -Cu<sub>6</sub>Sn<sub>5</sub>.

In addition, the the acid site numbers determined and calculated using NH<sub>3</sub>-TPD were following; 1.207 (Cu<sub>70</sub>Sn<sub>30</sub>), 0.131 (Cu<sub>70</sub>Sn<sub>30</sub>(HT)), 0.737 (Cu<sub>50</sub>Sn<sub>50</sub>), 0.84 (Cu<sub>50</sub>Sn<sub>50</sub>(HT)), 1.239(Cu<sub>30</sub>Sn<sub>70</sub>), 0.057 (Cu<sub>30</sub>Sn<sub>70</sub>(HT)), and 0.774 mmol/g (Cu). The acid site number of Sn was not detectable, since it was melted, as its melting point was 505 K, and loss its active sites when the NH<sub>3</sub>-TPD was ramped to 1073 K. The results showed that after the heat treatment the active sites was tremendous decreased in all cases, except Cu<sub>50</sub>Sn<sub>50</sub>(HT) due to the essemble crystal structure effect. Consequently, it can be stated that the increase in the crystal structure also increases in the number ofthe acid sites.



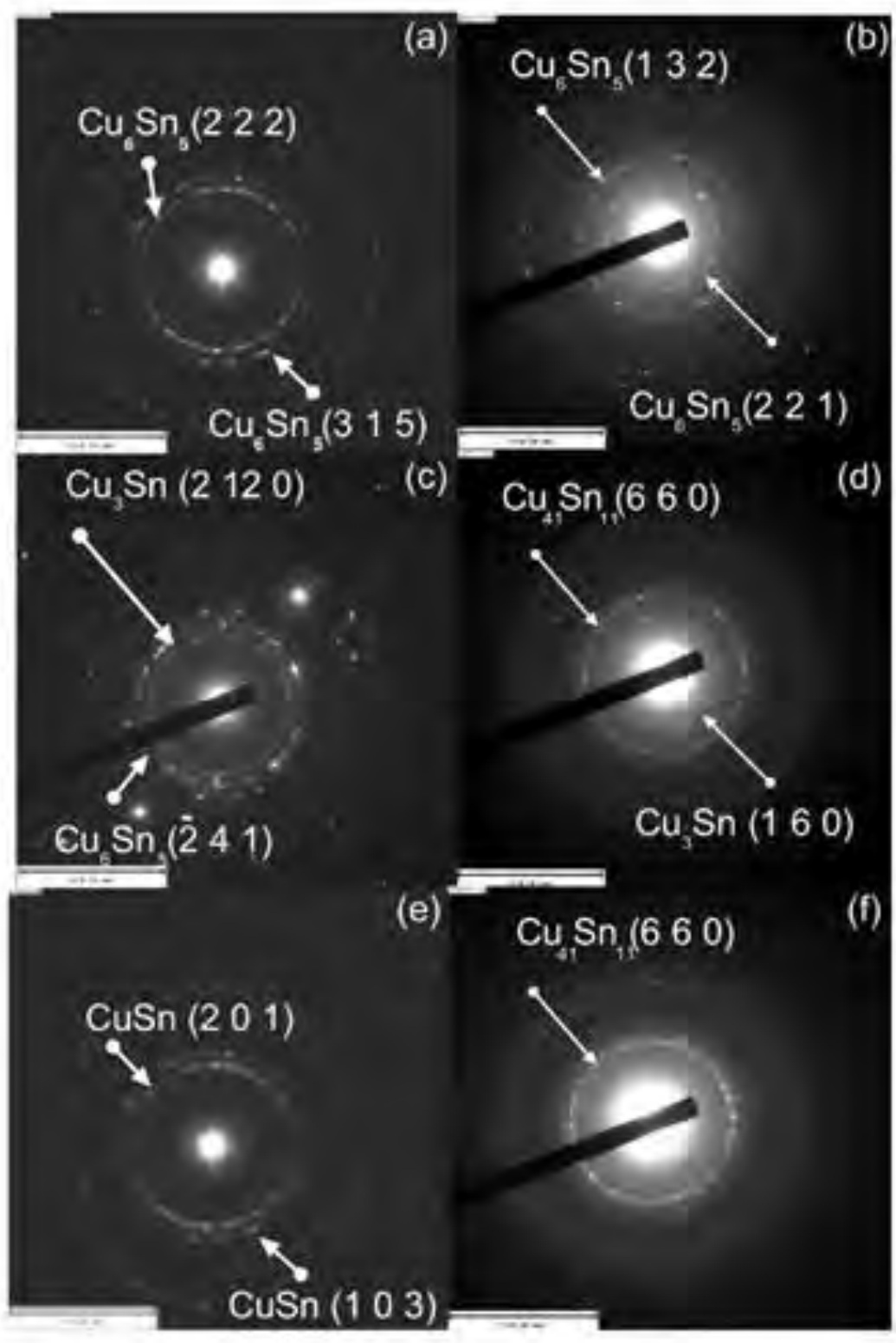


**Figure 6.3** Selected area electron diffraction (SAED) of a)  $\text{Cu}_{30}\text{Sn}_{70}$ , b)  $\text{Cu}_{30}\text{Sn}_{70}$ (HT), c)  $\text{Cu}_{50}\text{Sn}_{50}$ , d)  $\text{Cu}_{50}\text{Sn}_{50}$ (HT), e)  $\text{Cu}_{70}\text{Sn}_{30}$ , f)  $\text{Cu}_{70}\text{Sn}_{30}$ (HT).

The oxidation state number of Cu (i.e.  $\text{Cu}^+$  and  $\text{Cu}^{2+}$ ) and Sn (i.e.  $\text{Sn}^{2+}$  and  $\text{Sn}^{4+}$ ) were identified by XPS. Figures 6.4 (a-c) and 5 (a-c), showing the deconvoluted peak profile of Cu in  $\text{Cu}_x\text{Sn}_{1-x}$  intermetallics before and after the heat treatment and changes in the Cu peak shapes, suggested the presence of either one or two oxidation states of Cu in the intermetallic. The Cu  $2p_{3/2}$  peak was therefore

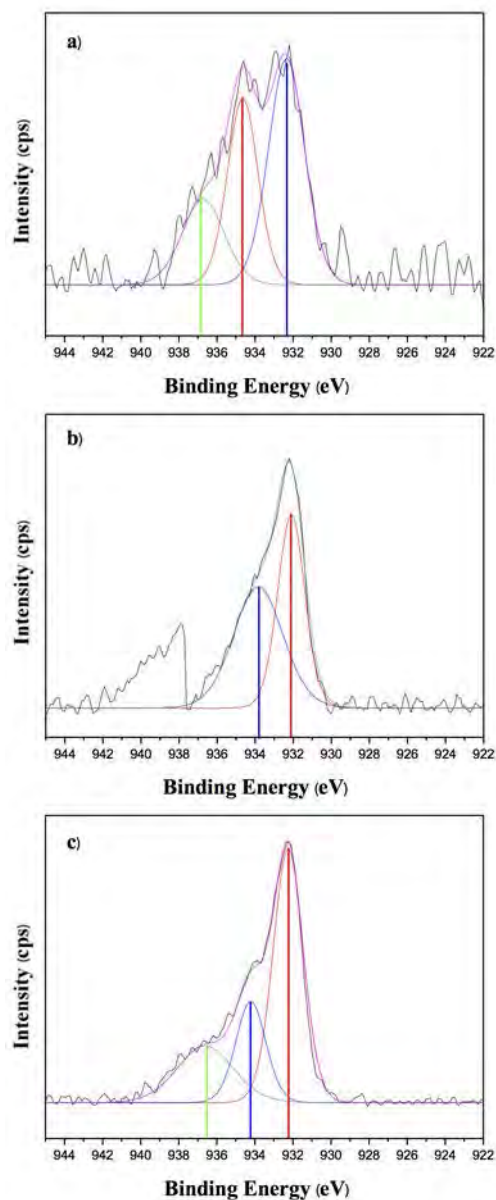


**Figure 6.4** Cu  $3p_{3/2}$  spectra of a)  $\text{Cu}_{30}\text{Sn}_{70}$ , b)  $\text{Cu}_{50}\text{Sn}_{50}$ , and c)  $\text{Cu}_{70}\text{Sn}_{30}$

deconvoluted by Gaussian-Lorentzian curves to fit two oxidation states of  $\text{Cu}^+$  and  $\text{Cu}^{2+}$ . From Figure 6.4a, the Cu  $2p_{3/2}$  peak of  $\text{Cu}_{30}\text{Sn}_{70}$  was 936.8, 934.8, and 932.3

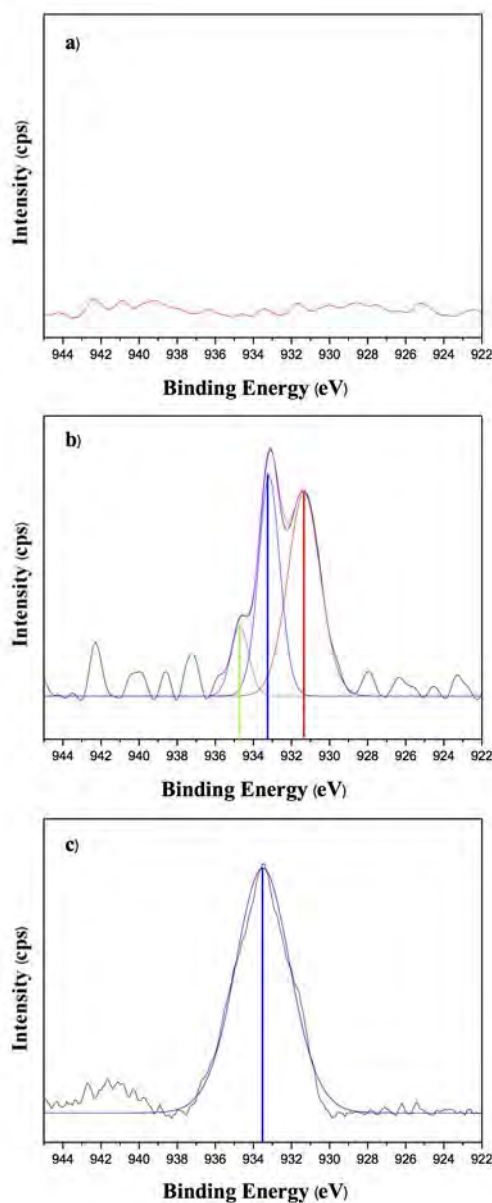


**Figure 6.5** Cu  $3p_{3/2}$  spectra of a)  $\text{Cu}_{30}\text{Sn}_{70}$ (HT), b)  $\text{Cu}_{50}\text{Sn}_{50}$ (HT), and c)  $\text{Cu}_{70}\text{Sn}_{30}$ (HT)

eV, corresponding to Cu (II) (Drouet *et al.*,2000). Likewise, Figure 6.4b and 6.4c show the Cu  $2p_{3/2}$  peak of  $\text{Cu}_{50}\text{Sn}_{50}$  and  $\text{Cu}_{70}\text{Sn}_{30}$  at 934.3, 932.2 and 936.5, 934.3, 936.5eV, respectively, corresponding to Cu (II) (Drouet *et al.*,2000; Klein *et al.*,1983). Figure 6.5a shows the Cu  $2p_{3/2}$  peak of  $\text{Cu}_{30}\text{Sn}_{70}$ (HT) with the absence of Cu ion because Cu completely diffused into the intersital site of Sn, while Figure

6.5b and 6.5c show the Cu  $2p_{3/2}$  peak of  $\text{Cu}_{50}\text{Sn}_{50}(\text{HT})$  and  $\text{Cu}_{70}\text{Sn}_{30}(\text{HT})$  at 934.8, 933.2, 931.5, and 933.5 eV, respectively, corresponding to Cu (II). The XPS results confirmed that Cu diffused into the interstitial site and formed the metal-metal bonds, as found the  $\text{Cu}^{2+}$  ion, since the binding energy (BEs) of Cu metallic (932.0 eV) was shifted to the higher BEs.

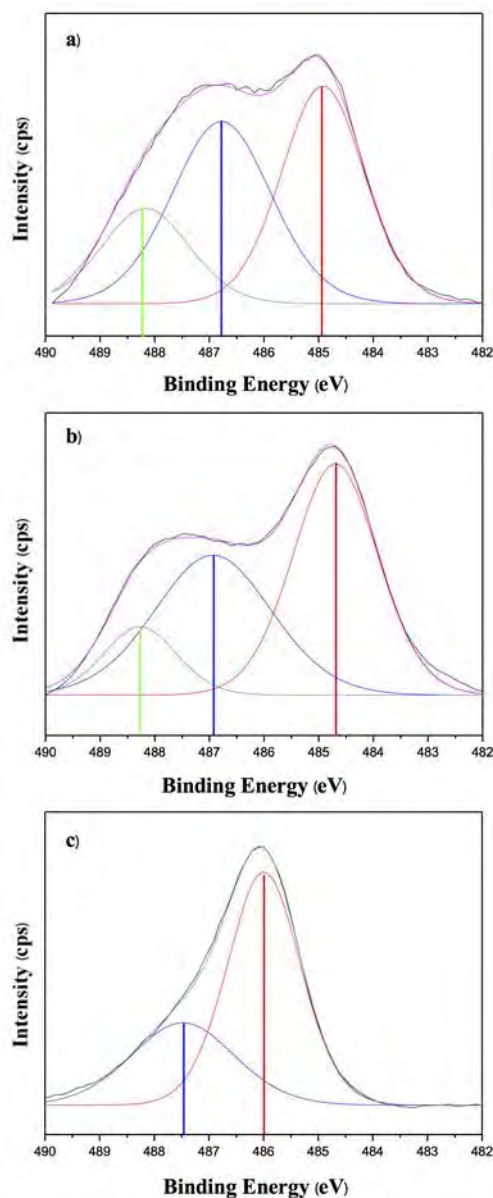


**Figure 6.6** Sn  $3d_{5/2}$  spectra of a)  $\text{Cu}_{30}\text{Sn}_{70}$ , b)  $\text{Cu}_{50}\text{Sn}_{50}$ , and c)  $\text{Cu}_{70}\text{Sn}_{30}$

Similarly, Figure 6.6 (a-c) and 6.7 (a-c), showing the deconvoluted peak profile of Sn in Cu-Sn before and after the heat treatment and changes in the Sn

peak shapes, suggested the presence of either one or two oxidation states of  $\text{Sn}^{2+}$  and  $\text{Sn}^{4+}$  in the intermetallics. The Sn  $3d_{5/2}$  peak was, therefore, deconvoluted by Gaussian-Lorentzian curves to fit the oxidation state number of Sn (i.e.  $\text{Sn}^{2+}$  and  $\text{Sn}^{4+}$ ). From Figure 6.6a, the Sn $3d_{5/2}$  peak of  $\text{Cu}_{30}\text{Sn}_{70}$  was at 488.2 (18.8%), 486.7 (40.7%), and 484.9 (40.5%), corresponding to  $\text{Sn}^{4+}$ ,  $\text{Sn}^{2+}$ , and Sn, respectively (Willemen *et al.*, 1979; Shuttleworth *et al.*, 1980; Okamoto *et al.*, 1979; Lin *et al.*, 1977), whereas,

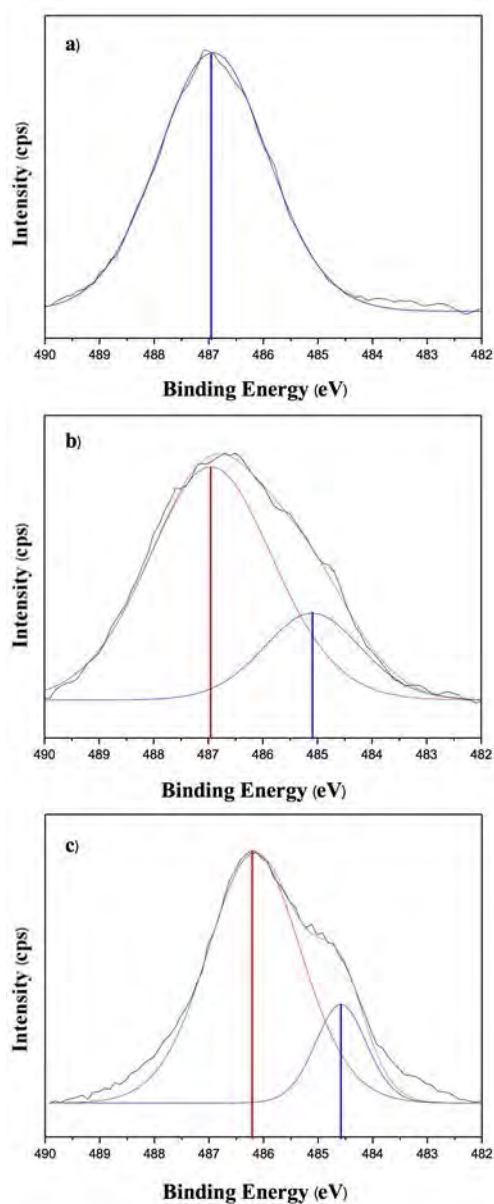


**Figure 6.7** Sn  $3d_{3/2}$  spectra of a)  $\text{Cu}_{30}\text{Sn}_{70}$ (HT), b)  $\text{Cu}_{50}\text{Sn}_{50}$ (HT), and c)  $\text{Cu}_{70}\text{Sn}_{30}$ (HT)

the Sn 3d<sub>5/2</sub> peak of Cu<sub>50</sub>Sn<sub>50</sub> in Fig. 6b was at 488.3 (12.2%), 486.9 (39.8%), and 484.4 eV (48%), belonging to Sn<sup>4+</sup>, Sn<sup>2+</sup>, and Sn, respectively [51-54]. Figure 6.6c shows the Sn 3d<sub>5/2</sub> peak of Cu<sub>70</sub>Sn<sub>30</sub>(HT) at 487.5 (33.3%) and 486 eV (66.7%), corresponding to Sn<sup>4+</sup> and Sn<sup>2+</sup> whereas Figure 6.7a shows the Sn3d<sub>5/2</sub> peak of Cu<sub>30</sub>Sn<sub>70</sub>(HT) at 486.9 eV (100%), corresponding to Sn<sup>2+</sup>. Figures 6.7b and 6.7c show the Sn 3d<sub>5/2</sub> peaks of Cu<sub>50</sub>Sn<sub>50</sub>(HT) and Cu<sub>30</sub>Sn<sub>70</sub>(HT) at 486.9(77.5%), 485.2 (22.5%) and 486.2 (82.2%), 484.6 eV (17.8%), respectively, corresponding to Sn<sup>2+</sup> and Sn. The XPS results indicated the shift of the binding energy (BEs) of Sn metallic (485.0 – 495.5 eV) to higher BEs since Cu diffused into interstitial site of Sn and formed the metal-metal bonds, as found the two oxidation states of Sn.

Figure 6.8, showing Fe-SEM-EDS elemental maps and back scattering images (BSE) of Cu-Sn intermetallic catalysts (Figure 6.8a-c, Cu<sub>30</sub>Sn<sub>70</sub>, Figure 6.8 d-f, Cu<sub>30</sub>Sn<sub>70</sub>(HT), Figure 6.8 g-i, Cu<sub>50</sub>Sn<sub>50</sub>, Figure 6.8 j-l, Cu<sub>50</sub>Sn<sub>50</sub>(HT), Figure 6.8 m-o, Cu<sub>70</sub>Sn<sub>30</sub>, and Figure 6.8 p-r, Cu<sub>70</sub>Sn<sub>30</sub>(HT)) confirmed the composition uniformity in the samples after the heat treatment. Table 6.1, listing the compositions of Cu/Sn in the Cu<sub>x</sub>Sn<sub>y</sub> intermetallic catalysts from the XPS technique, indicated that the values was close to the nominal weighing. In addition, the morphology of all prepared catalysts had random sphere shapes. Evidently, these results confirmed that the MA technique was a good method to successfully prepare Cu<sup>2+</sup> in the Cu<sub>x</sub>Sn<sub>y</sub> intermetallic catalysts since the Cu<sup>2+</sup> obtained was 100% in all compositions.

### 6.4.3 Catalytic activity testing

#### 6.4.3.1 *Kinetic modeling*

To study the electronic and geometric effects on different phases of the synthesized catalyst, quantitative analysis and the rate constant of the phenol consumption were studied. Moreover, qualitative analysis and the selectivity of products, viz. CAT, HQ, and BQ, were determined to indicate how selective the insertion of the hydroxyl group on ortho- or para-position was.

According to several studies, phenol hydroxylation using H<sub>2</sub>O<sub>2</sub> is fitted to the second-order kinetic expression, as recited elsewhere (Wilkenhoner *et al.*,2001);

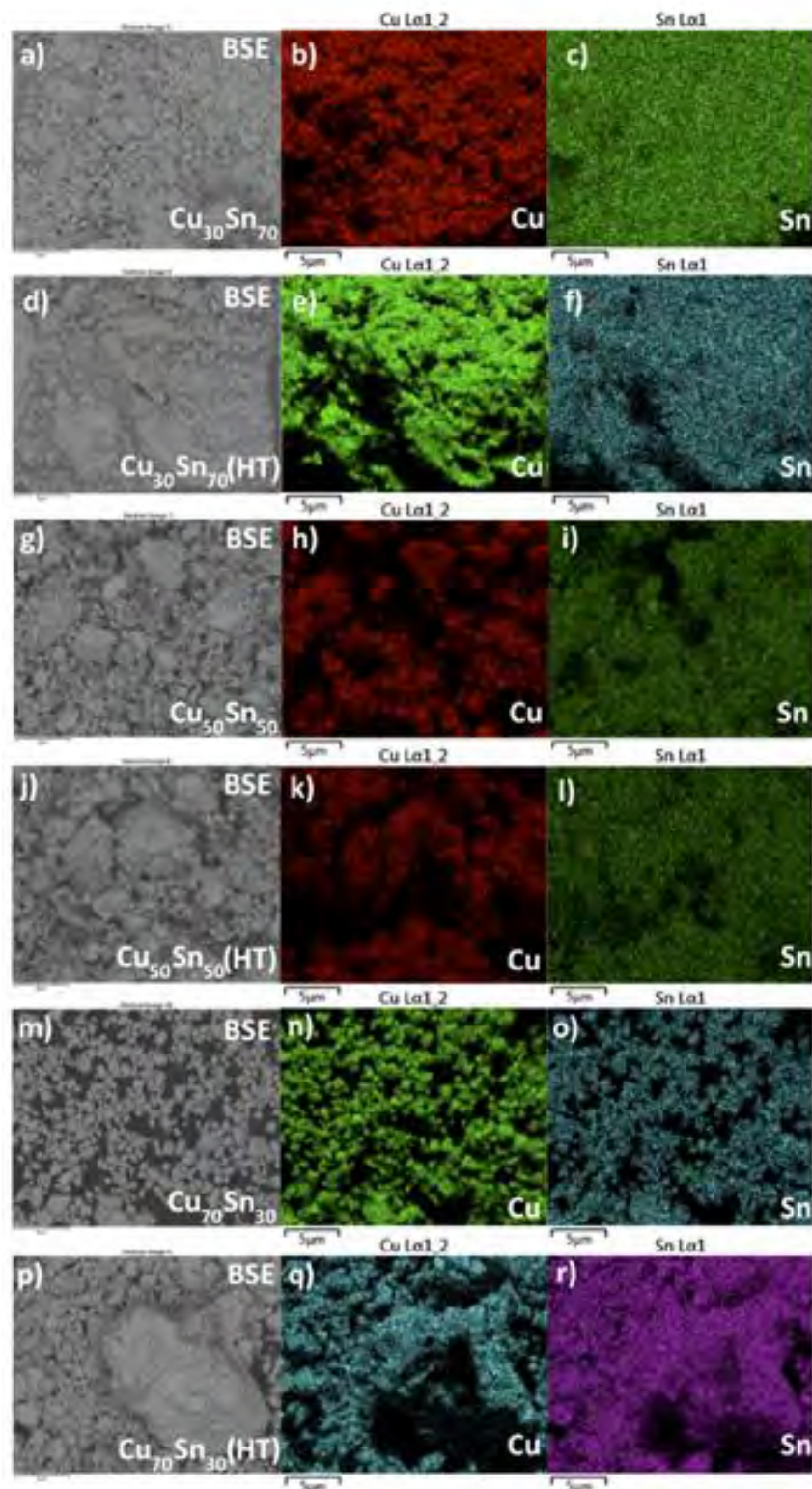


**Figure 6.8** FE-SEM-EDS elemental mapping and black scattering images (BSE) of a-c,  $\text{Cu}_{30}\text{Sn}_{70}$ , d-f,  $\text{Cu}_{30}\text{Sn}_{70}(\text{HT})$ , g-i,  $\text{Cu}_{50}\text{Sn}_{50}$ , j-l,  $\text{Cu}_{50}\text{Sn}_{50}(\text{HT})$ , m-o,  $\text{Cu}_{70}\text{Sn}_{30}$ , and p-r,  $\text{Cu}_{70}\text{Sn}_{30}(\text{HT})$ .



therefore, the concentration-time profile was used to determine the rate constant. Since the surface area generally has an effect on activity and selectivity, therefore, in order to compare the effects of  $\text{Cu}_x\text{Sn}_{1-x}$  intermetallics, it is critical that catalysts with different compositions should have close surface area. The  $\text{N}_2$  adsorption-desorption isotherms revealed that the prepared catalysts had surface area in a range of 3.8-4.2 ( $\text{m}^2/\text{g}$ ).

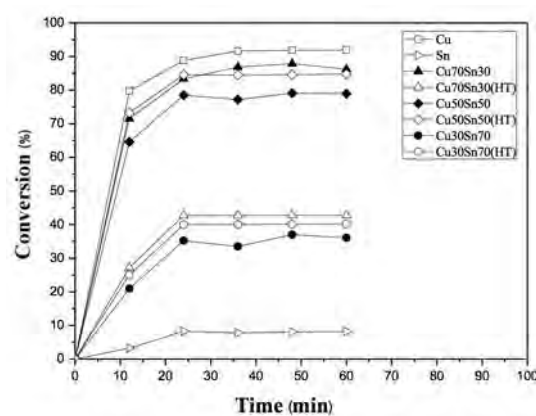


**Figure 6.9** Phenol conversion by time of  $\text{Cu}_x\text{Sn}_y$  intermetallic catalysts before and after the heat treatment.

Figure 6.9 shows conversion of phenol using all synthesized catalysts. It was found that from the starting point to 24 min reaction time, the catalysts provided the maximum conversion before reaching the steady state. Thereby, the concentration-time profiles for all catalysts were conducted from the beginning to 24 min with sampling every 3 min. The selectivity of the products was analyzed at 24 min reaction time.

#### 6.4.4 Geometric and Electronic effects on the catalysts

##### 6.4.4.1 Geometric effect

As mentioned previously, the geometric effect directly influenced the active site of the metal; therefore, the activity of the catalysts occurred by the production of hydroxyl radical from the  $\text{H}_2\text{O}_2$ . Experimentally, the reaction of phenol and  $\text{H}_2\text{O}_2$  without catalyst gave very little conversions (2.3%) (not shown), and the reaction of phenol and catalyst without  $\text{H}_2\text{O}_2$  hardly showed any conversion owing to the absence of the oxidizing agent. The reaction of phenol and  $\text{H}_2\text{O}_2$  in the presence of the catalyst produced remarkable conversion, depending on the type of



the catalysts. Unfortunately, the observation of the catalytic activity on  $\text{H}_2\text{O}_2$  was ambiguous since the dissociation of  $\text{H}_2\text{O}_2$  resulted in side reactions (Fathima *et al.*, 2008; Inchaurredo *et al.*, 2012). Hence, the activity of the catalysts was observed by the consumption of phenol concentration with time (Wilkenhoner *et al.*, 2001).

The rate constants of cubic Cu, tetragonal Sn,  $\text{Cu}_{30}\text{Sn}_{70}$  (cubic sorosite),  $\text{Cu}_{30}\text{Sn}_{70}(\text{HT})$  (cubic  $\delta\text{-Cu}_{41}\text{Sn}_{11}$ ),  $\text{Cu}_{70}\text{Sn}_{30}$  (monoclinic  $\eta\text{-Cu}_6\text{Sn}_5$ ), and  $\text{Cu}_{70}\text{Sn}_{30}(\text{HT})$  monoclinic  $\eta\text{-Cu}_6\text{Sn}_5$  (HT) calculated from the slopes are summarized in Table 6.1. Considering the crystal structures, Cu,  $\text{Cu}_{30}\text{Sn}_{70}$  (sorosite), and  $\text{Cu}_{30}\text{Sn}_{70}(\text{HT})$   $\delta\text{-Cu}_{41}\text{Sn}_{11}$  are in the group of the cubic structure, and showed that the rate constants decreased in the order of  $\text{Cu} > \text{sorosite} > \delta\text{-Cu}_{41}\text{Sn}_{11}$  due to their different crystallite sizes of 30, 29, and 50 nm, respectively. In the same case, the crystallite sizes of  $\text{Cu}_{70}\text{Sn}_{30}(\text{HT})$  (monoclinic  $\eta\text{-Cu}_6\text{Sn}_5$  (HT)) and  $\text{Cu}_{70}\text{Sn}_{30}$  ( $\eta\text{-Cu}_6\text{Sn}_5$ ) were 27.5 and 55.3 nm, respectively, and the rate constant increased with a decrease in the crystallite size. Evidently, this improvement could be used to explain the minimum energy structure due to an increase in the percentage of the under-coordinated metal atoms at the edges and the corners of facets of the nanoparticle. The decrease in the coordination of the edge and the corner atoms of the nanoparticle caused changes in the kinetics (Henry *et al.*, 1985; Dahl *et al.*, 1999; Dahl *et al.*, 2000; Vines *et al.*, 2009). As in agreement with theoretical prediction and related articles cited elsewhere (Vines *et al.*, 2009; Ludwig *et al.*, 2010; Schauer mann *et al.*, 2015), it can be concluded that as the coordinated sites (edges and corners) of  $\text{Cu}_x\text{Sn}_{1-x}$  nanoparticles are lowered, the diffusion rate of the hydroxyl radical over the surface and subsurface increased, hence the hydroxyl radicals were strongly facilitated to react to phenol. Consequently, the rate constant increased in conjunction with a decrease in the crystallite size (Henry *et al.*, 1992; Hammer *et al.*, 1996; Morikawa *et al.*, 1997; Hammer *et al.*, 2000; Alayoglu *et al.*, 2011; Schauer mann *et al.*, 2013). Based on the experimental results, it was revealed that the cubic structure produced a higher activity than the monoclinic structure and the same crystal structure since cubic structure contained a higher copper content than monoclinic crystal structure, as shown in Table 6.1, and, the smaller crystallite size produced the higher catalytic activity.

As observed from the addition of orthorhombic  $\varepsilon$ -Cu<sub>3</sub>Sn in the monoclinic  $\eta$ -Cu<sub>6</sub>Sn<sub>5</sub>(Cu<sub>50</sub>Sn<sub>50</sub>), the conversion and the rate constant tremendously jumped up to 77% and  $6.87 \times 10^{-5}$  dm<sup>3</sup>/mol.s, respectively. Moreover, the addition of around 50 %wt cubic  $\delta$ -Cu<sub>41</sub>Sn<sub>11</sub> phase (Cu<sub>50</sub>Sn<sub>50</sub>(HT)) yielded the highest conversion (84%) and rate constant ( $1.04 \times 10^{-4}$  dm<sup>3</sup>/mol.s) while the crystallite size was 46.3 nm. The result shows that the addition of orthorhombic  $\varepsilon$ -Cu<sub>3</sub>Sn and monoclinic  $\eta$ -Cu<sub>6</sub>Sn<sub>5</sub> phases governed the catalytic activity by enhancing the cleavage of H<sub>2</sub>O<sub>2</sub> (92% (Cu<sub>50</sub>Sn<sub>50</sub>) to 98% (Cu<sub>50</sub>Sn<sub>50</sub>(HT))), consistent with the results studied by adding another metal. As a result, the single phase of the cubic crystal structure with the higher percentage of copper provided the highest catalytic activity. The addition of another crystal structure containing the lower copper content (i.e. 50%wt Cu) showed a higher activity than the single phase. It could be implied that the ensemble crystal structure strongly affected the catalytic activities more than the metal content and the crystallite size.

#### 6.4.4.2 *Electronic effect*

As discussed from the geometric effect, there were both single (cubic and monoclinic) and multi phases (2 phases, i.e., Monoclinic and orthorhombic and 3 phases, i.e., Monoclinic, orthorhombic, and cubic) in the crystal structures. Therefore, to observe the electronic effect, the change in the crystallite size (degree of charge transfer and hybridization) and the surface geometry (ensemble crystal structures) were studied on how selective CAT (ortho) or HQ (para) was. Figure 6.10 shows the conversion and the product selectivity of the cubic copper, cubic sorosite (Cu<sub>30</sub>Sn<sub>70</sub>), cubic  $\delta$ -Cu<sub>41</sub>Sn<sub>11</sub> (Cu<sub>30</sub>Sn<sub>70</sub>(HT)), monoclinic  $\eta$ -Cu<sub>6</sub>Sn<sub>5</sub>(Cu<sub>70</sub>Sn<sub>30</sub>), and monoclinic  $\eta$ -Cu<sub>6</sub>Sn<sub>5</sub>(HT) (Cu<sub>70</sub>Sn<sub>30</sub>(HT)). The CAT product using cubic structure became constant, except cubic  $\delta$ -Cu<sub>41</sub>Sn<sub>11</sub>. The selectivity of CAT was higher than that of HQ since the crystallite size of cubic  $\delta$ -Cu<sub>41</sub>Sn<sub>11</sub> was 1.5 times larger than cubic copper and cubic sorosite. In addition, the large crystallite size of monoclinic  $\eta$ -Cu<sub>6</sub>Sn<sub>5</sub> showed a higher selectivity of CAT than HQ. The reason is that an increase in the crystallite size resulted in an increase of the coordinated sites (edges, corners), contributing to a decrease in either the geometric strain or the diffusion rate of the hydroxy radicals over the surface and

subsurface, hence making CAT more favourable [55, 72]. Furthermore, the results showed that the conversion decreases in conjunction with an increase in BQ selectivity because there was more oxidant left in the system and, therefore, HQ was

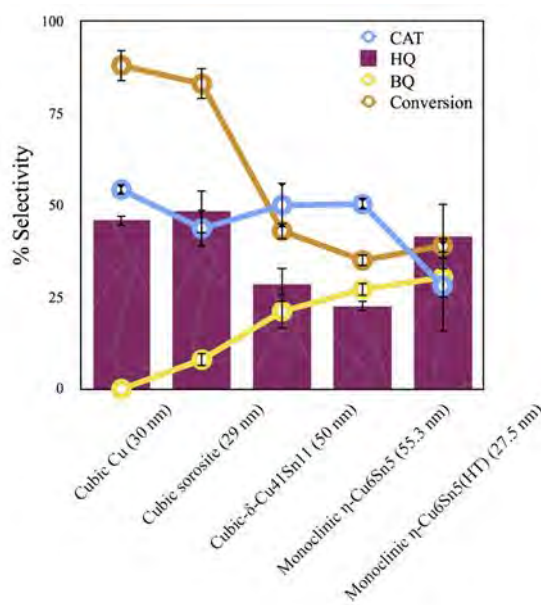


**Figure 6.10** Crystallite size and product selectivity of single phase catalysts.

further oxidized to BQ (Kulawong *et al.*, 2011). The results are in agreement with the surface studies that the large number of the acid site and  $\text{Sn}^{2+}$  ion could govern the reaction such that the acid sites prevented the  $\text{H}_2\text{O}_2$  scavenging and improvably absorbed phenol on its surface, in addition, the  $\text{Sn}^{2+}$  ion was selective to produce hydroxy radical. Thus, cubic  $\delta$ -Cu<sub>41</sub>Sn<sub>11</sub> having the acid site numbers of 1.20 mmol/g and containing 100%  $\text{Cu}^{2+}$  and 82.2 %  $\text{Sn}^{2+}$ , yielded 21.3% CAT and 12.1% HQ. Moreover, the  $\eta$ -Cu<sub>6</sub>Sn<sub>5</sub> having the acid site number of 1.23 mmol/g and containing 40%  $\text{Sn}^{2+}$  ion yielded 17.7% CAT (17.7%) and 7.9% HQ. Both catalysts have their  $\text{H}_2\text{O}_2$  efficiency of 92% ( $\delta$ -Cu<sub>41</sub>Sn<sub>11</sub>) and 62% ( $\eta$ -Cu<sub>6</sub>Sn<sub>5</sub>), as listed in Table 6.2. Moreover,  $\text{Cu}^{2+}$  ion governed the attraction of phenol to its surface and hydroxylation took place at ortho-position of phenol, meanwhile,  $\text{Sn}^{2+}$  generated hydroxy radicals. Consequently, the yields of CAT using  $\eta$ -Cu<sub>6</sub>Sn<sub>5</sub> and  $\delta$ -Cu<sub>41</sub>Sn<sub>11</sub> were more than HQ.

The crystallite size of monoclinic  $\eta$ -Cu<sub>6</sub>Sn<sub>5</sub>(HT) (Cu<sub>70</sub>Sn<sub>30</sub>(HT)) was half smaller than that of monoclinic  $\eta$ -Cu<sub>6</sub>Sn<sub>5</sub>(Cu<sub>70</sub>Sn<sub>30</sub>), leading to a higher conversion than the monoclinic  $\eta$ -Cu<sub>6</sub>Sn<sub>5</sub>[65, 70]. Indeed, the surface analysis reported that an amount of acid site of monoclinic  $\eta$ -Cu<sub>6</sub>Sn<sub>5</sub>(HT) dramatically dropped to 0.3 mmol/g and Cu<sup>2+</sup> was undetectable, yielding CAT, HQ, and BQ of 11.2, 16.6, and 12.13%, respectively. Depletion of Cu<sup>2+</sup> caused a lower yield of CAT, as mentioned earlier, and over oxidation of HQ to BQ. Evidently, among the catalysts studied in this work, as shown in table 6.2, monoclinic  $\eta$ -Cu<sub>6</sub>Sn<sub>5</sub>(HT) showed the highest yield of BQ because the system contained a large number of hydroxy radicals from 100% Sn content which its H<sub>2</sub>O<sub>2</sub> efficiency was 64%. The abundant hydroxy radicals preferred to react with HQ than free phenol, leading to over oxidation to BQ. Another electronic effect was from the surface geometry of monoclinic  $\eta$ -Cu<sub>6</sub>Sn<sub>5</sub> and orthorhombic  $\epsilon$ -Cu<sub>3</sub>Sn (Cu<sub>50</sub>Sn<sub>50</sub>); the ensemble of the crystal structure showed tremendous effect owing to the decrement of BQ in conjunction with increases of CAT and HQ, indicating that both monoclinic  $\eta$ -Cu<sub>6</sub>Sn<sub>5</sub> and orthorhombic  $\epsilon$ -Cu<sub>3</sub>Sn crystal structures were sensitive for activating either ortho or para position. In this case, CAT was higher than HQ due to the highly stable thermodynamics by the hydrogen intramolecular bonding (Winstanley *et al.*, 2007). Moreover, the addition of orthorhombic  $\epsilon$ -Cu<sub>3</sub>Sn (Cu<sub>50</sub>Sn<sub>50</sub>(HT)) showed a drastic decline of BQ due to the over oxidation of BQ to tar with respect to a high conversion (72%). Including cubic  $\delta$ -Cu<sub>41</sub>Sn<sub>11</sub> crystal structure, the HQ selectivity dramatically increased to 43.08% while the BQ was rarely detected because of the stronger oxidation reaction and the smaller crystallite, as mentioned earlier, and the over oxidation of BQ to tar was observed with respect to high conversion (84%). Evidently, the surface geometry showed the overwhelming effect more than the degree of charge transfer and hybridization. Surprisingly, the results were in agreement with the surface analysis that both Cu<sub>50</sub>Sn<sub>50</sub> and Cu<sub>50</sub>Sn<sub>50</sub>(HT) had 100%Cu<sup>2+</sup>, referring to the number of acid site, and 0.75 (39.8%) and 0.84 mmol/g (77.5%)Sn<sup>2+</sup>, respectively. It is indicated that the higher acid sites of Cu<sup>2+</sup> with the presence of Sn<sup>2+</sup> gave the higher CAT than HQ in all cases, as previously discussed and listed in Table 6.2. The increase in the number of Sn<sup>2+</sup> ion obviously affected to either the number of acid sites or the CAT selectivity.

## 6.5 Conclusion

The cubic phase exhibited a higher catalytic activity than the monoclinic phase, in which the cubic sorosite was the highest activity. Moreover, the smaller crystallite size showed a higher catalytic activity. In addition, the monoclinic crystal structure could improve its catalytic activity by ensemble with the orthorhombic crystal structure. The improvement by the crystal structure showed a much stronger effect than the metal content. Cubic  $\delta$ -Cu<sub>41</sub>Sn<sub>11</sub> (53.3%), monoclinic  $\eta$ -Cu<sub>6</sub>Sn<sub>5</sub>(19.8%), and orthorhombic  $\varepsilon$ -Cu<sub>3</sub>Sn (35.9%) gave the highest rate constant in the Cu<sub>x</sub>Sn<sub>1-x</sub> intermetallics, as called geometric effect. The electronic effect consisted of a change in the metal content (degree of charge transfer and hybridization) and the surface geometry (ensemble crystal structures). The surface geometry and the crystallite size showed a strong effect on the product selectivity. The monoclinic  $\eta$ -Cu<sub>6</sub>Sn<sub>5</sub> crystal structure gave higher CAT selectivity than the cubic phase crystal structure. The influence of orthorhombic  $\varepsilon$ -Cu<sub>3</sub>Sn could govern the reaction and provide CAT selectivity. It can be said that the Ma process is an alternative process for a green and large scale catalyst synthesis without using any solvent to improve characteristic properties of catalysts (i.e. acid site and oxidation number).

## 6.6 Acknowledgements

The authors gratefully acknowledge the mutual supports or the partial scholarship from Thailand Graduate Institute of Science and Technology (TIGIST-TG-33-09-58-058D), The Petroleum and Petrochemical College, Chulalongkorn University, and Powder Metallurgy Research and Development Unit (PM\_RDU) of the National Metal and Materials Technology Center (MTEC). The authors also would like to thank Mr. John M. Jackson for proof-reading the paper.

**Table 6.2** Surface analysis of Cu<sub>x</sub>Sn<sub>1-x</sub> intermetallics and H<sub>2</sub>O<sub>2</sub> efficiency

Catalyst	Crystal structure	Acid site (mmol/g)	Cu molar percentage			Sn molar percentage			Yield (%)			H <sub>2</sub> O <sub>2</sub> efficiency <sup>a</sup> (%)
			Cu	Cu <sup>+</sup>	Cu <sup>2+</sup>	Sn	Sn <sup>2+</sup>	Sn <sup>4+</sup>	CAT	HQ	BQ	
Cu <sub>70</sub> Sn <sub>30</sub>	Monoclinic η-Cu <sub>6</sub> Sn <sub>5</sub>	0.77	-	-	100	-	66.7	33.3	36.4	40.3	6.7	62
Cu <sub>70</sub> Sn <sub>30</sub> (HT)	Monoclinic η-Cu <sub>6</sub> Sn <sub>5</sub> (HT)	1.20	-	-	100	-	82.2	17.8	21.3	12.1	9.0	74
Cu <sub>50</sub> Sn <sub>50</sub>	Monoclinic η-Cu <sub>6</sub> Sn <sub>5</sub>	0.75	-	-	100	48	39.8	12.2	48.6	24.2	5.6	92
	Orthorhombic ε-Cu <sub>3</sub> Sn											
Cu <sub>50</sub> Sn <sub>50</sub> (HT)	Monoclinic η-Cu <sub>6</sub> Sn <sub>5</sub>	0.85	-	-	100	22.5	77.5	-	48.1	36.4	0	98
	Orthorhombic ε-Cu <sub>3</sub> Sn											
Cu <sub>30</sub> Sn <sub>70</sub>	Cubic δ-Cu <sub>41</sub> Sn <sub>11</sub>	1.23	-	-	100	40.5	40.7	18.8	17.7	8.0	9.5	92
	Cubic sorosite CuSn											
Cu <sub>30</sub> Sn <sub>70</sub> (HT)	Cubic δ-Cu <sub>41</sub> Sn <sub>11</sub>	0.05	-	-	0	-	100	-	11.2	16.6	12.1	92

<sup>a</sup> H<sub>2</sub>O<sub>2</sub> efficiency = (n<sup>o</sup> H<sub>2</sub>O<sub>2</sub> – n<sup>t</sup> H<sub>2</sub>O<sub>2</sub>)/(n<sup>o</sup> H<sub>2</sub>O<sub>2</sub>) x 100

## 6.7 References

- A. Donazzi, B. C. Michael and L. D. Schmidt, Chemical and geometric effects of Ce and washcoat addition on catalytic partial oxidation of CH<sub>4</sub> on Rh probed by spatially resolved measurements, J. Catal., 2008, 260, 270-275.
- A. K. Larsson, L. Stenberg and S. Lidin, The superstructure of domain-twinned η'-Cu<sub>6</sub>Sn<sub>5</sub>, Acta Crystallography. B., 1994, 50, 636-643.
- A. Kumar, D. Srinivas, Hydroxylation of phenol with hydrogen peroxide catalyzed by Ti-SBA-12 and Ti-SBA-16, Journal Molecular Catalyst A: Chemical., 368–369 (2013) 112-118.
- A. S. Bandarenka and M. T. M. Koper, Structural and electronic effects in heterogeneous electrocatalysis: Toward a rational design of electrocatalysts, J. Catal., 2013, 308, 11-24.
- A.B. Ahmed, B. Jibril, S. Danwittayahul, J. Dutta, Microwave-enhanced degradation of phenol over Ni-loaded ZnO nanorods catalyst, Applied Catalysis B. Environment., 156-157 (2014) 456-465.
- B.D. Cullity, "Elements of X-ray Diffraction:", 2nd ed., Addison-Wesley Publishing Company Inc. 2001.
- B.D. Cullity, "Elements of X-ray Diffraction:", 2<sup>nd</sup> ed., Addison-Wesley Publishing Company Inc. 2001.
- C. Borchers, C. Garve, M. Tiegel, M. Deutges, A. Herz, K. Edalati, R. Pippan, Z. Horita and R. Kirchheim, Nanocrystalline steel obtained by mechanical alloying of iron and graphite subsequently compacted by high-pressure torsion, Acta Mater., 2015, 97, 207-215.
- C. Perego, A. Carati, P. Ingallina, M. A. Mantegazza and G. Bellussi, Production of titanium containing molecular sieves and their application in catalysis, Applied Catalysis A: General, 2001, 221, 63-72.
- C. Perego, A. Carati, P. Ingallina, M.A. Mantegazza, G. Bellussi, Production of titanium containing molecular sieves and their application in

- catalysis, Applied Catalysis, A, 221 (2001) 63-72.
- C. Xia, L. Long, B. Zhu, M. Lin and X. Shu, Enhancing the selectivity of Pare-dihydroxybenzene in hollow titanium silicalite zeolite catalyzed phenol hydroxylation by introducing acid–base sites, Catalysis Communications, 2016, 80, 49-52.
- C.G. Silva, M.J. Sampaio, S.A.C. Carabineiro, J.W.L. Oliveira, D.L. Baptista, R. Bacsa, B.F. Machado, P. Serp, J.L. Figueiredo, A.M.T. Silva, J.L. Faria, Developing highly active photocatalysts: gold-loaded ZnO for solar phenol oxidation, Journal Catalysis, 316 (2014) 182-190.
- E. Buarod, S. Pithakratanayothin, S. Naknaka, P. Chaiyasith, T. Yotkaew, N. Tosangthum, R. Tongsri, Facile synthesis and characterization of tenorite nanoparticles from gas-atomized Cu powder, Powder Technology, 269 (2015) 118-126.
- E. Saboor Bagherzadeh, M. Dopita, T. Mütze, U.A. Peuker, Morphological and structural studies on Al reinforced by Al<sub>2</sub>O<sub>3</sub> via mechanical alloying, Advance Powder Technology., 26 (2015) 487-493.
- F. Shi, Y. Chen, L. Sun, L. Zhang and J. Hu, Hydroxylation of phenol catalyzed by different forms of Cu - alginate with hydrogen peroxide as an oxidant , Catalysis Communications, 2012, 25, 102-105.
- F. Viñes, C. Loschen, F. Illas and K. M. Neyman, Edge sites as a gate for subsurface carbon in palladium nanoparticles , Journal of Catalysis., 2009, 266, 59-63.
- F. Yu, W. Zhou, Progress in Natural Science: Alloying and dealloying of CuPt bimetallic nanocrystals, Material International, 23 (2013) 331-337.
- G. Busca, S. Berardinelli, C. Resini, L. Arrighi, J. Technologies for the removal of phenol from fluid streams: a short review of recent developments, Hazard Material, 160 (2008) 265-288.



- G. Langhendries, D. E. De Vos, G. V. Baron and P. A. Jacobs, Quantitative sorption experiments on Ti-zeolites and relation with  $\alpha$ -olefin oxidation by H<sub>2</sub>O<sub>2</sub>, Journal of Catalysis, 1999, 187, 453-463.
- G.H. Du, G. Van Tendeloo, Cu (OH)<sub>2</sub> nanowires, CuO nanowires and CuO nanobelts, Chemical Physics Letter, 393 (2004) 64-69.
- H. Maneesuwan, S. Tantisriyanurak, T. Chaisuwan, S. Wongkasemjit, On the synergistic catalytic properties of bimetallic mesoporous materials containing aluminum and zirconium: the prins cyclisation of citronellal, Applied Catalysis., A: General., 2016.
- H. Mostaan, F. Karimzadeh, M.H. Abbasi, Thermochim. Synthesis and formation mechanism of nanostructured NbAl<sub>3</sub> intermetallic during mechanical alloying and a kinetic study on its formation, Acta, 529 (2012) 36-44.
- H. Shi, T. Zhang, B. Li, X. Wang, M. He and M. Qiu, Photocatalytic hydroxylation of phenol with Fe–Al-silicate photocatalyst: A clean and highly selective synthesis of dihydroxybenzenes, Catalysis. Communication., 2011, 12, 1022-1026.
- H.-H. Huang, M.-C. Lu, J.-N. Chen and C.-T. Lee, Influence of surface modification on catalytic activity of activated carbon toward decomposition of hydrogen peroxide and 2-chlorophenol, Journal of Environmental Science and Health, Part A, 2003, 38, 1233-1246.
- H.S. Abbo, S.J.J. Titinchi, C. Shri, R. Prasad, Investigation of [Ni {Me<sub>4</sub>Bzo<sub>2</sub> [14] aneN<sub>4</sub>}] Cl<sub>2</sub> catalyzed selective hydroxylation of phenol to catechol by H<sub>2</sub>O<sub>2</sub> in the homogeneous medium, Journal Molecular Catalysis A: Chemical, 218 (2004) 125-132.
- I. Efremenko, Implication of palladium geometric and electronic structures to hydrogen activation on bulk surfaces and clusters, J. Mol. Catal. A: Chem., 2001, 173, 19-59.

- I.U. Castro, F. Stüber, A. Fabregat, J. Font, A. Fortuny, C. Bengoa, Supported Cu (II) polymer catalysts for aqueous phenol oxidation, Journal of Hazardous Materials, 163 (2009) 809-815.
- J.S. Benjamin, T.E. Volin, MT, Artificial neural network modeling of mechanical alloying process for synthesizing of metal matrix nanocomposite powders, Materials Science and Technology, 5 (1974) 1929-1934.
- K. Huang, Y. Xu, L. Wang, D. Wu, Heterogeneous catalytic wet peroxide oxidation of simulated phenol wastewater by copper metal–organic frameworks, RSC Advances, 5 (2015) 32795-32803.
- K. P. SA Howard, Mineralogical Society of America, Washington DC, 1989.
- K.-i. Shimizu, K. Shimura, K. Kato, N. Tamagawa, M. Tamura and A. Satsuma, Palladium - Catalysed Dehydrogenative Generation of Imines from Amines. A Nature - Inspired Route to Indoles via Cross - Couplings of Amines with Arylhydrazines, J. Mol. Catal. A: Chem., 2012, 353–354, 171-177.
- K.I. Toranosuke Saito, Hiroki Tsunomachi, Katsuya Sakaguchi, PROCESS FOR THE PREPARATION OF P-BENZOQUINONE, United States Patent, Sanko Kaihatsu, Kagaku Kenkyusho, USA, 1990.
- K.J. Winstanley, D.K. Smith, Ortho-substituted catechol derivatives: the effect of intramolecular hydrogen-bonding pathways on chloride anion recognition, Journal of Organic Chemistry, 2007, 72, 2803-2815
- Kurian M., Eldhose A., Thasleenabi R.M., Mild temperature oxidation of phenol over rare earth exchanged aluminum pillared montmorillonites, International Environment Reserve, 6 (2012) 669-375.
- L. Takacs, J.S. McHenry, Temperature of the milling balls in shaker and planetary mills, Journal Material Science 41 (2006) 5246-5249.

- L.-L. Lou and S. Liu, CuO-containing MCM-48 as catalysts for phenol hydroxylation, Catalysis Communications, 2005, 6, 762-765.
- M. Morakotjinda, K. Fakpan, T. Yotkaew, N. Tosangthum, R. Krataitong, A. Daraphan, P. Siriphol, P. Wila, B. Vetayanugul, R. Tongsri, Gas atomization of low melting-point metal powders, Chiang Mai J. Sci. 37 (2010) 55-63.
- M. Morakotjinda, K. Fakpan, T. Yotkaew, N. Tosangthum, R. Krataitong, A. Daraphan, P. Siriphol, P. Wila, B. Vetayanugul, R. Tongsri, Gas atomization of low melting-point metal powders, Chiang Mai Journal Science 37 (2010) 55-63
- M. R. Maurya, S. J. J. Titinchi and S. Chand, Oxidation of phenol with H<sub>2</sub>O<sub>2</sub> catalysed by Cu (II), Ni (II) and Zn (II) complexes of N, N' -bis-(salicylidene) diethylenetriamine (H<sub>2</sub>saldien) encapsulated in Y-zeolite, Journal of Molecular Catalysis A: Chemical, 2003, 201, 119-130.
- M. Sankar, N. Dimitratos, P.J. Miedziak, P.P. Wells, C.J. Kiely, G.J. Hutchings, Designing bimetallic catalysts for a green and sustainable future, Chemical Society Review, 41 (2012) 8099-8139.
- M. Xia, M. Long, Y. Yang, C. Chen, W. Cai, B. Zhou A highly active bimetallic oxides catalyst supported on Al-containing MCM-41 for Fenton oxidation of phenol solution,, Applied Catalysis., B: Environment, 110 (2011) 118-125.
- M.R. Maurya, S.J.J. Titinchi, S. Chand, Oxidation of phenol with H<sub>2</sub>O<sub>2</sub> catalysed by Cu (II), Ni (II) and Zn (II) complexes of N, N' -bis-(salicylidene) diethylenetriamine (H<sub>2</sub>saldien) encapsulated in Y-zeolite, Journal Molecular Catalysis A: Chemical, 201 (2003) 119-130.

- N. Inchaurredo, J. Cechini, J. Font and P. Haure, strategies for enhanced CWPO of phenol solutions, Applied Catalysis B, 2012, 111–112, 641-648.
- N.K. Mal, A.V. Ramaswamy, Hydroxylation of phenol over Sn-silicalite-1 molecular sieve: solvent effects, Journal Molecular Catalysis A: Chemical, 105 (1996) 149-158.
- N.N. Fathima, R. Aravindhan, J.R. Rao, B.U. Nair, Dye house wastewater treatment through advanced oxidation process using Cu-exchanged Y zeolite: A heterogeneous catalytic approach, Chemosphere, 70 (2008) 1146-1151.
- N.S. Inchaurredo, P. Massa, R. Fenoglio, J. Font, P. Haure, Efficient catalytic wet peroxide oxidation of phenol at moderate temperature using a high-load supported copper catalyst, Chemical Engineering Journal, 198–199 (2012) 426-434.
- P.S. Niphadkar, M.S. Kotwal, S.S. Deshpande, V.V. Bokade, P.N. Joshi, Tin-silicalite-1: Synthesis by dry gel conversion, characterization and catalytic performance in phenol hydroxylation reaction, Material Chemistry Physics, 114 (2009) 344-349.
- R. Klaewkla, S. Kulprathipanja, P. Rangsunvigit, T. Rirksomboon and L. Nemeth, Phenol hydroxylation using Ti-and Sn-containing silicalites, Chemical Communications, 2003, DOI: 10.1039/B303455K, 1500-1501.
- R. Klaewkla, S. Kulprathipanja, P. Rangsunvigit, T. Rirksomboon, W. Rathbun and L. Nemeth, Kinetic modelling of phenol hydroxylation using titanium and tin silicalite-1s: Effect of tin incorporation, Chemical Engineering Journal, 2007, 129, 21-30.
- R. Klaewkla, T. Rirksomboon, S. Kulprathipanja, L. Nemeth and P. Rangsunvigit, Light sensitivity of phenol hydroxylation with TS-1, Catalysis Communications, 2006, 7, 260-263.

- R. Tong Sri, T. Yotkaew, R. Krataitong, P. Wila, A. Sir-on, P. Muthitamongkol, N. Tosangthum, Characterization of Cu<sub>6</sub>Sn<sub>5</sub> intermetallic powders produced by water atomization and powder heat treatment, Material Characterization 86 (2013) 167-176.
- R.R. Zapico, P. Marín, F.V. Díez, S. Ordóñez, Influence of operation conditions on the copper-catalysed homogeneous wet oxidation of phenol: development of a kinetic model, Chemical Engineering Journal, 270 (2015) 122-132.
- S. Dahl, E. Törnqvist and I. Chorkendorff, Dissociative adsorption of N<sub>2</sub> on Ru (0001): a surface reaction totally dominated by steps, Journal of Catalysis, 2000, 192, 381-390.
- S. L. James, C. J. Adams, C. Bolm, D. Braga, P. Collier, T. Friscic, F. Grepioni, K. D. M. Harris, G. Hyett, W. Jones, A. Krebs, J. Mack, L. Maini, A. G. Orpen, I. P. Parkin, W. C. Shearouse, J. W. Steed and D. C. Waddell, Mechanochemistry: opportunities for new and cleaner synthesis, Chemical Society Reviews, 2012, 41, 413-447.
- S. Recchia, C. Dossi, N. Poli, A. Fusi, L. Sordelli and R. Psaro, Outstanding performances of magnesia-supported platinum–tin catalysts for citral selective hydrogenation, J. Catal., 1999, 184, 1-4.
- S. Schauermann and H.-J. Freund, Model approach in heterogeneous catalysis: kinetics and thermodynamics of surface reactions, Model approach in heterogeneous catalysis: kinetics and thermodynamics of surface reactions, Account of Chemical Research, 2015, 48, 2775-2782.
- S. Zamani, H.R. Bakhsheshi-Rad, A. Shokuhfar, M.R. Vaezi, M.R.A. Kadir, M.R.M. Shafiee, Synthesis and characterization of MoSi<sub>2</sub>-Mo<sub>5</sub>Si<sub>3</sub> nanocomposite by mechanical alloying and heat treatment, International Journal Refract Met Hard Material, 31 (2012) 236-241.

- S.-T. Kao, J.-G. Duh, Effect of Cu concentration on morphology of Sn-Ag-Cu solders by mechanical alloying, Journal Electron Material, 33 (2004) 1445-1451.
- SA Howard, K. Preston, Profile Fitting of Powder Diffraction Patterns, Mineralogical Society of America, Washington DC, 1989.
- T. Pino, P. Bréchnignac, E. Dartois, K. Demyk and L. d'Hendecourt, Electronic spectroscopy of a cyclopentafused PAH cation, the fluorene<sup>+</sup>: comparison between gas phase and matrix spectra , Chemical Physics Letters, 2001, 339, 64-70.
- V. S. Antonin, M. H. M. T. Assumpção, J. C. M. Silva, L. S. Parreira, M. R. V. Lanza and M. C. Santos, Synthesis and characterization of nanostructured electrocatalysts based on nickel and tin for hydrogen peroxide electrogeneration, Electrochimica. Acta, 2013, 109, 245-251.
- W. Ludwig, A. Savara, S. Schauermaann and H.-J. Freund, Role of Low - Coordinated Surface Sites in Olefin Hydrogenation: A Molecular Beam Study on Pd Nanoparticles and Pd (111) , Chem. Phys. Chem., 2010, 11, 2319-2322.
- W.D. Callister, "Materials Science and Engineering: An Introduction", Wiley & Sons 2003.
- Y. Morimoto, S. Bunno, N. Fujieda, H. Sugimoto and S. Itoh, Direct hydroxylation of benzene to phenol using hydrogen peroxide catalyzed by nickel complexes supported by pyridylalkylamine ligands , Journal of the American Chemical Society, 2015, 137, 5867-5870.
- Y. Yusuf, K. A. Savas, O. Ulker Bakir, Chemical Engineering Technology, 30 (2007) 548-552.
- Y. Zhao, G. He, W. Dai and H. Chen, High Catalytic Activity in the Phenol Hydroxylation of Magnetically Separable CuFe<sub>2</sub>O<sub>4</sub>-Reduced Graphene Oxide, Industrial & Engineering Chemistry Research, 2014, 53, 12566-12574.

## CHAPTER VII

### CONCLUSIONS AND RECCOMENDATIONS

#### CONCLUSIONS

The  $\text{Cu}_x\text{Sn}_{1-x}$  intermetallic catalysts prepared by mechanical alloying (Ma) were tested their catalytic activity on phenol hydroxylation. The optimal conditions found were at 70 °C reaction temperature for 1 h reaction time using 50 mg of  $\text{Cu}_{0.5}\text{Sn}_{0.5}$ , and 1:3 phenol: $\text{H}_2\text{O}_2$  ratio. Moreover, the crystal structure of the catalysts had an effect on the production distribution. Comparing the single crystal structures of  $\text{Cu}_x\text{Sn}_{1-x}$  and  $\text{Ni}_x\text{Sn}_{1-x}$  after replacing Cu with Ni, impressive activity enhancement of both Cu and Ni was achieved by adding Sn. The number of the strong acid sites and the  $\text{Sn}^{2+}$  ions increased in conjunction with an increase in the Sn content. At 343 K, 1:3 phenol: $\text{H}_2\text{O}_2$ , and 50 mg of the catalyst content, phenol hydroxylation showed that  $\text{Ni}_3\text{Sn}$  and  $\text{Ni}_3\text{Sn}_4$  intermetallic catalysts exhibited a prominent ability to produce only HQ at 30 and 42% yield, respectively. At the optimized conditions of 363 K, 1:4 phenol: $\text{H}_2\text{O}_2$ , and 50 mg of the catalyst content, both  $\text{Ni}_3\text{Sn}$  and  $\text{Ni}_3\text{Sn}_4$  intermetallic catalysts still showed a higher catalytic activity than the  $\text{Cu}_6\text{Sn}_5$  and  $\text{Cu}_6\text{Sn}_5(\text{HT})$  intermetallic catalysts.

Among the mixed crystal structures of  $\text{Cu}_x\text{Sn}_{1-x}$  intermetallic catalysts, the cubic phase exhibited a higher catalytic activity than the monoclinic phase, especially, the cubic sorosite provided the highest activity. The smaller crystallite size showed a higher catalytic activity. The catalytic activity of the monoclinic crystal structure could be improved by being ensemble with the orthorhombic crystal structure. The improvement from the crystal structure showed a much stronger effect than that from the metal content. Cubic  $\delta\text{-Cu}_{41}\text{Sn}_{11}$  (53.3%), monoclinic  $\eta\text{-Cu}_6\text{Sn}_5$  (19.8%), and orthorhombic  $\varepsilon\text{-Cu}_3\text{Sn}$  (35.9%) gave the highest rate constants. The surface geometry and the crystallite size showed a strong effect on the product selectivity. The monoclinic  $\eta\text{-Cu}_6\text{Sn}_5$  crystal structure gave a higher CAT selectivity than the cubic phase crystal structure.

Conclusively, the Ma technique was a plausible technique to synthesize catalysts modifiable both the crystal structure and the acid site number. Both  $\text{Cu}_x\text{Sn}_{1-x}$  and  $\text{Ni}_x\text{Sn}_{1-x}$  intermetallic catalysts were shown good results for oxidation reaction.

**RECOMENDATIONS**

Next steps should be studied other bimetallic catalysts using Ma technique and tested their activity. Comparison of the Ma technique with another technique should also be conducted.



## REFERENCES

- Adabavazeh, Z., Karimzadeh, F. and Enayati, M.H. (2012). Synthesis and structural characterization of nanocrystalline (Ni, Fe)<sub>3</sub>Al intermetallic compound prepared by mechanical alloying. Advanced Powder Technology 23(3), 284-289.
- Álvarez-Rodríguez, J., Rodríguez-Ramos, I., Guerrero-Ruiz, A., Gallegos-Suarez, E. and Arcoya, A. (2012). Influence of the nature of support on Ru-supported catalysts for selective hydrogenation of citral. Chemical Engineering Journal 204–206(0), 169-178.
- Chapuis, C. and Jacoby, D. (2001). Catalysis in the preparation of fragrances and flavours. Applied Catalysis A: General 221(1–2), 93-117.
- Du, W.Q., Rong, Z.M., Liang, Y., Wang, Y., Lu, X.Y., Wang, Y.F. and Lu, L.H. (2012). Chemoselective hydrogenation of  $\alpha,\beta$ -unsaturated aldehydes with modified Pd/C catalyst. Chinese Chemical Letters 23(7), 773-776.
- Ferrando, R., Jellinek, J. and Johnston, R.L. (2008). Nanoalloys: From Theory to Applications of Alloy Clusters and Nanoparticles. Chemical Reviews 108(3), 845-910.
- Gogebakan, M., Kursun, C. and Eckert, J. (2013). Formation of new Cu-based nanocrystalline powders by mechanical alloying technique. Powder Technology 247(0), 172-177.
- Gutierrez, V., Alvarez, M. and Volpe, M.A. (2012). Liquid phase selective hydrogenation of cinnamaldehyde over copper supported catalysts. Applied Catalysis A: General 413–414(0), 358-365.
- Gutiérrez, V., Nador, F., Radivoy, G. and Volpe, M.A. (2013). Highly selective copper nanoparticles for the hydrogenation of  $\alpha,\beta$ -unsaturated aldehydes in liquid phase. Applied Catalysis A: General 464–465(0), 109-115.
- Ide, M.S., Hao, B., Neurock, M. and Davis, R.J. (2012). Mechanistic Insights on the Hydrogenation of  $\alpha,\beta$ -Unsaturated Ketones and Aldehydes to Unsaturated Alcohols over Metal Catalysts. ACS Catalysis 2(4), 671-683.

- Lin, W., Cheng, H., He, L., Yu, Y. and Zhao, F. (2013). High performance of Ir-promoted Ni/TiO<sub>2</sub> catalyst toward the selective hydrogenation of cinnamaldehyde. Journal of Catalysis 303(0), 110-116.
- Margitfalvi, J.L., Borbáth, I., Hegedűs, M. and Tompos, A. (2002). Preparation of new type of Sn-Pt/SiO<sub>2</sub> catalysts for carbonyl activation. Applied Catalysis A: General 229(1–2), 35-49.
- Merlo, A.B., Vetere, V., Ruggera, J.F. and Casella, M.L. (2009). Bimetallic PtSn catalyst for the selective hydrogenation of furfural to furfuryl alcohol in liquid-phase. Catalysis Communications 10(13), 1665-1669.
- Mertens, P.G.N., Cuypers, F., Vandezande, P., Ye, X., Verpoort, F., Vankelecom, I.F.J. and De Vos, D.E. (2007). Ag<sup>0</sup> and Co<sup>0</sup> nanocolloids as recyclable quasihomogeneous metal catalysts for the hydrogenation of  $\alpha,\beta$ -unsaturated aldehydes to allylic alcohol fragrances. Applied Catalysis A: General 325(1), 130-139.
- Mertens, P.G.N., Vandezande, P., Ye, X., Poelman, H., Vankelecom, I.F.J. and De Vos, D.E. (2009). Recyclable Au<sup>0</sup>, Ag<sup>0</sup> and Au<sup>0</sup>–Ag<sup>0</sup> nanocolloids for the chemoselective hydrogenation of  $\alpha,\beta$ -unsaturated aldehydes and ketones to allylic alcohols. Applied Catalysis A: General 355(1–2), 176-183.
- Milone, C., Crisafulli, C., Ingoglia, R., Schipilliti, L. and Galvagno, S. (2007). A comparative study on the selective hydrogenation of  $\alpha,\beta$  unsaturated aldehyde and ketone to unsaturated alcohols on Au supported catalysts. Catalysis Today 122(3–4), 341-351.
- Mostaan, H., Karimzadeh, F. and Abbasi, M.H. (2012). Synthesis and formation mechanism of nanostructured NbAl<sub>3</sub> intermetallic during mechanical alloying and a kinetic study on its formation. Thermochimica Acta 529(0), 36-44.
- Plomp, A.J., van Asten, D.M.P., van der Eerden, A.M.J., Mäki-Arvela, P., Murzin, D.Y., de Jong, K.P. and Bitter, J.H. (2009). Catalysts based on platinum–tin and platinum–gallium in close contact for the selective hydrogenation of cinnamaldehyde. Journal of Catalysis 263(1), 146-154.

- Rojas, H., Díaz, G., Martínez, J.J., Castañeda, C., Gómez-Cortés, A. and Arenas-Alatorre, J. (2012). Hydrogenation of  $\alpha,\beta$ -unsaturated carbonyl compounds over Au and Ir supported on SiO<sub>2</sub>. Journal of Molecular Catalysis A: Chemical 363–364(0), 122-128.
- Serra, S., Fuganti, C. and Brenna, E. (2005). Biocatalytic preparation of natural flavours and fragrances. Trends in Biotechnology 23(4), 193-198.
- Taniya, K., Jinno, H., Kishida, M., Ichihashi, Y. and Nishiyama, S. (2012). Preparation of Sn-modified silica-coated Pt catalysts: A new PtSn bimetallic model catalyst for selective hydrogenation of crotonaldehyde. Journal of Catalysis 288(0), 84-91.
- Wienhöfer, G., Westerhaus, F.A., Junge, K. and Beller, M. (2013). Fast and selective iron-catalyzed transfer hydrogenations of aldehydes. Journal of Organometallic Chemistry 744(0), 156-159.
- Zamani, S., Bakhsheshi-Rad, H.R., Shokuhfar, A., Vaezi, M.R., Kadir, M.R.A. and Shafiee, M.R.M. (2012). Synthesis and characterization of MoSi<sub>2</sub>-Mo<sub>5</sub>Si<sub>3</sub> nanocomposite by mechanical alloying and heat treatment. International Journal of Refractory Metals and Hard Materials 31(0), 236-241.

## CURRICULUM VITAE

**Name:** Sakollapath Pithakratanayothin

**Date of Birth:** August 17, 1989

**Nationality:** Thai

**University Education:**

2017 Student internship at Paul Scherrer Institute (6 months)

2012-2014 Master Degree of Science (Petrochemical Technology),  
Petroleum and Petrochemical College, Chulalongkorn University, Bangkok, Thailand

2008-2012 Bachelor Degree of Science (Petrochemical Technology),  
Faculty of Engineer, King Mongkut's University of Technology Lardkrabang,  
Bangkok, Thailand

**1. Publications:**

1. Pithakratanayothin, S, Thongsri, R, Chaisuwan, T, and Wongkasemjit, S (2017) Influences of M-Sn intermetallics (M=Cu, Ni) prepared by mechanical alloying on phenol hydroxylation. *Catalysis Science and Technology*, 2017
2. Pithakratanayothin, S, Thongsri, R, Chaisuwan, T, and Wongkasemjit, S (2016) a simple route to  $\text{Cu}_x\text{Sn}_{1-x}$  intermetallic nanoparticle catalysts for ultra phenol hydroxylation. *Materials Chemistry and Physics*, 2016
3. Pithakratanayothin, S. and Jitkarnka, S. (2014) Comparison of components in oil derived from tyre pyrolysis with and without KL catalyst using GC  $\times$  GC / TOF-MS. *Chemical Engineering Transactions*, 2014

**2. Proceedings:**

1. Pithakratanayothin, S, Thongsri, R, Chaisuwan, T, and Wongkasemjit, S, (2018, November 6) Structural effect of  $\text{Cu}_x\text{Sn}_{1-x}$  intermetallic catalyst prepared by mechanical alloying technique in phenol hydroxylation. *Proceeding of the International Conference on Catalysis and Pyrolysis 2018*, San Francisco, USA.
2. Pithakratanayothin, S, Thongsri, R, Chaisuwan, T, and Wongkasemjit, S, (2017, May 15) A simple mechanical alloying technique for green catalyst synthesis. *Proceeding of the TechConnect World Innovation Conference 2017*, Washington D.C., USA.

3. Pithakratanayothin, S. and Jitkarnka, S. (2014, March 31) analysis of a tire-derived oil using GC × GC – TOF/MS for better identification and grouping of hydrocarbon compounds. Proceeding of the 29<sup>th</sup> ICSW 2014, Philadelphia, USA.
4. Pithakratanayothin, S. and Jitkarnka, S. (2014, April 24) analysis of a tire-derived oil using GC × GC – TOF/MS for better identification and grouping of sulphur compounds. Proceeding of the 5<sup>th</sup> Research Symposium on Petrochemical and Materials Technology and the 20<sup>th</sup> PPC Symposium on Petroleum, Petrochemicals, and Polymers, Bangkok, Thailand.
5. Pithakratanayothin, S. and Jitkarnka, S. (2014, August 23) comparison of components in oil derived from tyre pyrolysis with and without KL catalyst using GC × GC / TOF-MS. Proceeding of the 17<sup>th</sup> Conference Process Integration, Modelling and Optimisation for Energy Saving and Pollution Reduction, Prague, Czech Republic.